Quantum Electrodynamics and Relativistic Corrections of the g-factor and hyper fine structure splitting in Li- and B-like ions

Submitted by Ekaterina Berseneva to the University of Exeter as a thesis for the degree of
Doctor of Philosophy by Publication in Engineering
In AUGUST 2020

I certify that all material in this thesis which is not my own work has been identified and that no material has previously been submitted and approved for the award of a degree by this or any other University.

Signature: .....

1 Abstract

The investigations in the field of the quantum computer brings the importance of the understanding of the Quantum Electrodynamics (QED) properties of particles to the front line. By the various techniques of molecular cooling and trapping we remove the kinetics characteristics of the system. Thus, when the particle is trapped and doesn't perform any movement we can test the physical characteristics such as total electronic energies of atoms and ions, energies of optical and X-ray transitions, hyperfine splitting constants that show the energy levels splitting, g-factors of bound electrons, that describe the magnetic and angular momentum of a particle, isotopic shifts, probabilities of electrical and magnetic transitions in atoms etc.

The objective of this thesis is the high precision calculations of G-factor and Hyperfine structure splitting of different elements. By considering the existing results and literature, we perform the high accuracy calculations on H-like (one electron and nucleus), Li-like(three electrons orbiting nucleus) and B-like(five electrons orbiting nuclues) elements. Moreover working closely with experimental groups we perform calculations on lanthanide atoms.

For these type of calculations, different type of contributions are to be taken into account, including correlation, relativistic, quantum electrodynamic, higher radiative corrections, and the contribution of the negative Dirac spectrum. It is also necessary to calculate the corrections arrising from the the electric charge distribution and nucleus magnetic moment.

We propose the approximate radiative single-particle potential that significantly improves the high-accuracy of the non empirical calculations of the QED corrections for calculating the electronic structure of atoms and molecules.

In conjunction with the experimental measurements and fits, using the Multi Configurational Dirac-Fock-Sturm method (MCDFS), we have executed the extensive high-precision calculation for the electronic structure calculations of one of the

lanthanide atoms, the Er. The interest of these calculations is explained in their multiple unpaired valence electrons, that have rich atomic energy spectra and exhibit various types of coupling between the electronic angular momentum J and the nuclear spin I of the atom. These calculations allowed us to obtain the magnetic dipole and electric quadrupole constants for the only stable fermionic isotope, $167^{E}r$ and thus explain the theory behind the experiment of the laser cooling transitions.

We then do various calculations to improve existing results for the determination of the fine-structure constant. The approach of the calculations by the MCDFS method has been proposed for the calculations for the specific weighted differences of the g-factors of H-and Li-like ions of the same element. An accurate formula was obtained for the weight parameter, determined by requiring cancellation of the nonrelativistic finite nuclear size corrections to various orders. We then demonstrated that weighted differences can be used for an effective cancellation of nuclear structural effects. This independent scheme may be used to extract the fine-structure constant from a comparison of experimental and theoretical bound-electron g-factors with an accuracy improvement by orders of magnitude.

The future prospect of the calculations for the many-electron systems like B-like particles are also outlined.

2 Acknowledgements

As my thesis writing days come to a close I would like to take this opportunity to express gratitude to those who supported me through the years of my PhD research and made it all possible.

I would like to give thanks to my supervisors, Prof. Anna Baldycheva and Prof. Ilya I. Tupitsyn, for their ideas, inspiration, encouragement and helpful discussion, guidance and supervision throughout this PhD. Because of them, the project exists and became successful. I would also like to thank all the members of the Theoretical Quantum Dynamics and Quantum Electrodynamics group at Max Planck Institute of Core Physics in Heidelberg, in particular, Prof. Christoph Keitel, Dr. Zoltan Harman, Dr. Natalia Oreshkina for their help with theoretical investigations of g-factor and HFS of Li-like elements. But it was not just the scientific supervision that was provided, I've also been very lucky to participate in the scientific life of their outstanding theoretical group. Many thanks to Svetlana Kotochigova group at National Institute of Standards and Technology for her kind supervision, long fruitful conversations and my first opportunity to work closely in the same project with an experimental Ultracold Atoms and Quantum Gases group of Prof. Francesca Ferlaino at the University of Innsbruck. A very special thank you I would like to say to the Yury Kozhedub, a member of the Quantum physics department of the Saint-Petersburg State University. You are the kindest person on Earth, you were always supporting me during my PhD, thank you for answering on my endless questions and looking through my calculations.

I would like to acknowledge the full financial support from the Max Planck Institute and German-Russian Interdisciplinary Science Center that made my international theoretical investigation possible.

Further thanks are to my parents and my family that were always very supportive. Especially to my mother for always been there for me and spending endless

hours over the phone, advising me always wisely. There are many others not mentioned here, I am sorry for not including you, but I wanted to keep this short.

3 List of Contents

Contents

4 List of Tables

List of Tables

5 List of Figures

List of Figures

6 List of Publications

1. V. A. Yerokhin, E. Berseneva, Z. Harman, I. I. Tupitsyn, and C. H. Keitel. Weighted difference of g-factors of light Li-like and H-like ions for an improved determination of the fine-structure constant, Phys. Rev. A. 94, 022502 (2016).

2. V. A. Yerokhin, E. Berseneva, Z. Harman, I. I. Tupitsyn, and C. H. Keitel. G-factor of light ions for an im proved determination of the fine-structure constant, Phys. Rev. Lett. 116, 100801 (2016).

3. I. Tupitsyn, E. Berseneva. A Single-Sartical Nonlocal Potential for Taking into Account Quantum-Electrody namic Corrections in Calculations of the Electronic Structure of Atoms. Optics and Spectroscopy 2013, vol 114, No. 5, pp. 743-749.

4. Albert Frisch, Kiyotaka Aikawa, Michael Mark, Francesca Ferlaino, Ekaterina Berseneva, Svetlana Ko tochigova. Hyperfine Structure of Laser-Cooling Transitions in Fermionic Erbium-167, Phys. Rev. A. 88, 032508 (2013).

7 Presentations

1) SPb-POEM2020: SPb-Photonic and OptoElectronic Materials Conference, 27-30 April, St. Petersbourg, 2020

2) SNAIA2019: Smart NanoMaterials 2018 - Advances, Innovation and Applications, 9-12 December, Paris, 2019

3) POEM2019: Photonic and OptoElectronic Materials Conference, 9-12 April, London, 2019

4) SNAIA2018: Smart NanoMaterials 2018 - Advances, Innovation and Applications, 9-12 December, Paris, 2018

5) PSAS2014: International Conference on Precision Physics of Simple Atomic Systems, 25-30 May, Rio de Janeiro, Brazil.

6) ISNP: International School of Nanophotonics and Photovoltaics, August 30 –September 6, 2013, Maratea, Italy.

7) ECAMP 11: European Conference on Atoms, Molecules and Photons conference, 24-28 June, Aarhus, Denmark.

8) EAS: Extreme Atomic Systems conference, 9-14 February, 2013, Riezlern, Austria.

9) SPARC: Stored Particles Atomic Physics Research Collaboration, 26-28 November, 2012, Vienna, Austria.

10) D18-2011-118: Precision Physics and Fundamental Physical Constants, December 2011, Dubna, Russia.

11) 2nd Conference of Applied Mathematics and Physics Jazz , March 2008, Saint-Petersburg, Russia.

8 Abbreviations

Abbreviations	
Notation	Definition
DC	Dirac-Coulomb
DCB	Dirac-Coulomb-Breit
DFB	Dirac-Fock-Breit
HF	Hartree-Fock
HFD	Hartree-Fock-Dirac
DF	Dirace-Fock
DFB	Dirace-Fock-Breit
DS	Dirace-Sturm
IS	Isotopic Shift
QED	Quantum Electrodynamics
MCDF	Multiconfigurational Dirac-Fock method
MCDFS	MultiConfigurational Dirac-Fock-Sturm method
MS	Mass Shift
MO	molecular orbitals
RHF	Restricted Hartree-Fock
PT	Perturbation theory
HFS	Hyperfine Splitting Structure
CI	Configuration interaction
DFR	Dirac-Fock-Roothaan orbitals
UDFR	Unrestricted Dirac-Fock-Roothaan
CSF	Configuration State Functions
RAS	Restricted Active Space
MOT	Magneto-Optical Trapping
ZS	Zeeman slowing
HCL	Cathode Discharge Lamp
EOM	Electro-Optical Modulator
LO	Local oscillator
DKB	Dual Kinetic Balance method
NRQED	Nonrelativistic Quantum Electrodynamics

9 Introduction

Over the past decades there has been made a significant development of computer technology and new theoretical methods. It resulted in the progress in study of the various physical properties of atoms and molecules. Comparison of theoretical data with high-precision experimental data gives a possibility not only to interpret the results of measurements, but also for testing a number of fundamental theories and the precise determination of fundamental constants.

The determination of fundamental constants like the mass of the electron and the fine structure constant with high accuracy in highly charged ions comprise an ultra sensitive tool for testing Quantum Electrodynamic (QED) effects in the strongest electric and magnetic fields. The first high-precision measurements of the ground-state hyperfine splitting were performed for various H-like ions, including ^{209}Bi, ^{165}Ho, ^{185}Re, ^{207}Pb, ^{203}Tl and ^{205}Tl in Ref. [58]. This experimental progress has motivated theoretical community for high-precision calculations.

There are several well-known theoretical methods for the evaluation of the g-factor and Hyper Fine Structure (HFS). The most widely used method is perturbation theory. Unfortunately, it might be applied only in high-Z ions with a small number of electrons. The reason is that this method does not provide accurate results for the inter-electronic interaction for low-Z ions. However, to reach the accuracy of theoretical prediction for Li-like ions comparable to the one for H-like ions, accurate evaluation of the QED, nuclear and inter-electronic interaction corrections is required. Moreover, in the case of heavy H-like ions, the leading uncertainty of the theoretical prediction for the g-factor is determined by the nuclear effects. In the high-Z region it is comparable to the binding QED correction of second order in α, and, therefore, it restricts probing the QED effects to first order in α. This theoretical uncertainty of the hyperfine splitting is dominated by the nuclear effects, especially by the Bohr-Weisskopf effect caused by the inhomogeneous nuclear magnetization

distribution [39]. Recent theoretical research has proved that when a specific difference between the HFS for H- and Li-like ions (or H- and B-like ions) of the same isotope is considered, the Bohr-Weisskopf effect can be largely cancelled, the same nucleus the uncertainty due to the nuclear effects can be significantly reduced and a higher accuracy for testing strong-field QED can be reached than with studies on the binding energy. Thus, an extension of the measurements to the three-electron ions is needed and anticipated.

Over the last decades, there has been a growing interest in the g-factor of a bound-electron, both theoretically (see e.g. [9–11]) and experimentally (see e.g. [3, 4, 12]). This interest is rising partly due to the development of experiments on highly charged ions utilizing ion traps. The study of these systems also provides the opportunity to determine fundamental constants such as the mass of the electron [2, 12]. Experimental investigations of ions with high charge-number Z are expected in the nearest future. Currently, high-precision experiments of the g-factor of Li-like Ca are being performed [12]. Furthermore, the precision theory of the g-factor of heavy B-like and H-like ions including higher-order QED and nuclear corrections is anticipated to yield, in combination with planned experiments, an independent determination of the fine-structure constant α [1].

In this thesis, we outline the different scientific background relevant to the Hartree Fock method, Breit interaction, g-factor and Hyperfine Structure Splitting (Section 10). Then, we then discuss the key computing method, the Dirac-Fock-Strum method, for calculation of the electronic structure of atoms (Section 11) and we show the way the fitting of the virtual orbitals to obtain the different configurations of ions is performed. In Section 12 we propose a novel single-particle effective potential that can be used in the Dirac–Fock (DF) method, the relativistic density functional, the multi-configuration DF method, and the relativistic method of superposition of configurations. Applying this potential in the atomic electronic

structure equations gives us a possibility to further improve the accuracy of the QED corrections calculations. In Section 13 we describe the experiment and ab initio calculations approach to the hyperfine structure of laser-cooling transitions in fermionic Erbium-167. These calculations allowed us to obtain the magnetic dipole and electric quadrupole constants for the only stable fermionic isotope, 167Er and thus explain the theory behind the experiment of the laser cooling transitions. In Section 14 we outline the implementation of the high accuracy MCDFS computational method for the weighted difference of the g-factors of H-and Li-like ions of the same element for am improved determination of the fine structure constant. We demonstrate the results for various Z from 6 to 60 for the fns corrections to the bound-electron g-factor of the ground state of Li-like and H-like ions and their weighted difference. We also observe that the leading term of the Za expansion of Eq. (14.21), $H^{(1,0)}$, should not depend on the nuclear charge radius R and on the speed of light c. All dependence of $H^{(1,0+)}$ on R and c comes only through the relativistic effects, which are small corrections in the low-Z region. Therefore, numerical calculations of $H^{(1,0+)}$ performed with different choices of R and c should have the same low-Z limit. We further show that this weighted difference and its combination for two different elements can be used to extract the fine-structure constant from near-future bound-electron g-factor experiments with an accuracy improvement by orders of magnitude as compared to its present literature value. In Section 15, we draw the final conclusions, outline the future prospects for the development and application of high accuracy calculations for the many-electron systems.

10 Background.

10.1 The restricted Hartree-Fock method for approximating the center of gravity of a configuration.

To obtain high-precision results for the electronic structure calculations, it is necessary to take into account various contributions of different nature. These contributions include quantum electrodynamic (QED) corrections, higher radiative corrections, and the contribution of the negative Dirac spectrum. Moreover, for some of the physical values, largely determined by the behaviour of the wave functions near the nucleus, the corrections caused by the distribution of the electric charge and magnetic moment over the nucleus should also be taken into account.

The main contribution of these corrections can be obtained by the implementation to the calculations of the one-electron approximation by the Hartree-Fock (HF) method or the relativistic Dirac-Fock (DF) method. However, in the HF or DF method, the interelectron interaction is only partially taken into account. Therefore, it is extremely important to accurately take into account the effects of correlation.

The non-relativistic Hartree-Fock method has been developed by various scientific groups, including [15–17] and others. The non-relativistic Hartree-Fock method developed and briefly described in this section is based on algorithms and earlier versions of programs created by V. F. Brattsev [15, 17, 19].

We consider the Hamiltonian of the N-electron system

$$\hat{H} = \sum_{i}^{N} \hat{h}_i + \frac{1}{2} \sum_{i \neq j} u_{ij} \,, \tag{10.1}$$

where $\hat{h}$ is the single-electron Hamiltonian and u_{ij} are the electron-electron operator interactions. Let the index α number all the Slater determinants of this configura-

tion. The expression for the total energy, obtained as the average Hamiltonian with the wave function $\det_\alpha$, has the same form as in the single-determinant Hartree-Fock (HF) method.

$$E_\alpha^{HF} \,=\, \langle \alpha \mid \hat{H} \mid \alpha \rangle \,=\, \sum_{i\in\alpha}^{N} \langle i \mid \widehat{h} \mid i \rangle \,+\, \sum_{i\neq j\in\alpha} \left[\langle ij|ij\rangle \,-\, \langle ij|ji\rangle \right]. \qquad (10.2)$$

where the index i numbers the occupied single-electron states ϕ_i, from which the Slater determinant $\det_\alpha$ is constructed. Hereafter, we use the following notation for two-electron integrals

$$\langle ij|kl\rangle \,=\, \int dx \int dx'\, \phi_i^*(x)\, \phi_j^*(x')\, u(x,x')\, \phi_k^*(x)\, \phi_l^*(x')\,, \qquad (10.3)$$

where x is the set of spatial and spin coordinates of the electron.

In the restricted Hartree-Fock method (RHF), single-electron functions are limited. It is required that they be transformed according to irreducible representations of the group G of symmetry of the Hamiltonian $\hat{H}$. Therefore, single-electron states can also be numbered with three indices n, γ, μ, where γ is the number of the irreducible representation, μ is the line number of the irreducible representation, and n is the main quantum number that numbers different states of the same symmetry. The set of states with fixed quantum numbers n and γ form a shell. The number of different states of one shell n_γ coincides with the dimension of the irreducible representation. Hereafter, we denote the various shells $(n\gamma)$ by the letters $a, b, c, d, ...$ The number of electrons in the shell a will be denoted by q_a. Let $N_a = n_\gamma$ be the number of different single-electron states of a given shell. If $q_a < N_a$, then the shell is open.

10.2 The non-relativistic Hartree-Fock method in the central field.

We consider the nonrelativistic Hamiltonian in the case of a central field.

$$\hat{h} = \hat{T} + V(r)\,, \qquad \hat{T} = \frac{p^2}{2m}\,, \qquad u_{ij} = \frac{e^2}{|\boldsymbol{r}_i - \boldsymbol{r}_j|} \tag{10.4}$$

Then the orbital quantum number l plays the role of the number of the irreducible representation of the group of three-dimensional rotations O_3. The atomic shell number a corresponds to a pair of indices $a \equiv (n_a, l_a)$, and the index μ contains two projections of the orbital and spin angular momenta $\mu \equiv (m_a, m_{s_a})$. The total number of single-electron states of this shell is $N_a = 2(2l_a + 1)$. Single electron orbitals in the restricted Hartree-Fock method (or in the central field approximation) have the form

$$\phi_{a,m_a,m_{s_a}}(\boldsymbol{r}, \sigma) = \frac{P_a(r)}{r} \cdot Y_{l_a m_a}(\boldsymbol{r}) \cdot \eta_{m_{s_a}}(\sigma)\,. \tag{10.5}$$

Here $P_a(r)$ is the single-electron radial wave function of the shell a.

10.3 Relativistic Hartree-Fock method.

The relativistic Hartree-Fock method in the central field approximation, which is also called the Dirac-Fock (DF) or Hartree-Fock-Dirac (HFD) method, was described and implemented by several authors and groups [18, 20–25]. In the restricted relativistic HFD method, single-electron states with quantum numbers nlj and μ ($\mu = -j, \ldots, j$), which are transformed according to irreducible representations of the rotation group, are the Dirac bispinor

$$\phi_{n\kappa\mu}(\boldsymbol{r},\tau) \;=\; \left(\begin{array}{c} \dfrac{P_{n\kappa}(r)}{r}\,\chi_{\kappa\mu}(\boldsymbol{r},\sigma) \\ i\,\dfrac{Q_{n\kappa}(r)}{r}\,\chi_{-\kappa\mu}(\boldsymbol{r},\sigma) \end{array} \right) , \tag{10.6}$$

where $\kappa = (-1)^{j+1/2-l}(j+1/2)$ is the relativistic quantum number, and the index $\tau = 1, 2, 3, 4$ numbers the components of the Dirac bispinor and $\chi_{\kappa\mu}$is the spherical Pauli spinor

$$\chi_{\kappa\mu}(\boldsymbol{r},\sigma) \;=\; \sum_{m}\sum_{m_s} C^{j\mu}_{lm,\frac{1}{2}m_s}\, Y_{lm}(\boldsymbol{r})\cdot\eta_{m_s}(\sigma)\,. \tag{10.7}$$

Dirac-Coulomb Hamiltonian

The relativistic Dirac-Coulomb Hamiltonian has the form

$$\hat{H} \;=\; \sum_{i}^{N} \hat{h}^{\mathrm{D}}_{i} \;+\; \frac{1}{2}\sum_{i\neq j} u_{ij}\,, \tag{10.8}$$

where $\hat{h}^{\mathrm{D}}$ is the single-electron Dirac operator

$$\hat{h}^{\mathrm{D}} \;=\; c\,(\boldsymbol{\alpha}\cdot\boldsymbol{p}) \;+\; (\beta \;-\; 1)\,c^2 \;+\; V(\boldsymbol{r})\,. \tag{10.9}$$

Here $\boldsymbol{\alpha}$, β are the Dirac matrices. The electron-electron interaction in the Dirac-Coulomb Hamiltonian has a simple form

$$u_{ij} \,=\, \frac{1}{r_{ij}}\,, \qquad \boldsymbol{r}_{ij} \,=\, \boldsymbol{r}_i - \boldsymbol{r}_j\,. \tag{10.10}$$

10.4 Breit interaction.

In our calculation we aim to include the relativistic effects with an accuracy of v^2/c^2. However, it is insufficient to pass from the many-electron Schrödinger Hamiltonian to the many-electron Hamiltonian Dirac-Coulomb. It is also necessary to take into account the Breit interaction.

In the Coulomb gauge, the electron-electron interaction in the Coulomb-Breit Hamiltonian , in addition to the Coulomb interaction $u_C(i,j)$ also includes the Breit interaction $u_B(i,j)$

$$u_{ij} \;=\; u_C(i,j) \;+\; u_B(i,j)\,, \tag{10.11}$$

where

$$u_C(i,j) \;=\; \frac{1}{r_{ij}}\,, \qquad \boldsymbol{r}_{ij} \;=\; \boldsymbol{r}_i - \boldsymbol{r}_j\,. \tag{10.12}$$

The Breit interaction can in turn be divided into two parts

$$u_B(i,j) \;=\; u_M(i,j) \;+\; u_R(i,j)\,, \tag{10.13}$$

where $u_M(i,j)$ is usually called the magnetic interaction or the Gaunt interaction

$$u_M(i,j) \;=\; -\frac{\boldsymbol{\alpha}_1\,\boldsymbol{\alpha}_2}{r_{ij}} \tag{10.14}$$

and the term $u_R(i,j)$ is a time delay,

$$\begin{aligned} u_R(i,j) \;&=\; -\frac{1}{2}(\boldsymbol{\alpha}_i\,\boldsymbol{\nabla}_i)\cdot(\boldsymbol{\alpha}_j\,\boldsymbol{\nabla}_j)r_{ij} \;=\; \frac{1}{2}\,\frac{([\boldsymbol{\alpha}_i\times\boldsymbol{r}_{ij}]\cdot[\boldsymbol{\alpha}_j\times\boldsymbol{r}_{ij}])}{r_{ij}^3} \\ &=\; -\frac{1}{2}\left[\frac{(\boldsymbol{\alpha}_i\,\boldsymbol{r}_{ij})\cdot(\boldsymbol{\alpha}_j\,\boldsymbol{r}_{ij})}{r_{ij}^3} - \frac{\boldsymbol{\alpha}_i\,\boldsymbol{\alpha}_j}{r_{ij}}\right]. \end{aligned} \tag{10.15}$$

10.5 G-factor and HFS

Though they have similar nature both and come from the interaction with a magnetic field, the g-factor comes as a result of an interaction of the particle with an external magnetic field, while HFS comes from the interaction with a magnetic dipole moment of a nucleus.

G-factor could be described as a dimensionless quantity that is used to describe the magnetic and angular momentum of a particle. To describe the HFS constant, let us imagine the simple example of the H-like ions, that consist of a proton and an orbiting electron. Both proton and electron have a spin that could be either up or down and thus the system can take different configurations, where spin is either ”up” or ”down”. We can derive that this system can has four possible spin states. All these fours possible states could be described as ground states. However there will be a slight energy difference between them. These shifts are much smaller than the energy difference between the ground state and next state that is above. As a result each of these different states have their energy levels split very closely.

The shift of the energy levels of an atom exposed to the external magnetic field is called the Zeeman effect. The external magnetic field couples with the magnetic momentum of the particles and causes the energy shift.

10.6 G-factor formulation

The total value of the g-factor of an ion can be written as

$$g = g_{\rm D} + \Delta g_{\rm int} + \Delta g_{\rm QED} + \Delta g_{\rm SQED} + \Delta g_{\rm NS} + \Delta g_{\rm rec} \tag{10.16}$$

- $g_{\rm D}$ – Dirac value
- $\Delta g_{\rm int}$ – interelectronic interaction
- $\Delta g_{\rm QED}$ – one-electron QED correction
- $\Delta g_{\rm SQED}$ – screened QED correction
- $\Delta g_{\rm NS}$ – contribution of the nuclear size
- $\Delta g_{\rm rec}$ – nuclear recoil (finite nuclear mass)

10.7 G-factor interelectronic-interaction correction

High-precision measurements of the g-factors of multiply charged ions provide an opportunity to study QED corrections and test quantum electrodynamics. However, for this it is necessary to have high-precision theoretical data, in which both relativistic and correlation effects were taken into account. The possibility of obtaining such data is provided by the DFS method developed by I. I. Tupitsyn. The multi-configuration DFS method could be used in systematic calculations of g-factors of Li-like ions [26–29] as well as for B-like ions [30].

Relativistic Hamiltonian in a magnetic field.

The atomic g-factor for a spinless nucleus is determined by the expression

$$g = \frac{1}{\mu_B J}\frac{\partial E(\mathcal{H})}{\partial \mathcal{H}}\bigg|_{\mathcal{H}=\prime} = \frac{1}{\mu_B J}\frac{\partial}{\partial \mathcal{H}}\langle \Psi \mid H \mid \Psi \rangle\bigg|_{\mathcal{H}=\prime}, \tag{10.17}$$

where H is the Hamiltonian of the atomic system in an external magnetic field $\boldsymbol{\mathcal{H}}$, $\mathcal{H} = |\boldsymbol{\mathcal{H}}|$ and the z axis is directed along the magnetic field $\boldsymbol{\mathcal{H}}$, $E(\mathcal{H})$ is the energy of the state with the maximum projection ($M_J = J$) of the angular momentum J and $\mu_B = |e|/(2mc)$ the Bohr magneton. In the first order of perturbation theory in the magnetic field $\mathcal{H}$, the energy shift is $\Delta E(\mathcal{H})$, and (10.17) has the form

$$g = \frac{1}{\mu_B J}\frac{\Delta E(\mathcal{H})}{\mathcal{H}}\,, \qquad \Delta E(\mathcal{H}) = \langle \Psi \mid \hat{\mathrm{H}}_m \mid \Psi \rangle\,, \tag{10.18}$$

where the operator of interaction of an electron with an external uniform magnetic field $\hat{\mathrm{H}}_m$ has the form

$$\hat{\mathrm{H}}_m \,=\, e\sum_i (\boldsymbol{\alpha}_i \cdot \boldsymbol{A}) \,=\, -\frac{e}{2}\sum_i (\boldsymbol{\mathcal{H}} \cdot [\boldsymbol{\alpha}_i \times \boldsymbol{r}_i]) \tag{10.19}$$

Here $\boldsymbol{A} = -[\boldsymbol{r} \times \boldsymbol{\mathcal{H}}]/2$ is the vector potential.

Thus, for the g factor, we obtain

$$g \,=\, \frac{mc}{J}\,\langle \Psi \mid \sum_i [\boldsymbol{\alpha}_i \times \boldsymbol{r}_i]_z \mid \Psi \rangle \tag{10.20}$$

The magnetic Hamiltonian can be written in another form [31–33]

$$\hat{\mathrm{H}}_m \,=\, [\hat{H}_{\mathrm{DC}}, \hat{P}] + \frac{e}{2mc}\,\beta\,\Big([\hat{\boldsymbol{S}} + \hat{\boldsymbol{J}}] \cdot \boldsymbol{\mathcal{H}}\Big) \tag{10.21}$$

where $\hat{H}_{\mathrm{DC}}$ is the Dirac-Coulomb Hamiltonian (10.8) (without the Breit interaction) and the operator $\hat{P}$ is defined by the expression

$$\hat{P} \,=\, \frac{e}{2mc}\,\beta(\boldsymbol{\alpha}\,\boldsymbol{A})\,. \tag{10.22}$$

Assuming that $\langle \Psi \mid \hat{H}, \hat{P}] \mid \Psi \rangle = 0$ for the exact wave function Ψ, the g-factor can

be calculated by the formula

$$g \;=\; \frac{1}{J}\,\langle\Psi \mid \beta\,(\hat{S}_z + \hat{J}_z) \mid \Psi\rangle \;-\; \frac{1}{\mu_b\, J\, \mathcal{H}}\langle\Psi[U_B, \hat{P}] \mid \Psi\rangle \tag{10.23}$$

Here U_B is the Breit electron-electron interaction operator. Expression (10.23) was used in [33] calculating the g-factors of ions by the method of coupled clusters.

In the nonrelativistic limit, it is easy to obtain the well-known expression for the g-factor [34]

$$g^{\rm nr} \;=\; 1 \;+\; \frac{J(J+1) \;-\; L(L+1) \;+\; S(S+1)}{2J(J+1)}\,. \tag{10.24}$$

For atoms with one s-electron outside the closed shells, $g^{\rm nr} = 2$.

10.8 Hyperfine Structure Splitting

In relativistic theory the interaction of the electron with the nucleus is described by the relativistic operator of the hyperfine magnetic dipole interaction has the form:

$$\hat{h}^{(m)}_{\rm hfs} \,=\, \frac{e}{r^3}\,(\boldsymbol{\alpha},\,[\boldsymbol{\mu}\times\boldsymbol{r}]) \,=\, \frac{e}{r^3}\,(\boldsymbol{\mu},\,[\boldsymbol{r}\times\boldsymbol{\alpha}]) \,=\, (\boldsymbol{\mu},\,\boldsymbol{T}), \qquad \boldsymbol{T} \,=\, \frac{e}{r^3}\,[\mathbf{r}\times\boldsymbol{\alpha}]\,, \tag{10.25}$$

where $\boldsymbol{\mu}$ is the magnetic dipole moment of the nucleus, and $\boldsymbol{\alpha}$ are the Dirac matrices, that are the components of the. The correction to the atomic energy due to the magnetic HFS has the form [36]:

$$W(FIJ) \,=\, \langle FIJ \mid \widehat{h}^{(m)}_{\rm hfs} \mid FJI\rangle \,=\, \frac{1}{2}\,C(FJI)\cdot A(J)\,, \tag{10.26}$$

where J is the total moment of the electron system, I is the spin of the nucleus and F is the total moment, $C(FJI) \,=\, F(F+1) - J(J+1) - I(I+1)$ and $A(j)$ is the magnetic HFS constant, defined by the expression

$$A(J) = \frac{\mu}{I}\,\frac{1}{M}\,\langle JM \mid \hat{\boldsymbol{T}}_0 \mid JM\rangle \,=\, \frac{\mu}{\mu_N}\,\frac{\mu_N}{I}\,\frac{\langle J \parallel \hat{T} \parallel J\rangle}{\sqrt{J(J+1)(2J+1)}} \tag{10.27}$$

where I is the nuclear spin, and μ_N is the nuclear magneton:

$$\mu_N \,=\, \frac{m}{M_p}\,\mu_B, \qquad \mu_B = \frac{e\hbar}{2mc} \tag{10.28}$$

Here μ_B is the Bohr magneton, and M_p is the proton mass. If we measure the magnetic moment μ in nuclear magnetons, then:

$$\begin{aligned} A(J) &= 1.987131207 \cdot 10^{-6} \quad \frac{1}{I}\,\frac{\mu}{\mu_N}\,\frac{\langle J \parallel \hat{\boldsymbol{T}} \parallel J\rangle}{\sqrt{J(J+1)(2J+1)}}\ \text{(a.u.)} \\ &= 1.307469525 \cdot 10^{4} \quad \frac{1}{I}\,\frac{\mu}{\mu_N}\,\frac{\langle J \parallel \hat{\boldsymbol{T}} \parallel J\rangle}{\sqrt{J(J+1)(2J+1)}}\ \text{(MHz)}. \end{aligned} \tag{10.29}$$

The reduced matrix element $\langle J \parallel \hat{\boldsymbol{T}} \parallel J\rangle$ can be calculated using wave functions calculated by the DFS method for a fixed value of the projection of the angular momentum $\overline{M}$. For this we use the Eckart-Wigner theorem [35]

$$\langle J \parallel \hat{\boldsymbol{T}} \parallel J\rangle = \frac{\sqrt{2J+1}}{C^{J\overline{M}}_{J\overline{M},10}}\,\langle J\overline{M} \mid \hat{\boldsymbol{T}} \mid J\overline{M}\rangle\,, \qquad C^{J\overline{M}}_{J\overline{M},10} = \frac{\overline{M}}{\sqrt{J(J+1)}} \tag{10.30}$$

The matrix element $\langle J\overline{M} \mid \hat{\boldsymbol{T}} \mid J\overline{M}\rangle$ can be calculated if the single-particle density matrix D_{ij} is known as:

$$\langle J\overline{M} \mid \hat{\boldsymbol{T}} \mid J\overline{M}\rangle = \sum_{i,j} D_{a\mu_a,b\mu_b}(J\overline{M})\,\langle a\mu_a \mid \hat{T}_0 \mid b\mu_b\rangle\,, \tag{10.31}$$

where $\langle a\mu_a \mid \hat{T}_0 \mid b\mu_b\rangle$ is the single-electron matrix elements of the operator $\hat{T}_0$ (10.25). Single-electron matrix elements can be calculated by the formula:

$$\langle a\mu_a \mid \widehat{T}_\nu \mid b\mu_b\rangle = (\kappa_a+\kappa_b)\,g^1(j_a\mu_a;\, j_b\mu_b)\int\limits_0^\infty dr\,\frac{F(r)}{r^2}\,(P_aQ_b+P_bQ_a), \tag{10.32}$$

where $(\kappa_a + \kappa_b)$ is an even number and $\nu = \mu_a - \mu_b$ and $g^1(j_a\mu_a;\, j_b\mu_b)$ are the relativistic Gaunt coefficients. The function $F(r)$, which is included in the expression for the radial integral, ensures that the Bohr-Weisskopf correction is taken into account.

The total value of the HFS of a many-electron ion can be written as

$$\Delta E^{(a)}_{\rm HFS} = E_{\rm F}\Bigg[A(\alpha Z)(1-\delta)(1-\varepsilon)+ \\ + \frac{1}{Z}B(\alpha Z) + \frac{1}{Z^2}C(Z,\alpha Z) + x_{\rm QED} + x_{\rm SQED}\Bigg] \tag{10.33}$$

- $E_{\rm F}$ – Fermi energy
- $A(\alpha Z)$ – one-electron relativistic factor
- δ – correction for distribution of the nuclear charge
- ε – correction for distribution of magnetic moment over the nucleus (Bohr-Weisskopf correction)
- $B(\alpha Z)$, $C(Z,\alpha Z)$ – interelectronic interaction corrections
- $x_{\rm QED}$ – one-electron QED correction
- $x_{\rm SQED}$ – screening QED correction

References

[1] V.F.Bratzev, Atomic wave functions tables, Science, L., 1966, 157 p.

[2] V.F.Bratzev, Atomic wave functions tables, Science, L., 1971, 456 p.

[3] V.I. Baranovsky, V.F. Bratzev, A.I. Panin, V.M. Tretiyak, Calculation methods of electronic structure of atoms and molecules, LGU, 1976, 204 p.

[4] V.F. Bratzev, G.B. Daineka, I.I. Tupitsyn, Izv AN USSR, Physics, 2655 p (1977).

[5] Sharlotte Frose Fisher, The Hartree-Fock Method for atoms, John Willet & Sons, NY, (1977).

[6] I.P.Grant, Relativistic effects in Atoms, Molecules and Solids, v.87 of Advanced Study Institute Series, Ed. G.L.Malli, Plenum Press, New-York (1983).

[7] M.A. Coulthard, J.Phys.B., v.7, p.440 (1974).

[8] J.P.Desclaux, J.Phys.B., v.4, p.631 (1971).

[9] J.B.Mann and W.R.Johnson, Breit interaction in Multielectron Atoms., Phys.Rev.A, v.4, N.1, p.41-51, (1971).

[10] I.M. Band and V.I. Fomichev, Computer Program Complex RAINE V: Description of Code for Calculations of Atomic Field Using the Self-Consistent Dirac-Fock Method, Leningrad Nuclear Physics Institute Report LNPI-498 (1979)

[11] L.V.Chernysheva, V.L.Yakhontov, Computer Physics Communications, v.119, p.232 (1999).

[12] V.M.Shabaev, D.A.Glazov, M.B.Shabaeva, I.I.Tupitsyn, V.A.Yerokhin, T.Beier, G.Plunien, G.Soff, Nuclear Instruments and Methods in Physics Research B, v.205, pp. 20-24 (2003).

[13] D.A.Glazov, V.M. Shabaev, I.I.Tupitsyn, A.V.Volotka, V.A.Yerokhin, G.Plunien, and G.Soff, Phya.Rev.A, v.70, pp.062104(1-9) (2004).

[14] D.A. Glazov, V.M. Shabaev, I.I. Tupitsyn, A.V. Volotka, V.A. Yerokhin, P. Indelicato, G. Plunien and G. Soff, Nuclear Instruments and Methods in Physics Research B, v. 235, pp. 55-60, (2005)

[15] D.A. Glazov, A.V. Volotka, V.M. Shabaev, I.I. Tupitsyn, G. Plunien, Physics Letters A, v.357, p.330-333, (2006)

[16] R.Soria Orts, J.R. Crespo Lopez-Urrutia, H.Bruhns, A.J. Gonzalez Martinez, Z.Harman, U.D.Jentschura, C.H.Keitel, A.Lapierre, H.Tawara, I.I.Tupitsyn, J.Ullrich and A.V.Volotka Phys.Rev.A., v76, p.052501(1-7) (2007).

[17] P.G.H. Sandars, J.Phys.B.,**1**, 511 (1968).

[18] E.Lindroth, B.W.Lynn and P.G.H. Sandars, J.Phys.B.,**22**, 559 (1989).

[19] E.Lindroth and A.Ynnerman, Phys.Rev.A, v.47, p.961 (1993).

[20] I.I.Sobelman, Atomic Spectra, and Radiative Transitions, Berlin, Springer (1979).

[21] D.A. Varshalovich, A.N. Moskalev, V.K. Hersonsky, Quantum theory of angular momentum, Science, L., 439 p (1975).

[22] McWeeny R., Methods in Computational Molecular Physics. ed. Wilson S., Diercksen G. H. F., Plenum Press, New York, Ser.B, 325p (1992).

[23] B.H.Brandow, Int.J.Quant.Chem, **15**, p.207 (1979).

[24] M.Svreĕcek, Int.J.Quant.Chem, **31**, p.625 (1987).

[25] V.M.Shabaev, Physics Reports v.356, p.119-228 (2002).

[26] A.N. Artemyev, V.M. Shabaev, I.I. Tupitsyn, G.Plunien, and V. A. Yerokhin, Phys.Rev.Lett., v.98, p.173004-(1-4) (2007).

[27] E.Dalgaard, P.Jørgensen, J.Chem.Phys. **69**, p.3833 (1978).

[28] Ron Shepard, The Multiconfigurational Self- Consistent Field Method, Advances in Chemical Physics, LXIX, Ab Initio Methods in Quantum Chemistry - II, Ed. by K.P.Lawley, pp.63-200, (1987).

[29] Jeppe Olson, The method of Second Quantization, in "Lecture Notes in Chemistry", pp.38-88, ed. B.O.Roos, Springer-Verlag, (1992).

[30] Björn O.Roos, The Multi-configurational (MC) Self- Consistent Field (SCF) Theory, in "Lecture Notes in Chemistry", pp.177-254, ed. B.O.Roos, Springer-Verlag, (1992).

[31] B.Levy and G.Berthier, Int.J.Quant.Chem., v.2, p.307 (1968).

[32] Rotenberg M., Adv. Atom. and Molec. Phys., v. 6, p. 233 (1970).

[33] P.P.Pavinsky, A.I. Sherstyuk, Problems of theoretical physics, L., t. 1, 66-107 p, (1974).

[34] A.I. Sherstyuk, TMF, v.21, 224–231 (1974).

[35] P.F. Gruzdev, A.I. Sherstyuk, Izv USSR, physics, v 41, 2477 p, (1977)

[36] P.F. Gruzdev, A.I. Sherstyuk, G.S. Solovieva, Optics and Spectroscopy, 1198 p (1977)

[37] C.C.J.Roothaan and P.Bagus, Methods in Computational Physics, **2**, Academic Press, N.Y. (1963).

[38] E. Trabert, P. Beiersdorfer, S. B. Utter, G. V. Brown, H. Chen, C. L. Harris, P. A. Neill, D. W. Savin and A. J. Smith, Astrophys.J., v.541, p.506, (2000).

11 Dirac-Fock-Sturm method for the calculation of the electronic structure of atoms.

11.1 Outline of the method.

Our calculations were based on the large-scale configuration-interaction Dirac-Fock-Sturm method that was developed by I. I. Tupitsyn.

First, let us introduce the general scheme of the relativistic calculation of the electronic structure of atoms (or ions) by the Dirac-Fock-Sturm (DFS) method, that can also be reprdofuced in a non-relativistic fashion.

1. First, the single-electron wave functions are calculated by the Dirac-Fock (DF), or Multiconfiguration Dirac-Fock (MCDF), method.
2. Then, for each value of the relativistic quantum number κ, the Dirac-Sturm (DS) equations are derived. The set of DF or MCDF orbitals previously obtained for occupied or partially-occupied states is supplemented by virtual DS orbitals. This set of functions forms the single-electron basis, which is necessary in order to carry out further calculations using the configuration interaction (CI) method.
3. To take into account the contribution of the negative Dirac spectrum to the average values of physical quantities and to the transition amplitudes, the basis is supplemented by the DS orbitals, which are the solutions of the DS equations corresponding to the negative Dirac spectrum. This leads to a doubling of the single-electron basis. The basis obtained in this way satisfies the kinetic balance condition.
4. In order to construct an orthonormal set of single-electron functions and to enable the subsequent use of perturbation theory (PT), a transition from the DS basis to Dirac-Fock-Roothaan orbitals (DFR) takes place. DFR orbitals

are obtained by solving the equations of the restricted Dirac-Fock-Roothaan (RDFR) method.

5. If the calculation of the physical quantity described by the Hermitian operator $\hat{A}$ is carried out using the Hellman-Feynman theorem, then the operator $\hat{A}$, with some multiplier, is included in the Hamiltonian. Thus, the task is reduced to the calculation for an atom in an external field, which can lead to a violation of the symmetry of the central field. In this case, the orthonormal single-electron basis is constructed using the unrestricted Dirac-Fock-Roothaan (UDFR) method.

6. In the next step, using the concept of restricted active space (RAS), a set of non-relativistic configurations is constructed that are taken into account in the CI and PT methods. A list of all relativistic configurations is produced, which corresponds to the set of non-relativistic configurations obtained by the RAS method. Then, for a fixed value M of the projection of the total angular momentum, a complete set of the Slater determinants is generated that corresponds to the list of relativistic configurations. The resulting set of Slater determinants forms the multi-electron basis used in the CI and PT methods.

7. In the case of central field symmetry preservation, for each relativistic configuration, linear combinations of the Slater determinants are found, which are in turn eigenfunctions of the square of the angular momentum $\hat{J}^2$. These linear combinations are commonly called "Configuration State Functions" (CSF). The transition from the Slater determinants to CSF reduces the size of the multi-electron basis.

11.2 Dirac-Fock-Sturm orbitals

To implement the configuration interaction (CI) methods and the many-particle perturbation theory (PT), it is necessary to first build a basis of single-electron functions. The natural choice for such functions is the populated orbitals of the DF or MCDF method. The set of these functions must then be supplemented with additional vacant (virtual) orbitals.

In Breit approximation, the multi-electron system can be described by the Hamiltonian

$$H = \sum_i h_D(i) + \sum_{i,j} V(i,j), \tag{11.1}$$

where h_D is a one-electron Dirac Hamiltonian

$$h_D = c(\alpha \cdot \rho) + (\beta - 1)c^2 + V(r) \tag{11.2}$$

and $V(i,j)$ is a two-electron interaction Coulomb-Breit operator

$$V(i,j)\alpha\left[\frac{1}{r_{ij}} - \frac{\alpha_i \cdot \alpha_j}{r_{ij}} - \frac{(\alpha_i \cdot r_{ij})(\alpha_j \cdot r_{ij})}{2r_{ij}^3}\right] \tag{11.3}$$

Then the Dirac bispinor for one-electron basis can be represented as:

$$\phi_{n\kappa m}(\boldsymbol{r},\sigma) = \begin{pmatrix} \dfrac{P_{n\kappa}(r)}{r}\,\chi_{\kappa m}(\Omega,\sigma) \\ i\,\dfrac{Q_{n\kappa}(r)}{r}\,\chi_{-\kappa m}(\Omega,\sigma) \end{pmatrix} \tag{11.4}$$

The one-electron functions for the occupied state $|a\rangle = |n\kappa m\rangle$ can be calculated

from the Dirac equation:

$$\begin{cases} c\left(-\dfrac{d}{dr}+\dfrac{\kappa_a}{r}\right)Q_a(r)+\Big(V(r)+c^2\Big)P_a(r)=\varepsilon_a P_a(r) \\ c\left(\dfrac{d}{dr}+\dfrac{\kappa_a}{r}\right)P_a(r)+\Big(V(r)-c^2\Big)Q_a(r)=\varepsilon_a Q_a(r), \end{cases} \tag{11.5}$$

In the other word, virtual orbitals can, for example, be obtained as the eigenfunctions of an operator $\hat{h}^{\rm DF}$:

$$\hat{h}^{\rm DF} \,=\, c\boldsymbol{\alpha}\cdot\boldsymbol{p} \,+\, (\beta-1)c^2+\hat{V}^{\rm DF}(r)\,, \tag{11.6}$$

where $\hat{V}^{\rm DF}(r)$ is the non-local Dirac-Fock potential. However, the spectrum of the DF operator includes a continuous spectrum, the contribution of which to the correlation energy can be 60%-70%. In addition, the average radius of the excited bound states grows rapidly with the increasing principal quantum number n, and therefore these orbitals are poorly adapted to take into account the correlation effects of the ground and low-excited states of atoms and ions. One of the ways to eliminate the states of the continuous spectrum is to 'place' the atom (or ion) in a spherically symmetric "box" with infinitely high walls of radius $R_{\mathbf{box}}$. However, the dimensions of the "box" should be large enough so as not to distort busy or partially occupied states. For neutral atoms, the radius $R_{\mathbf{box}}$ should be about 20-30 a.u. In this case, to obtain high-precision data, it is necessary to include on the order of 30-40 radial basis functions for each value of the relativistic quantum number κ, leading to a very large (over 2000) number of single-electron functions. Such a large single-electron basis cannot reasonably be used in calculations by the CI method taking into account 3-fold and 4-fold excitations. Here, the Sturm orbital basis is used to give the virtual states. This basis is devoid of the above disadvantages. The full procedure for constructing non-relativistic Sturm orbitals is described in [46–48, 48],and one of its first implementations in the framework of the non-relativistic HF method is

contained in [50].

As a brief description of the method, one first considers the relativistic or non-relativistic Fock operator $\hat{h}^{\rm F}$ and the generalized eigenvalue problem for the Sturm operator $\hat{h}^{\rm S}$:

$$\hat{h}^{\rm S}\varphi_j \,=\, \lambda_j\, W(r)\,\varphi_j\,, \qquad \hat{h}^{\rm S} = \hat{h}^{\rm F} - \varepsilon_0\,. \tag{11.7}$$

- ε_0 is usually an one-electron energy of one of the valence states.
- φ_j are Sturm functions.

When the parameter $\varepsilon_0 < 0$, the single-electron energy of the HF or DF of one of the valence states of the atom is usually selected. The weight function $W(r)$ is positive, and $W(r) \to 0$ as $r \to \infty$. It is trivially verifiable that all the Sturm functions $\varphi_j(r)$ have the same exponential asymptotics at infinity:

$$\varphi_j(r) \to A_j\, e^{-\sqrt{-2\,\varepsilon_0}r}, \qquad \text{as} \quad r \to \infty$$

Therefore the Sturm operator has a purely discrete spectrum. The Sturm functions form an orthonormal system with weight $W(r)$

$$\langle \varphi_i \mid W \mid \varphi_j \rangle \,=\, \delta_{i,j} \tag{11.8}$$

The set of functions $\{\varphi_j\}$ forms a complete set, at least in the non-relativistic case. The spectrum of the Sturm operator depends on the choice of ε_0 and the weight function $W(r)$. If ε_0 is chosen from one of the eigenvalues of the Fock operator, then the corresponding Hartree-Fock orbital φ_0 will be an eigenfunction of the Sturm operator for $\lambda_j = 0$.This orbital will be referred to as a reference. Here, the set of Sturm functions was constructed separately for each symmetry, i.e. for each value of the quantum number l. The typical choice for the weight function is $W(r) = 1/r$,

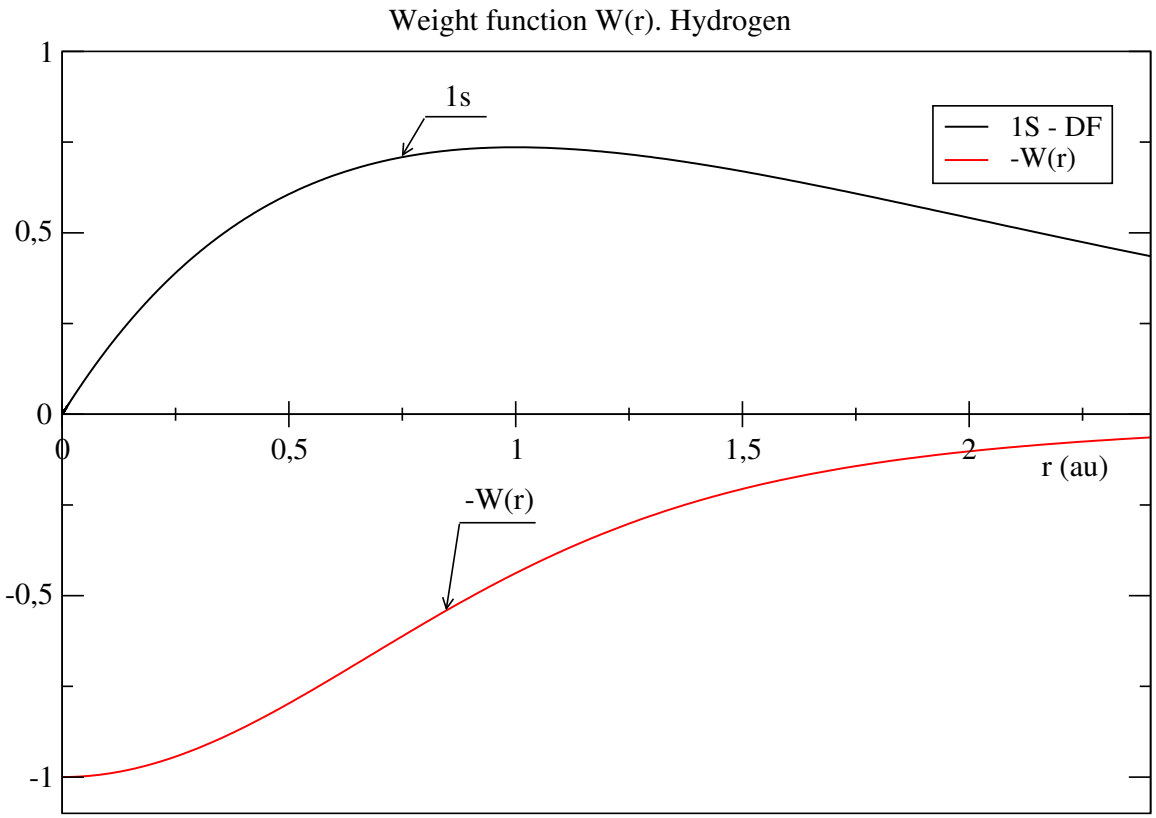

Figure 1: Weight function W (r). Reference orbital - 1s of the H atom.

which leads to the problem of quantisation of charge $Z^* = Z - \lambda_j$. However, such a choice of $W(r)$ is inconvenient in relativistic calculations, since it changes the behaviour of the functions $\varphi_j(r)$ near 0.

$$\varphi_j(r) \to A\, r^{\gamma_j^*} \qquad \gamma_j^* = \sqrt{\kappa_j^2 - \left(\frac{Z^*}{c}\right)^2} \tag{11.9}$$

If the weight function $W(r)$ tends to a constant value as $r \to 0$, then the asymptotic behaviour of the Sturm functions near zero coincides with the asymptotic behavior of the DF orbitals, since in this case $Z^* = Z$. Here, the weight function was defined in the form:

$$W(r) = \left[\frac{1 - \exp(-(\alpha r)^2)}{(\alpha r)^2}\right]^n . \tag{11.10}$$

Usually, in the calculations herein, $n = 2, 3$ were chosen and the parameter α defined so as to achieve rapid convergence of the Sturmian expansions. Fig.1, shows as an example the graph of the weight function $W(r)$ and the reference 1s wave function of the hydrogen atom. Fig.2 shows the Sturm functions derived from the 1s orbital and the weight fucntion $W(r)$. The Sturm orbitals for $\lambda_j < 0$, are localised in the region where the weight function $W(r)$ is close to constant. They approximately coincide with the occupied HF or DF states. Such orbitals are hence excluded from consideration and, in their place, the HF or DF orbitals are included in the basis. The relativistic Sturm operator, like the DF operator, has a negative Dirac spectrum, which corresponds to a value of λ of the order $-2c^2$. However, unlike the DF operator, the negative spectrum of the Sturm operator is discrete, and the corresponding orbitals decay exponentially with increasing r. Thus, in the nonrelativistic case, the single-electron basis (of dimension M) was constructed as follows. The basic functions of the occupied states φ_j ($j = 1, \ldots, M_0$) were chosen as numerical solutions of the HF equations. As virtual states φ_j ($j = M_0 + 1, \ldots, M$) the eigenfunctions of the Sturm operator for $\lambda_j > 0$ were used. In the relativistic case, the basis doubles due to the addition of the M Sturm orbitals corresponding to the negative Dirac spectrum. In what follows, the combined relativistic basis of the DF orbitals and the Sturm functions will be called the Dirac-Sturm (DS) basis.

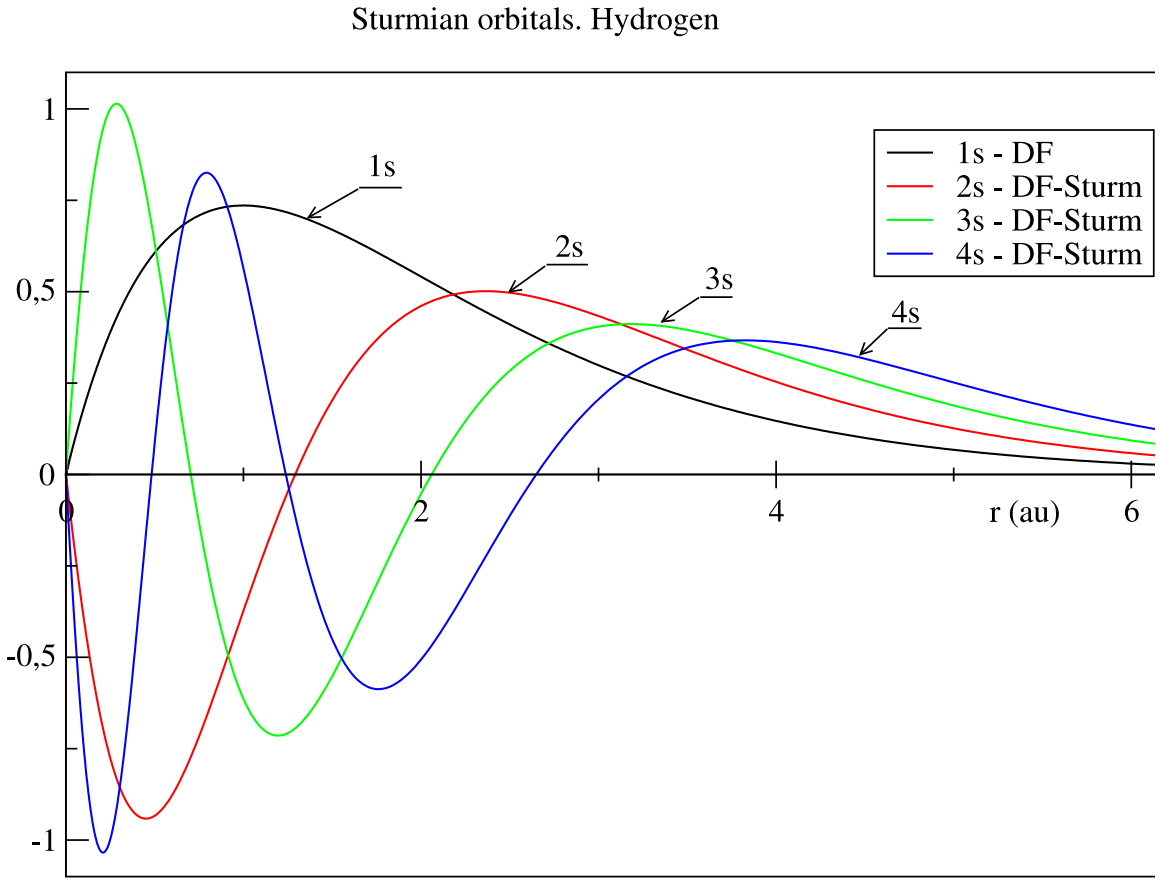

Figure 2: Sturm s-functions of the H atom.

11.3 Building a basis for the Slater determinants using the concept of limited active space.

Herein, the set of all Slater determinants which is included in the expansion of the multiconfiguration wave function, is obtained by generating all determinants from a given list of non-relativistic atomic configurations. The list of all non-relativistic configurations is constructed by considering single, double, triple, and quadruple excitations from one or more reference configurations. Reference configurations include those whose atomic terms and wave functions are to be determined. When generating a list of configurations herein, we used the concept of Restricted Active Space (RAS), introduced by B.O. Roos (see, for example, [4]). According to this model, the entire space of single-electron radial wave functions is divided into four subspaces RAS0, RAS1, RAS2 and RAS3:

1. RAS0 - inactive occupied cores (frozen core). This space includes orbitals from which excitations are excluded from consideration.
2. RAS1 - occupied cores (closed shells). This space includes orbitals for which the number of excitations is limited in RAS2 and RAS3 by a given number of holes N_h
3. RAS2 - active inhabited (valence orbitals). This space includes the valence orbitals (unfilled shells) and vacant shells whose energies are close to the energies of the valence shells in the DFS method; these include the DF orbitals obtained by the single-configuration rational or multiconfiguration DF methods. The number of excitations from RAS2 to RAS2 and RAS3 is limited by the number of electrons N_2.
4. RAS3 - vacant inhabited (unfilled, highly-excited orbitals). In the DFS method, the DS orbitals belong to this space. The number of excitations from RAS1 and RAS2 to the vacant shells of RAS3 is limited by the number of electrons

N_3.

The method described above generates a list of all non-relativistic configurations that are included in the calculation using the CI or PT method. In the next stage, a list of all relativistic configurations corresponding to a given set of non-relativistic configurations of the atom is constructed. Then, Slater determinants $\det_\alpha\{\phi_i(x_j)\}$, corresponding to a given set of relativistic configurations is generated. The indices α and β will number the various Slater determinants. The Slater determinants $\det_\alpha\{\phi_i(x_j)\}$ are constructed from single-electron functions, which in the central field approximation are determined by expression (10.5) or (10.6). Moreover, only those determinants that have a given projection value M of the total angular momentum J are included in the multi-electron basis. Herein, we have created algorithms and programs that implement the above described procedure for generating Slater determinants and which are an integral part of the program complex of the DFS method. Usually, in relativistic and non-relativistic calculations of atoms and ions, we restrict ourselves to double excitations of core shells from RAS1 ($N_h \leq 2$), quadruple excitations of active (valence) shells ($N_2 \leq 4$) and double and triple excitations to the space of vacant shells ($N_3 \leq 3$). Thus, the list of determinants for a given value of the projection M can be on the order of $10^6 - 10^8$.

11.4 Excluding frozen core occupiers from RAS0.

The complexity of the calculation by the DFS method can be significantly reduced if we exclude from the calculation the frozen core orbitals assigned to the RAS0 space. The full wave function in the DFS method is sought in the form of an expansion of the basis of the Slater determinants:

$$\Psi(x_1, x_2, ..., x_N) = \sum_\alpha C_\alpha \det_\alpha\{\phi_i(x_j)\}\,. \tag{11.11}$$

We divide the number of electrons N into the number N_c of frozen core electrons assigned to the RAS0 space plus the number N_v of remaining electrons, which we shall conditionally call valence, $N = N_c + N_v$. Similarly, all single-electron orbitals $\{\phi_i(x_j)\}$ are divided into core $\{\phi_i^c(x_j)\}$ and valence $\{\phi_i^v(x_j)\}$ orbitals. Since no excitations from the RAS0 space are considered, the core N_c electrons are represented in the same way in each of the Slater determinants, which can be represented as:

$$\det_\alpha\{\phi_i(x_j)\} \;=\; \sqrt{\frac{N!}{N_c!N_v!}}\,\hat{A}\;\det{}^c\{\phi_i^c(x_j)\}\,\det{}^v_\alpha\{\phi_i^v(x_j)\}\,, \tag{11.12}$$

where $\hat{A}$ is an antisymmetrisation operator:

$$\hat{A} \;=\; \frac{1}{N!}\sum_P (-1)^{\varepsilon_P}\;\cdot\hat{P}. \tag{11.13}$$

and ε_P is the parity of the permutation P. A determinant that is composed only of spanning orbitals, $\det_c\{\phi_i^c(x_j)\}$ is independent of the index α. Therefore, the full wave function can be represented as:

$$\Psi(x_1,x_2,...,x_N) = \sqrt{\frac{N!}{N_c!N_v!}}\,\hat{A}\,\Psi^c(x_1,x_2,...,x_{N_c})\cdot\Psi^v(x_{N_c+1},...,x_N)\,, \tag{11.14}$$

where $\Psi^c(x_1,x_2,...,x_{N_c})$ is the core Slater determinant, and $\Psi^v(x_{N_c+1},...,x_N)$ is a linear combination of Slater determinants composed only of the valence orbitals $\det^v_\alpha$:

$$\Psi^v(x_{N_c+1},x_{N_c+2},...,x_N) = \sum_\alpha C_\alpha\,\det{}^v_\alpha\{\phi_i(x_j^v)\}\,. \tag{11.15}$$

Thus, the system of electrons and single-electron functions is divided into two groups: core and valence. Using the group function method [36], for the total

energy of the system $E_{\rm tot}$, we obtain:

$$E_{\rm tot} \,=\, \langle \Psi \mid \hat{H} \mid \Psi \rangle \,=\, E_{\rm core} \,+\, \langle \Psi^v \mid \hat{H}^v \mid \Psi^v \rangle \,, \tag{11.16}$$

where the total energy of the core $E_{\rm core}$ is determined by the expression:

$$E_{\rm core} \,=\, \langle \Psi^c \mid \hat{H}^c \mid \Psi^c \rangle \,, \qquad \hat{H}^c = \sum_{i=1}^{N_c} \hat{h}_i + \frac{1}{2} \sum_{i \neq j=1}^{N_c} u_{ij} \tag{11.17}$$

and the effective Hamiltonian $\hat{H}^v$ of the valence electrons has the form:

$$\hat{H}^v = \sum_{i=N_c+1}^{N_v} \left(\hat{h}_i + \hat{V}_i^{\rm core} \right) + \frac{1}{2} \sum_{i \neq j=N_c+1}^{N_v} u_{ij} \,. \tag{11.18}$$

The single-particle core potential $\hat{V}^{\rm core}$ in expression (11.18) contains the Coulomb potential $\hat{V}^{\rm core}_{\rm coul}$ and the exchange potential $\hat{V}^{\rm core}_{\rm ex}$ such that $\hat{V}^{\rm core} = \hat{V}^{\rm core}_{\rm coul} - \hat{V}^{\rm core}_{\rm ex}$, can be defined by the expressions:

$$\begin{aligned} \hat{V}^{\rm core}_{\rm coul}\, \phi(x) \;&=\; \int dx' \, \rho_{\rm core}(x') \, u(x, x^{\prime)} \, \phi(x) \\ \hat{V}^{\rm core}_{\rm ex}\, \phi(x) \;&=\; \int dx' \, \rho_{\rm core}(x, x') \, u(x, x^{\prime)} \, \phi(x') \,, \end{aligned} \tag{11.19}$$

where the single-particle density $\rho_{\rm core}(x')$ and the single-particle density matrix $\rho_{\rm core}(x, x')$ of core electrons have the form:

$$\rho_{\rm core}(x) \,=\, \sum_{i=1}^{N_c} |\phi_i^c(x)|^2 \,, \qquad \rho_{\rm core}(x, x') \,=\, \sum_{i=1}^{N_c} \phi_i^c(x)^* \, \phi_i^c(x') \,. \tag{11.20}$$

Thus, the problem of calculating the total wave function Ψ (11.11), which depends on N variables, reduces to determining the valence wave function Ψ^v (11.15), which depends only on the coordinates of valence electrons, the number of which N_v can

be markedly smaller than N. Thus, the dimension of the problem, especially for heavy atoms, is significantly reduced. The interaction with the frozen core is taken into account by introducing into the Hamiltonian of valence electrons the single-particle core potential $\hat{V}^{\rm core}$, of which the calculation of the matrix elements is not difficult.

11.5 Construction of the eigenfunctions of the operator J^2.

For the many-electron basis the many-electron wave function $\Psi(\gamma J M_J)$ with a total angular momentum and projection J and M_J and other quantum numbers γ is expanded in a terms of a large number of configuration state functions with the same J and M_J can be represented as:

$$\Psi(\gamma J M_J) = \sum_\alpha \Phi_\alpha(J M_J). \tag{11.21}$$

For each relativistic atomic configuration $\Phi_\alpha(JM_J)$ are eigenfunctions of J^2, J_z and can be obtained as linear combination of the Slater determinants

$$\Phi(\boldsymbol{x}) = \frac{1}{\sqrt{N!}}\,\det\{\psi_i(x_j)\} = \frac{1}{\sqrt{N!}}\begin{vmatrix} \phi_1(x_1) & \phi_2(x_1) & \dots & \phi_N(x_1) \\ \phi_1(x_2) & \phi_2(x_2) & \dots & \phi_N(x_2) \\ \dots & \dots & \dots & \dots \\ \phi_1(x_N) & \phi_2(x_N) & \dots & \phi_N(x_N) \end{vmatrix} \tag{11.22}$$

So, in the case when the central field symmetry is preserved, we pass from the basis of the Slater determinants to the basis of the so-called Configuration State Functions (CSF), which are eigenfunctions of the operator J^2. The CSFs $\Phi_I(JM)$ are constructed separately for each relativistic configuration and are linear combinations of the Slater determinants $\det{}^{\rm M}_\alpha\{\phi_{\rm i}({\rm x_j})\}$ with a given value of the projection of the

angular momentum M:

$$\Phi_I(JM) = \sum_{\alpha \in Q} A^I_\alpha(JM)\, \mathrm{det}^{\mathrm{M}}_\alpha\{\phi_{\mathrm{i}}(\mathrm{x_j})\}\,. \tag{11.23}$$

Here, the index Q numbers the relativistic configurations, and the index I numbers the specific CSF. The unknown coefficients $A^I_\alpha(JM)$ can be found by various methods, including by adding up moments, design methods, etc. Herein, we used a simple procedure based on the diagonalization of the matrix $\boldsymbol{J^2}$ of the operator $\hat{J}^2$ in the basis of the Slater determinants with a fixed value M:

$$\left(\boldsymbol{J^2}\right)_{\alpha\beta} = \langle \alpha \mid \hat{J}^2 \mid \beta \rangle\,, \qquad \alpha, \beta \in Q\,. \tag{11.24}$$

By diagonalizing such a matrix, we obtain the eigenfunctions of the operator $\hat{J}^2$, corresponding to the values of the total angular momentum $J \geq |M|$. As the CSF basis, we chose our own functions for $J = |M|$. Note that the $A^I_\alpha(JM)$ coefficients were calculated only for one of the group of equivalent configurations. By equivalent configurations, we mean here configurations having the same filling numbers for the shells and differing from each other only in the main quantum numbers of the shells.

Calculations of g-factors of Li-like ions.

For the calculations of the g-factors of Li-like ions, we divide the full value of the g-factor into separate contributions

$$g = g_{\mathrm{D}} + \Delta g_{\mathrm{int}} + \Delta g_{\mathrm{qed}} + \Delta g_{\mathrm{nuc}}\,, \tag{11.25}$$

where g_{D} is the g-factor calculated with the Dirac wave functions of the Coulomb field, Δg_{int} is the correction taking into account the electron-electron interaction

(Coulomb and Breit), $\Delta g_{\rm qed}$ is the contribution of the higher radiation and QED corrections, and $\Delta g_{\rm nuc}$ is the correction, taking into account the final dimensions of the core. We perform DFS calculations for different values of the parameter λ, which was introduced as a factor in front of the interelectron interaction operator. By numerically differentiating $g(\lambda)$ we obtained the coefficients $g^{(n)}$ of the expansion of the g-factor $g(\lambda)$ in a perturbation theory series. For $\lambda = 1$ we obtain

$$g = g^{(0)} + g^{(1)} + g^{(2)} + \dots .$$

Here $g^{(0)} = g_{\rm D}$ and $\Delta g_{\rm int} = g^{(1)} + g^{(2)} + \dots$. The first-order contribution $g^{(1)}_{\rm DFS}$, calculated by the DFS method can be compared with the value $g^{(1)}_{\rm PT}$, obtained by the standard Perturbation Theory (PT) method in a much larger splines basis. When calculating the correction for the electron-electron interaction $\Delta g_{\rm int}$ one can use a more accurate value of $g^{(1)}_{\rm PT}$, and obtain higher orders of magnitude PT $\Delta g_{\rm DFS}$ as follows

$$\Delta g_{\rm DFS} = g_{\rm DFS} - g^{(0)} - g^{(1)}_{\rm DFS}$$

Here $g_{\rm DFS}$ is the total g-factor calculated by the DFS method for $\lambda = 1$. In general, the interelectronic-interaction correction $\Delta g_{\rm int}$ can be cast in the form:

$$\Delta g_{\rm int} = 2\left[\frac{(\alpha Z)^2}{Z} B(\alpha Z) + \frac{(\alpha Z)^2}{Z^2} C(\alpha Z) + \frac{(\alpha Z)^2}{Z^3} D(\alpha Z) + ...\right], \quad (11.26)$$

Here, functions $B(\alpha Z)$, $C(\alpha Z)$, and $D(\alpha Z)$ are applied to define the interelectronic-interaction correction terms of first, second, and third orders in $1/Z$, respectively. The derivation of the interelectronic-interaction correction in first order in the expansion parameter $1/Z$ was considered in detail in Ref. [26]. To perform the accurate calculations this contribution should be divided into two parts, namely, the part

which may be also derived from standard quantum mechanical perturbation theory,

$$
\begin{aligned}
&\Delta E_{int} \\
&= \sum_{m_c} \left[\sum_P (-1)^P \sum_n^{\varepsilon_n \neq \varepsilon_v} \frac{\langle PvPc\,|I(\triangle_{P_{cc}})|\,nc\rangle\langle\, n|\delta V|v\,\rangle}{\varepsilon_v - \varepsilon_n} \right. \\
&+ \sum_P (-1)^P \sum_n^{\varepsilon_n \neq \varepsilon_v} \frac{\langle\, v|\delta V|n\,\rangle\,\langle nc\,|I(\triangle_{P_{cc}})|\,PvPc\rangle}{\varepsilon_v - \varepsilon_n} \\
&+ \sum_P (-1)^P \sum_n^{\varepsilon_n \neq \varepsilon_v} \frac{\langle PvPc\,|I(\triangle_{P_{vv}})|\,vn\rangle\langle\, n|\delta V|c\,\rangle}{\varepsilon_v - \varepsilon_n} \\
&\left. + \sum_P (-1)^P \sum_n^{\varepsilon_n \neq \varepsilon_v} \frac{\langle\, c|\delta V|n\,\rangle\,\langle\, vn\,|I(\triangle_{P_{vv}})|\,PvPc\rangle}{\varepsilon_v - \varepsilon_n} \right],
\end{aligned}
\tag{11.27}
$$

and a QED part involving derivatives with respect to the frequency of the exchanged photon:

$$
-\sum_{m_c} \left[\langle\, cv|\, I'(\triangle_{vc})\,|\,vc\,\rangle(\langle v\,|\,\delta V\,|\,v\rangle - \langle\, c\,|\delta V|\,c\,\rangle) \right]. \tag{11.28}
$$

Here, v and c are the valence and core electron states, respectively, m_c denotes the angular momentum projection of the core electron, $\triangle_{ab} = \varepsilon_a - \varepsilon_b$, $\delta V(\boldsymbol{x}) = e\,\boldsymbol{\alpha}\cdot\boldsymbol{A}_{\rm cl}(\boldsymbol{x})$ is the interaction operator of the external magnetic field, $I(\omega) = e^2\,\alpha^\rho\,\alpha^\sigma\,D_{\rho\sigma}(\omega)$, $D_{\rho\sigma}(\omega, \boldsymbol{x}-\boldsymbol{y})$ is the interaction operator which can be derived from the exchange of a virtual photon between two electrons. In the latter definition, the photon propagator is given by

$$
D_{\rho\sigma}(\omega, \boldsymbol{x}-\boldsymbol{y}) = {\rm g}_{\rho\sigma}\frac{\exp({\rm i}|\omega||\boldsymbol{x}-\boldsymbol{y}|)}{4\pi|\boldsymbol{x}-\boldsymbol{y}|} \tag{11.29}
$$

in the Feynman gauge, and its derivative is $I'(\omega) = dI(\omega)/d\omega$. The related contribution to the g-factor is defined as $\Delta g_{\rm int} = \Delta E_{\rm int}/\mu_0 \mathcal{H} m_v$, where $\mu_0 = |e|/2m$ is the Bohr magneton and m_v is the angular momentum projection of the valence

electron.

Eq. (11.27) contains sums over intermediate states excluding the valence $2s$ reference state. We use a relativistic Sturmian basis set of single-electron wave functions (see the next section for more details) to perform the summation numerically. In order to saturate these sums, we take into account all virtual orbitals with s and d symmetries with principal quantum numbers up to 50.

Table 1: G-factor and HFS virtual orbits fitting for Li Z=3, Li-like ions

configuration	g-factor	HFS, Fc(Z)	HFS, (Mhz)
real	3.48137529	0.49323671	919.48533
s-orbitals			
40s	-6.99402556	-0.88621998	-1652.07954
45s	-6.99402558	-0.88621998	-1652.07954
50s	-6.99402556	-0.88621998	-1652.07954
d-orbitals			
40d	3.60798797	0.49323755	919.48689
45d	3.60798797	0.49323755	919.48689
50d	3.60798796	0.49323755	919.48689

11.6 Li-like elements, Calculation of the 1 photon exchange diagrams and virtual orbitals fitting

In this Session we show the procedure of the fitting of the calculation of the 1 photon exchange diagrams by perturbation theory method to the DFS method for the Li-like elements with different Z. In general, to obtain the maximum accuracy of higher order corrections to g-factor and HFS corresponding to the 2-photon exchange and scattering one should firstly run calculations for the 1-photon exchange diagrams and then compare them to the results obtained by the perturbation theory. The results are shown in the Table 1, Table 2, Table 3, Table 4, Table 5, Table 6, Table 7, Table 8,Table 9.

11.7 B-like elements, Li-like elements, Calculation of the 1 photon exchange diagrams and virtual orbitals fitting.

In this Session we show the procedure of the fitting of the calculation of the 1 photon exchange diagrams by perturbation theory method to the DFS method for the B-like elements with different Z. In general, to obtain the maximum accuracy of higher

Table 2: G-factor and HFS virtual orbits fitting for F, Z=9, Li-like ions

configuration	g-factor	HFS, Fc(Z)	HFS, (Mhz)
real	10.50961990	0.16650845	20297.29954
s-orbitals			
40s	-21.00566444	-0.29807899	-36335.68333
45s	-21.00566444	-0.29807899	-36335.68333
50s	-21.00566444	-0.29807899	-36335.68333
d-orbitals			
40d	10.88939969	0.16651095	20297.60328
45d	10.88939967	0.16651095	20297.60324
50d	10.88939967	0.16651095	20297.60324

Table 3: G-factor and HFS virtual orbits fitting for Si, Z=14, Li-like ions

configuration	g-factor	HFS, Fc(Z)	HFS, (Mhz)
real	16.51109399	0.10923139	-10586.61367
s-orbitals			
40s	-32.73437665	-0.19441604	18842.63752
45s	-32.73437665	-0.19441602	18842.63536
50s	-32.73437665	-0.19441602	18842.63536
d-orbitals			
40d	17.10170720	0.10923529	-10586.99130
45d	17.10170721	0.10923529	-10586.99128
50d	17.10170721	0.10923529	-10586.99129

Table 4: G-factor and HFS virtual orbits fitting for Ca, Z=20, Li-like ions

configuration	g-factor	HFS, Fc(Z)
real orbitals	24.00017568	0.07926459
s-orbitals		
5s	-26.29109881	-0.09812332
10s	-42.59679536	-0.11841094
15s	-45.83447315	-0.14147007
20s	-46.91483827	-0.13979494
25s	-46.91393425	-0.13966595
30s	-46.91394237	-0.13966974
33s	-46.91394237	-0.13966978
36s	-46.91394237	-0.13966977
40s	-46.91394237	-0.13966977
45s	-46.91394237	-0.13966977
50s	-46.91394237	-0.13966977
d-orbitals		
5d	24.84378950	0.07927066
10d	24.84346597	0.07927024
15d	24.84346181	0.07927024
20d	24.84345960	0.07927025
25d	24.84346830	0.07927022
30d	24.84346841	0.07927022
35d	24.84346839	0.07927022
40d	24.84346839	0.07927022
45d	24.84346839	0.07927022
50d	24.84346839	0.07927022

Table 5: G-factor and HFS virtual orbits fitting for Xe, Z=54, Li-like ions

configuration	g-factor	HFS, Fc(Z)	HFS, (Mhz)
real orbitals	78.72786629	0.04636356	-361268.34775
s-orbitals			
40s	-132.09574656	-0.07365508	573925.88886
45s	-132.09574656	-0.07365509	573925.93648
50s	-132.09574656	-0.07365509	573925.93660
d-orbitals			
40d	80.97513052	0.04638082	-361402.80640
45d	80.97513052	0.04638082	-361402.80527
50d	80.97513052	0.04638082	-361402.80527

Table 6: G-factor and HFS virtual orbits fitting for Bi, Z=83, Li-like ions

configuration	g-factor	HFS, Fc(Z)	HFS, (Mhz)
real orbitals	157.30515231	0.06963483	-1156722.79423
s-orbitals			
40s	-219.54450036	-0.10016078	1663797.52523
45s	-219.54450036	-0.10016080	1663797.86124
50s	-219.54450036	-0.10016080	1663797.85925
d-orbitals			
40d	160.57085198	0.06966871	-1157285.59605
45d	160.57085198	0.06966871	-1157285.58718
50d	160.57085198	0.06966871	-1157285.58541

Table 7: G-factor and HFS virtual orbits fitting to the PT 1-photon exchange calculations for Ca, Z=20, Li-like ions

configuration	g-factor	HFS, Fc(Z)	HFS, (Mhz)
PT	-46.0706616	-0.1396643	
s orbitals			
25s-16d	-46.07067092	-0.13966444	32459.68904
30s-16d	-46.07065623	-0.13966409	32459.60655
31s-16d	-46.07065621	-0.13966418	32459.62786
32s-16d	-46.07065621	-0.13966409	32459.60659
33s-16d	-46.07065621	-0.13966415	32459.62077
34s-16d	-46.07065621	-0.13966411	32459.61013
35s-16d	-46.07065621	-0.13966414	32459.61723
36s-16d	-46.07065621	-0.13966412	32459.61368
d orbitals			
33s-16d	-46.07065621	-0.13966415	32459.62077
33s-19d	-46.07065595	-0.13966415	32459.62079
33s-20d	-46.07065846	-0.13966414	32459.61767
33s-21d	-46.07064825	-0.13966418	32459.62636
33s-22d	-46.07064958	-0.13966417	32459.62593
33s-23d	-46.07064966	-0.13966416	32459.62374
33s-24d	-46.07064909	-0.13966416	32459.62396
33s-25d	-46.07064975	-0.13966416	32459.62398
33s-26d	-46.07064972	-0.13966417	32459.62400
33s-27d	-46.07064971	-0.13966417	32459.62401
33s-28d	-46.07064971	-0.13966417	32459.62401
33s-29d	-46.07064974	-0.13966417	32459.62400
33s-30d	-46.07064964	-0.13966416	32459.62394
33s-31d	-46.07064965	-0.13966417	32459.62399
s,d random			
34s-21d	-46.07064825	-0.13966413	32459.61572
34s-24d	-46.07064909	-0.13966413	32459.61687

Table 8: G-factor and HFS virtual orbits fitting to the PT 1-photon exchange calculations for Si, Z=14, Li-like ions

configuration	g-factor	HFS, Fc(Z)	HFS, (Mhz)
PT	-32.1437718	-0.1944122	
d fitting			
33s-16d	-32.14376404	-0.19441218	18842.26270
33s-17d	-32.14376407	-0.19441218	18842.26268
33s-18d	-32.14376409	-0.19441218	18842.26267
33s-19d	-32.14376410	-0.19441218	18842.26265
33s-20d	-32.14376410	-0.19441218	18842.26265
33s-21d	-32.14376410	-0.19441218	18842.26267
33s-22d	-32.14376278	-0.19441218	18842.26278
33s-23d	-32.14376415	-0.19441218	18842.26291
33s-24d	-32.14376360	-0.19441218	18842.26295
33s-25d	-32.14376356	-0.19441218	18842.26296
33s-26d	-32.14376356	-0.19441218	18842.26296
33s-27d	-32.14376354	-0.19441218	18842.26297
33s-28d	-32.14376352	-0.19441218	18842.26298
33s-29d	-32.14376356	-0.19441218	18842.26297
33s-30d	-32.14376340	-0.19441218	18842.26296
33s-31d	-32.14376344	-0.19441218	18842.26296
33s-32d	-32.14376344	-0.19441218	18842.26308

Table 9: G-factor and HFS virtual orbits fitting to the PT 1-photon exchange calculations for Bi Z=83, Li-like ions

configuration	g-factor	HFS, Fc(Z)	HFS, (Mhz)
PT	-216.2788605		
s fitting			
20s-15d	-216.27199791	-0.09991762	1659758.34765
30s-16d	-216.28657368	-0.10013322	1663339.79504
31s-16d	-216.28657966	-0.10014557	1663544.87859
32s-16d	-216.28659159	-0.10013409	1663354.27336
34s-16d	-216.28660430	-0.10013681	1663399.41165
35s-16d	-216.28660680	-0.10014405	1663519.70212
d fitting			
33s-16d	-216.28659559	-0.10014401	1663519.05602
33s-17d	-216.28696505	-0.10014366	1663513.19505
33s-18d	-216.28659158	-0.10014376	1663514.81484
33s-19d	-216.30078597	-0.10013214	1663321.76109
33s-20d	-216.27828962	-0.10015039	1663624.95882
33s-21d	-216.27873073	-0.10015000	1663618.56214
33s-22d	-216.27875518	-0.10014997	1663618.04881
33s-23d	-216.27875696	-0.10014997	1663618.02509
33s-24d	-216.27875797	-0.10014994	1663617.44261
33s-25d	-216.27875711	-0.10014997	1663617.94596
33s-26d	-216.27875711	-0.10014997	1663617.97655
33s-27d	-216.27875712	-0.10014997	1663617.99074
33s-28d	-216.27875711	-0.10014997	1663617.99362
33s-29d	-216.27875711	-0.10014996	1663617.87415
33s-30d	-216.27875710	-0.10014998	1663618.08826

order corrections to g-factor and HFS corresponding to the 2-photon exchange and scattering one should firstly run calculations for the 1-photon exchange diagrams and then compare them to the results obtained by the perturbation theory. Compared to the Li-like calculations with 3 electrons in B-like systems we have to take into account all exchanges and interelectronic interactions for 5 electrons. The results are shown in the Table 10, Table 11.

Table 10: G-factor and HFS virtual orbits fitting to the PT 1-photon exchange calculations for Ca, Z=20, B-like ions

configuration	g-factor	HFS, Fc(Z)
PT	-134.64245839	-0.00055149
s-orbitals		
5s	-136.97471693	0.00032891
10s	-136.99181399	0.00192111
15s	-136.95912926	0.00171015
20s	-136.99279042	0.00183877
25s	-136.99276162	0.00185399
29s	-136.99276246	0.00185318
35s	-136.99276246	0.00185316
40s	-136.99276246	0.00185316
p-orbitals		
5p	-96.04879787	-0.31457129
10p	-96.09187776	-0.31211174
15p	-96.07063509	-0.31220221
20p	-96.07072578	-0.31239218
25p	-96.07072402	-0.31238674
30p	-96.07072545	-0.31239222
35p	-96.07072545	-0.31239222
43p	-96.07072545	-0.31239222
47p	-96.07072545	-0.31239220
51p	-96.07072545	-0.31239219
d-orbitals		
5d	-109.43798041	0.00381065
10d	-109.66152760	0.00582419
15d	-109.64287934	0.00590209
20d	-109.64450896	0.00574181
25d	-109.64909597	0.00579825
30d	-109.64909636	0.00579813
35d	-109.64909637	0.00579814
40d	-109.64909637	0.00579814
45d	-109.64909637	0.00579815
50d	-109.64909637	0.00579815
55d	-109.64909637	0.00579814

Table 11: G-factor and HFS virtual orbits fitting to the PT 1-photon exchange calculations for B-like ions in one table

Element	g-factor	HFS, Fc(Z)	HFS, (Mhz)
Li, Z=3			
PT	10.873707177	-1.905478645	
PW	10.87371255	-1.90547880	-1184.05610
Si, Z=14			
PT	51.055844715	-0.420237136	
PW	51.05586938	-0.42023708	13626.55241
Ca, Z=20			
PT	73.427632786	-0.303637971	
PW	73.42766750	-0.30363788	

References

[1] V. M. Shabaev, D. A. Glazov, N. S. Oreshkina, A. V. Volotka, G. Plunien, H.-J. Kluge, and W. Quint, Phys. Rev. Lett. 96, 253002 (2006).

[2] P. Beiersdorfer, A. L. Osterheld, J. H. Scofield, J. R. Crespo Lopez-Urrutia, and K. Widmann, Phys. Rev. Lett. 80, 3022 (1998).

[3] J. Verdu S.c, S. Stahl, T. Valenzuela, M. Vogel, G. Werth, T. Beier, H.-J. Kluge, and W. Quint, Phys. Rev. Lett. 92, 093002 (2004).

[4] H. Haffner, T. Beier, N. Hermanspahn, H.-J. Kluge, W. Quint, S. Stahl, J. Verdu, and G. Werth, Phys. Rev. Lett. 85, 5308 (2000).

[5] V.M.Shabaev, Physics Reports v.356, p.119-228 (2002).

[6] V.M. Shabaev, Phys. Rev. A **57**, 59 (1998).

[7] D.A.Glazov, V.M. Shabaev, I.I.Tupitsyn, A.V.Volotka, V.A.Yerokhin, G.Plunien, and G.Soff, Phya.Rev.A, v.70, pp.062104(1-9) (2004).

[8] V.M. Shabaev, K. Pachucki, I.I. Tupitsyn, and V.A. Yerokhin, Phys.Rev.Lett. **94**, 213002 (2005).

[9] V.M.Shabaev, I.I.Tupitsyn, K.Pachucki, G.Plunien, and V.A.Yerokhin, Phys.Rev.A, **72**, p.062105 (2005).

[10] V. A. Yerokhin, P. Indelicato and V. M. Shabaev, Phys. Rev. A 69, 052503 (2004).

[11] K. Pachucki, U. D. Jentschura, and V. A. Yerokhin, Phys. Rev. Lett. 93, 150401 (2004).

[12] S. Sturm, F. Kohler, J. Zatorski, A. Wagner, Z. Harman, G. Werth, W. Quint, C.H. Keitel, K. and K. Blaum, Nature 506, 7489 (2014).

[13] V. M. Shabaev, M. Tomaselli, T. Kuhl, A. N. Artemyev and V. A. Yerokhin, Phys. Rev. A 56, 252–255 (1997).

[14] A. V. Volotka, D. A. Glazov, I. I. Tupitsyn, N. S. Oreshkina, G. Plunien and V. M. Shabaev, Phys. Rev. A 78, 062507 (2008).

[15] V.F.Bratzev, Atomic wave functions tables, Science, L., 1966, 157 p.

[16] V.F.Bratzev, Atomic wave functions tables, Science, L., 1971, 456 p.

[17] V.I. Baranovsky, V.F. Bratzev, A.I. Panin, V.M. Tretiyak, Calculation methods of electronic structure of atoms and molecules, LGU, 1976, 204 p.

[18] V.F. Bratzev, G.B. Daineka, I.I. Tupitsyn, Izv AN USSR, Physics, 2655 p (1977).

[19] Sharlotte Frose Fisher, The Hartree-Fock Method for atoms, John Willet & Sons, NY, (1977).

[20] I.P.Grant, Relativistic effects in Atoms, Molecules and Solids, v.87 of Advanced Study Institute Series, Ed. G.L.Malli, Plenum Press, New-York (1983).

[21] M.A. Coulthard, J.Phys.B., v.7, p.440 (1974).

[22] J.P.Desclaux, J.Phys.B., v.4, p.631 (1971).

[23] J.B.Mann and W.R.Johnson, Breit interaction in Multielectron Atoms., Phys.Rev.A, v.4, N.1, p.41-51, (1971).

[24] I.M. Band and V.I. Fomichev, Computer Program Complex RAINE V: Description of Code for Calculations of Atomic Field Using the Self-Consistent

Dirac-Fock Method, Leningrad Nuclear Physics Institute Report LNPI-498 (1979)

[25] L.V.Chernysheva, V.L.Yakhontov, Computer Physics Communications, v.119, p.232 (1999).

[26] V.M.Shabaev, D.A.Glazov, M.B.Shabaeva, I.I.Tupitsyn, V.A.Yerokhin, T.Beier, G.Plunien, G.Soff, Nuclear Instruments and Methods in Physics Research B, v.205, pp. 20-24 (2003).

[27] D.A.Glazov, V.M. Shabaev, I.I.Tupitsyn, A.V.Volotka, V.A.Yerokhin, G.Plunien, and G.Soff, Phya.Rev.A, v.70, pp.062104(1-9) (2004).

[28] D.A. Glazov, V.M. Shabaev, I.I. Tupitsyn, A.V. Volotka, V.A. Yerokhin, P. Indelicato, G. Plunien and G. Soff, Nuclear Instruments and Methods in Physics Research B, v. 235, pp. 55-60, (2005)

[29] D.A. Glazov, A.V. Volotka, V.M. Shabaev, I.I. Tupitsyn, G. Plunien, Physics Letters A, v.357, p.330-333, (2006)

[30] R.Soria Orts, J.R. Crespo Lopez-Urrutia, H.Bruhns, A.J. Gonzalez Martinez, Z.Harman, U.D.Jentschura, C.H.Keitel, A.Lapierre, H.Tawara, I.I.Tupitsyn, J.Ullrich and A.V.Volotka Phys.Rev.A., v76, p.052501(1-7) (2007).

[31] P.G.H. Sandars, J.Phys.B.,**1**, 511 (1968).

[32] E.Lindroth, B.W.Lynn and P.G.H. Sandars, J.Phys.B.,**22**, 559 (1989).

[33] E.Lindroth and A.Ynnerman, Phys.Rev.A, v.47, p.961 (1993).

[34] I.I.Sobelman, Atomic Spectra, and Radiative Transitions, Berlin, Springer (1979).

[35] D.A. Varshalovich, A.N. Moskalev, V.K. Hersonsky, Quantum theory of angular momentum, Science, L., 439 p (1975).

[36] McWeeny R., Methods in Computational Molecular Physics. ed. Wilson S., Diercksen G. H. F., Plenum Press, New York, Ser.B, 325p (1992).

[37] B.H.Brandow, Int.J.Quant.Chem, **15**, p.207 (1979).

[38] M.Svreĕcek, Int.J.Quant.Chem, **31**, p.625 (1987).

[39] V.M.Shabaev, Physics Reports v.356, p.119-228 (2002).

[40] A.N. Artemyev, V.M. Shabaev, I.I. Tupitsyn, G.Plunien, and V. A. Yerokhin, Phys.Rev.Lett., v.98, p.173004-(1-4) (2007).

[41] E.Dalgaard, P.Jørgensen, J.Chem.Phys. **69**, p.3833 (1978).

[42] Ron Shepard, The Multiconfigurational Self- Consistent Field Method, Advances in Chemical Physics, LXIX, Ab Initio Methods in Quantum Chemistry - II, Ed. by K.P.Lawley, pp.63-200, (1987).

[43] Jeppe Olson, The method of Second Quantization, in "Lecture Notes in Chemistry", pp.38-88, ed. B.O.Roos, Springer-Verlag, (1992).

[44] Björn O.Roos, The Multi-configurational (MC) Self- Consistent Field (SCF) Theory, in "Lecture Notes in Chemistry", pp.177-254, ed. B.O.Roos, Springer-Verlag, (1992).

[45] B.Levy and G.Berthier, Int.J.Quant.Chem., v.2, p.307 (1968).

[46] Rotenberg M., Adv. Atom. and Molec. Phys., v. 6, p. 233 (1970).

[47] P.P.Pavinsky, A.I. Sherstyuk, Problems of theoretical physics, L., t. 1, 66-107 p, (1974).

[48] A.I. Sherstyuk, TMF, v.21, 224–231 (1974).

[49] P.F. Gruzdev, A.I. Sherstyuk, Izv USSR, physics, v 41, 2477 p, (1977)

[50] P.F. Gruzdev, A.I. Sherstyuk, G.S. Solovieva, Optics and Spectroscopy, 1198 p (1977)

[51] C.C.J.Roothaan and P.Bagus, Methods in Computational Physics, **2**, Academic Press, N.Y. (1963).

[52] Kotochigova S.A., Tupitsyn I.I., J.Phys.,B, v.20, p.4759-4771 (1987).

[53] S.Kotochigova, K.P.Kirby and I.Tupitsyn Phys.Rev.A, v.76, p.05213 (1-9), (2007).

[54] P.Pyykkö, E.Pajanne, M.Inokuti, Int.J.Quant.Chem., v.7, p.785 (1973).

[55] Woods R.D., Saxon D.S., Phys. Rev., v.95, p.577 (1954).

[56] T.V.Back, H. S. Margolis, P. K. Oxley, J. D. Silver, and E. G. Myers, Hyperfine Int., v.114, p.203, (1998).

[57] D. P. Moehs and D. A. Church, Phys.Rev.A, v.58, p.1111, (1998).

[58] E. Trabert, P. Beiersdorfer, S. B. Utter, G. V. Brown, H. Chen, C. L. Harris, P. A. Neill, D. W. Savin and A. J. Smith, Astrophys.J., v.541, p.506, (2000).

[59] E. Trabert, P. Beiersdorfer, G. Gwinner, E. H. Pinnington and A. Wolf, Phys.Rev.A, v.66, p.052507 (2002).

[60] Z.Harman, U.D.Jentschura1, C.H.Keitel, A.Lapierre, R.Soria Orts, J.R.Crespo Lopez-Urrutia, H.Tawara, J.Ullrich, A.N.Artemyev, I.I.Tupitsyn, A.V.Volotka and V.M.Shabaev, J.Phys. Conference Series, v.58, p.133, (2007).

[61] A.V. Volotka, D.A. Glazov, G. Plunien, V.M. Shabaev, and I.I. Tupitsyn, Eur.Phys.J.D v.48, p.167-170, (2008).

[62] R.A.Hegstrom, Phys.Rev. A, **7**, p.451 (1973).

[63] I.P. Grant, Gauge invariance and relativistic radiative transitions, J.Phys.B: Atom.Molec.Phys, **7**, N12, pp 1458-1475 (1974).

[64] A Lapierre, J.R.Crespo López-Urrutia and J Ullrich, EBIT MPI-Heidelberg, Private communication (2004).

[65] W R Johnson, Private communication (2004).

[66] C.Z.Dong, S.Fritzsche, B.Fricke and W.-D.Sepp, Phys. Scripta, **T92**, p.296 (2001)

12 Single-Particle Nonlocal Potential to Take into Account Quantum-Electrodynamic Corrections

A new single-particle effective potential is proposed. This potential allows one to take into account quantum-electrodynamic (QED) corrections in relativistic calculations of many-electron ions and neutral atoms. In particular, it can be used in the Dirac–Fock (DF) method, the relativistic density functional, the multi-configuration DF method, and the relativistic method of superposition of configurations. The potential is constructed without fitting parameters. Self-energy corrections have been calculated for a number of neutral alkali atoms and Li-like ions to check the quality of the nonlocal potential proposed. Comparison with the data in the literature on the QED corrections obtained in non empirical calculations based on the use of QED perturbation theory is performed

12.1 Introduction

The accuracy of experimental and theoretical atomic and molecular spectroscopic data has increased so much in the last decades that it has become urgent to take into account the radiativequantum-electrodynamic (QED) corrections in calculations of the electronic structure of atoms and molecules. It is especially important to consider QED corrections when calculating the energies and probabilities of transitions with participation of core electrons,for example, for radiative X-ray and nonradiative Auger transitions. QED corrections can also play an important role in calculations of the energies of optical transitions and ionization potentials of valence electrons for heavy and super heavy neutral atoms and ions.

Non empirical calculations of radiative corrections based on the use of the QED perturbation theory for many-electron systems are extremely cumbersome and time-consuming. To date, these high-accuracy non empirical calculations can be per-

formed for only hydrogen-like ions and for multiply charged ions and light atoms with a small number of electrons. In this context, it is an urgent problem to construct an approximate radiative single-particle potential, addition of which to the many-electron Hamiltonian of the system would make it possible to take into account QED corrections in such methods for calculating the electronic structure of atoms and molecules as the Dirac–Fock (DF) method, the density functional method, and more complex methods that take into account the electronic correlation (multiconfiguration DF method, method of superposition of configurations, and coupled-cluster method). To date, many attempts have been made to take into account QED corrections in calculations of the electric structure of atoms using different interpolation schemes for corrections to total energies and transition energies (see, for example, [1–6]). In addition,various local radiative potentials have been proposed(see, for example, [7, 9–14]), which can be added to the Hamiltonian of the system to take into consideration QED corrections. The dominant contributions to a QED correction are vacuum polarization and self-energy. The contribution of vacuum polarization can be taken into account with high accuracy by adding a local Uehling potential [15] to the Hamiltonian. Therefore, were stricted ourselves to only the self-energy correction(ΔE^{SE}). The purpose of this study was to construct a nonlocal radiative potential in order to take into consideration correction ΔE^{SE}. Having chosen some local radiative potential as a starting one, we build a nonlocal potential, such that its addition to the hydrogen-like Dirac Hamiltonian shifts energies $\delta\varepsilon_i^{\mathrm{SE}}$ of all states under consideration exactly by the value of self-energy correction $\delta\varepsilon_i^{\mathrm{SE}}$ for a hydrogen like ion. We chose the radiative potential proposed in [14] as a starting local potential. Corrections $\delta\varepsilon_i^{\mathrm{SE}}$ for H-like ions were taken from [16, 17]. The self-energy shift of the energy levels in a hydrogen-like ion is proportional Z^4/n^3, where Z is thenucleus charge and n is the principal quantum number. Therefore, correction ΔE^{SE} is often expressed in terms of dimensionless

smooth function $F(\alpha Z)$ [16], which is found from the relation

$$\Delta E^{\rm SE} = \frac{\alpha}{\pi}\frac{(Z\alpha)^4}{n^3}F(\alpha Z)mc^2, \tag{12.1}$$

Here, α is the fine-structure constant, m is the electron mass, and c is the speed of light. This paper is organized as follows. Different versions of effective local potentials, which could be used as starting ones when constructing a nonlocal radiative potential, are enumerated in Section 12.2. The way to construct the nonlocal radiative potential proposed in this study is described in Section 12.3. Calculations of the self-energy corrections for the ionization potentials of some neutral atoms and some Li-like ions are reported in Section 12.4, which also contains a discussion of the results obtained. Instead of the relativistic system of units, which is natural for quantum electrodynamics, we used the atomic system of units ($\hbar = e = m = 1$), because the radiative potential is applied in the calculations of electronic structure, where this system of units is conventional.

12.2 Effective Local Radiative Potential.

Below, we enumerate the local radiative potentials (known to us) that could be used as starting ones to construct the nonlocal effective potential proposed here. A detailed analysis of different local radiative potentials can also be found in [7, 8].

1. The following simple expression for the radiative local potential was proposed in an old study [9].

$$V_{\rm Pais}(r) = \frac{e^2}{r}\,2e^{-r/r_0}\,, \qquad r_0 = \frac{e^2}{mc^2} \tag{12.2}$$

2. Bethe [10] expressed the self-energy correction in terms of the electron den-

sity at the zero point (or at the nucleus). The corresponding potential can be written as

$$V_{\rm Bethe}(r) = \frac{4\alpha^3 Z}{3}\left[-2\ln(\alpha Z) - \ln(2K_{n0}/(\alpha Z)^2) + \frac{19}{30}\right]\,\delta(r)\,, \quad (12.3)$$

where K_{n0} is the so-called Bethe logarithm [18]. This potential can be used in non relativistic calculations of self-energy correction $\Delta E^{\rm SE}$ for the s states of light atoms.

3. A local potential in the form of a Gaussianfunction was proposed in [11]

$$V_{\rm Fricke}(r) = \exp(-r^2/r_0^2)\,, \qquad r_0 = \frac{2\alpha^3}{\pi}\,\ln\left(\frac{1}{Z\alpha}\right)\,. \quad (12.4)$$

4. A radiative potential proportional to nucleus potential $V_{\rm rnucl}(r)$ (formed by a uniformly charged sphere) was used in [12]

$$V_{\rm Pak}(r) = V_0\begin{cases} 1 - \dfrac{r^2}{R_{\rm n}^2} & r \le R_{\rm n} \\ 0 & r > R_{\rm n}\,, \end{cases} \quad (12.5)$$

where $R_{\rm n}$ is the radius of spherical nucleus and V_0 is afitting parameter.

5. A non relativistic radiative potential in the form was proposed in [13].

$$V_{\rm Eides}(r) = \frac{8\alpha^4 Z(2\pi)^{1/2}}{3r^3} \quad (12.6)$$

6. A Gaussian like radiative potential was alsoused in [7] to take into account

the self-energy correction:

$$V_{\rm SE}(r) = B\, e^{-\beta r^2}\,, \tag{12.7}$$

where fitting parameters B and β were determined formany elements of the periodic table.

7. A more complex local radiative potential for taking into account the self-energy QED correction was proposed in [14] ; later, it was used in calculations of the electronic structure of many-electron atoms[19, 20]. Specifically this potential was used in this study as a starting one to construct the nonlocal potential; therefore, we will consider this potential in more detail.

   According to [21], the self-energy part of the total radiative potential can be divided into three parts.

$$\Phi_{\rm rad}(r) = \Phi_{\rm mag}(r) + \Phi_{\rm hf}(r) + \Phi_{\rm lf}(r) \tag{12.8}$$

The first part, $\Phi_{\rm mag}(r)$, which is referred to as the magnetic form factor, can be written in atomic units

$$\Phi_{\rm mag}(r) = \frac{i\,\alpha}{4\pi}\,(\boldsymbol{\alpha}\cdot\boldsymbol{\nabla})\,\beta\,\left[-\frac{Z}{r}\,\left(\int\limits_1^\infty dt \frac{e^{-2tr/\alpha}}{t^2\,\sqrt{t^2-1}} - 1\right)\right]\,, \tag{12.9}$$

where vector quantity $\boldsymbol{\alpha}$ and scalar quantity β are standard Dirac matrices. The addition of this potential to the relativistic central-field Hamiltonian is equivalent to supplementing the radial Dirac equation with a potential in the form

$$V_{\rm mag}(r) = -\frac{\alpha Z}{2\pi r}\left[K_1(2r/\alpha) - \frac{\alpha}{2r}\right]\begin{pmatrix} 0 & 1 \\ 1 & 1 \end{pmatrix}, \tag{12.10}$$

where K_1 is a modified Bessel function [22]. Radial magnetic potential $V_{\rm mag}(r)$ transposes the large and small components of the two-component Dirac radial wave function.

The second $\Phi_{\rm hf}(r)$ and third $\Phi_{\rm hf}(r)$ terms in expression (12.8) are, respectively, the high- and low-frequency parts of the electric form factor. High-frequency part $\Phi_{\rm hf}(r)$ of the electric form factor, according to [14] , is determined by the expression

$$\Phi_{\rm hf}(r) = A(Z,r)\,\frac{\alpha^2 Z}{\pi r}\int\limits_1^\infty dt\,\frac{e^{-2tr/\alpha}}{\sqrt{t^2-1}}\left[\left(1-\frac{1}{2t^2}\right)\left(\ln(t^2-1)+L(\alpha Z)\right)-\frac{3}{2}+\frac{1}{t^2}\right], \tag{12.11}$$

where

$$L(t) = 4\,\ln\left(\frac{1}{\alpha Z}+\frac{1}{2}\right). \tag{12.12}$$

The function $A(Z,r)$ has the form

$$A(Z,r) = (1.071-1.976\,x^2-2.128\,x^3+0.169\,x^4)\,\frac{r}{r+0.07\,\alpha^3 Z^2}, \qquad x = \alpha\,(Z-80), \tag{12.13}$$

where the numerical coefficients were obtained by fitting the values of high-frequency corrections to theenergies of the $s-$ states of hydrogen-like ions

using the data of [17].

The expression for potential $\Phi_{\rm hf}(r)$ can be rewrittenin the form.

$$\Phi_{\rm hf}(r) = I_{\log}(r) + L(t)\left[K_0(\rho) - \frac{1}{2}\,Ki_2(\rho)\right] - 1.5\,K_0(\rho) + Ki_2(\rho)\,. \quad (12.14)$$

where $\rho = 2r/\alpha$, K_0 is a modified Bessel function [22], Ki_2 is a double integral of the modified Bessel function [22]

$$I_{\log}(r) = \int\limits_1^\infty dt\,\frac{e^{-2tr/\alpha}}{\sqrt{t^2-1}}\,\left(1 - \frac{1}{2t^2}\right)\ln(t^2-1)\,. \quad (12.15)$$

Low-energy part $\Phi_{\rm lf}(r)$ of the radiative potential in [14] was approximated by the expression.

$$\Phi_{\rm lf}(r) = B(Z)\,Z^4\,\alpha^3\,e^{-Zr}\,. \quad (12.16)$$

where $B(z) = 0.074 + 0.35\alpha Z$.

12.3 Nonlocal Radiative Potential

Let us assume that there is some local or nonlocal single-particle potential $\hat{V}$, addition of which to the Hamiltonian of a many-electron system allows one to take into account QED corrections. The basic concept of the construction of a nonlocal radiative potential is that any single-particle Hermitian potential $\hat{V}$ can approximately be replaced with finite-dimensional $\hat{V}_{\rm sep}$ (separable) Hermitian potential as follows

$$\hat{V} \simeq \hat{V}_{\rm sep} = \sum_{k,j} \mid \hat{V}\,\psi_k\rangle\,\left(G^{-1}\right)_{kj}\,\langle\hat{V}\psi_j\mid, \quad (12.17)$$

where

$$G_{kj} = \langle \psi_k \mid V \mid \psi_j \rangle, \tag{12.18}$$

It is easy to verify that the result of the action of potential $\hat{V}_{\rm sep}$ on set of functions ψ_j coincides with the result of the action of initial potential $\hat{V}$ on the same function:

$$\hat{V}_{\rm sep}\,\psi_i = \sum_k \left(G^{-1}\,G\right)_{ki}\,\hat{V}\,\psi_k = \hat{V}\,\psi_i\,. \tag{12.19}$$

Let us assume that there is some local or nonlocal single-particle potential $\hat{V}_{\rm SE}$, the addition of which to the Hamiltonian of a many-electron system allows one to take into account the self-energy correction.The expectation value of this potential, calculated on the wave functions of H-like ions, $\psi_i^{(0)}$, can be considered equal to self-energy corrections of hydrogen-like ions $\delta\varepsilon_i^{\rm SE}$ (the values of the latter can be found in the literature for practically all chemical elements):

$$\langle \psi_i^{(0)} \mid \hat{V}_{\rm SE} \mid \psi_i^{(0)} \rangle = \delta\varepsilon_i^{\rm SE}\,. \tag{12.20}$$

Let us set some local potential $V_{\rm loc}$ approximating radiative potential. Having used representation (12.17) for local potential $V_{\rm loc}$, one can replace radiative potential with a separable potential in form (12.17). In this case, the expectation values of potentials $\hat{V}_{\rm sep}$ and $V_{\rm loc}$ calculated on functions $\psi_i^{(0)}$ will be the same and, at the same time, differ from the expectation value of potential $\hat{V}_{\rm SE}$. We can refine the representation of the radiative potential in the form of a Hermitian separable potential by introducing diagonal matrix Λ into representation (12.17), i.e., search for the

radiative potential in the form

$$\hat{V}_{\rm SE} = \frac{1}{2} \sum_{k,j} \mid V_{\rm loc}\, \psi_k^{(0)} \rangle \, \left(\Lambda\, G^{-1} + G^{-1}\, \Lambda \right)_{kj} \, \langle V_{\rm loc} \psi_j^{(0)} \mid , \tag{12.21}$$

where the matrix elements of matrix G are equal to the matrix elements of local potential $V_{\rm loc}$ in the basis of hydrogen-like functions

$$G_{kj} = \langle \psi_k^{(0)} \mid V_{\rm loc} \mid \psi_j^{(0)} \rangle \, . \tag{12.22}$$

Matrix elements λ_{ii} of diagonal matrix Λ can be found from condition (12.20) by equating the diagonal matrix elements of potential to self energy corrections for hydrogen-like ions $\delta\varepsilon_i^{\rm SE}$

$$\langle i \mid \hat{V}_{\rm SE} \mid i \rangle = \frac{1}{2} \sum_{k,j} G_{ik} \, \left(\Lambda\, G^{-1} + G^{-1}\, \Lambda \right)_{kj} \, G_{ji} = \delta\varepsilon_i^{\rm SE} \, . \tag{12.23}$$

So, we find the diagonal elements of matrix Λ

$$\lambda_{ii} = \delta\varepsilon_i^{\rm SE} / G_{ii} \tag{12.24}$$

Thus, we have the following expression for the non-local radiative potential:

$$\hat{V}_{\rm SE} = \sum_{k,j} \mid V_{\rm loc}\, \psi_k^{(0)} \rangle \, D_{kj} \, \langle V_{\rm loc} \psi_j^{(0)} \mid , \tag{12.25}$$

where

$$D_{kj} = \frac{1}{2}\left[\frac{\delta\varepsilon_k^{\rm SE}}{G_{kk}} + \frac{\delta\varepsilon_j^{\rm SE}}{G_{jj}}\right]\left(G^{-1}\right)_{kj} . \tag{12.26}$$

Separable potential has the following property: the expectation value of this operator calculated with hydrogen-like wave functions exactly coincide with self-energy corrections for H-like ions. Nonlocal potential (12.25), along with the Uehling potential, can be added to the many-electron relativistic Dirac–Coulomb–Breit Hamiltonian to take into account the radiative corrections in calculations of the electronic structure of multiply charged ions and neutral atoms. The matrix elements of nonlocal operator (12.25) can easily be calculated in methods applying a finite basis set. However, in DF and other methods,where integrodifferential equations are solved using grid techniques, the large nonlocal part of the total potential may lead to divergences during the self-consistency procedure. Therefore, it is desirable to "attenuate" the nonlocality of potential (12.25). This can be done by adding the local potential $V_{\rm loc}$ and substracting representation $V_{\rm loc}$ in the form of separable potential (12.17) on the right hand side of equality (12.25). Thus,we can rewrite expression (12.25) for radiative potential in the form

$$\hat{V}_{\rm SE} = V_{\rm loc} + \sum_{k,j} \mid V_{\rm loc}\,\psi_k^{(0)}\rangle\,\Delta D_{kj}\,\langle V_{\rm loc}\psi_j^{(0)}\mid , \tag{12.27}$$

where

$$\Delta D_{kj} = \frac{1}{2}\left[\frac{\delta\varepsilon_k^{\rm SE} - G_{kk} - \delta_k}{G_{kk}} + \frac{\delta\varepsilon_j^{\rm SE} - G_{jj} - \delta_j}{G_{jj}}\right]\left(G^{-1}\right)_{kj} . \tag{12.28}$$

The expression for matrix elements ΔD_{kj} was supplemented with small corrections δ_k for the following reason. When potential (12.27) is added to the Hamiltonian of a hydrogen-like ion, the energy shifts will differ from self-energy corrections, because

the wave functions change as a result of adding the potential. Being a second-order effect, this shift is insignificant.

Nevertheless, this effect can be taken into account by adding small corrections δ_k to the mean of local potential G_{kk}. The δ_k value can be found iteratively by solving the Dirac equation for hydrogen-like ions, based on the following requirement: addition of potential (12.27) should result in an energy shift equal to known self-energy corrections $\delta\varepsilon_k^{\rm SE}$ for H-like ions. Note that, in central-field problems, the angular parts of potential $\hat{V}_{\rm SE}$ are readily separated and one can easily pass from the operator in the general form to a radial potential,which (as well as the initial potential) does not mix states with different values of relativistic quantum number κ.

12.4 Results and Discussion

The calculations were performed using nonlocal potential (12.27), having included $\psi_k^{(0)}$ and $\psi_j^{(0)}$ j hydrogen-like wave functions and f all s-, p-, and d- states with principal quantum numbers n not more than $n = 5$ in the sum over k and j. Self-energy corrections for hydrogen-like ions with a point nucleus for the 1s, 2s, $2p_{1/2}$, and $2p_{3/2}$ states were taken from [16]. For other s-, p-, and d- states with quantum numbers $n = 3, 4, 5$, we used the data of [17] and the interpolation schemes described in [23]. Radiative potential $\Phi_{\rm rad}$ (see([14])) was applied as local starting potential $V_{\rm loc}$

To check the quality of the proposed nonlocal potential, we calculated the self-energy correction for the ionization potentials of a number of neutral alkali atoms and several Li-like ions. The calculation was performed on the basis of the single-configuration DFmethod and the Dirac–Fock–Slater (DFS) methodusing modified versions of the Hartree–Bock–Dirac(HFD) program [24].

The following potential was used as an exchangepotential in the DFS method:

$$V_x(r) = -x_\alpha \left(\frac{81}{32\,\pi^2}\,4\pi\rho(r)\right)^{1/3}, \qquad \int\limits_0^\infty dr\rho(r) = N \tag{12.29}$$

where $\rho(r)$ is the total radial electron density normalized to number of electrons N. The value of coefficient $x_\alpha = 1$ corresponds to the Slater exchange potential [25], and the value $x_\alpha = 2/3$ corresponds to the Kohn–Sham potential [26]. The irregular asymptotics of these potentials at large distances was correlated using the Latter correction [27]. We used precisely this self-action correction to compare our data with the results of non empirical calculations of QED corrections [28, 29] based on the local exchange potential (12.29).

Note that the DF and DFS calculations of the contributions of QED corrections can be performed indifferent approximations. The simplest way to do this is to calculate the mean of the radiative potential using the single-electron DF and DFS functions. In the second and third approaches, it is necessary to perform calculations for an atom or ion including radiative potential $\hat{V}_{\rm SE}$ in the self-consistency procedure and neglecting it. In the second approach, one uses the difference in single-electron energies. The third approach, in which QED corrections are determined as the differences in the corresponding total energies, is most logical. Our experience shows that these three calculation techniques may yield significantly different results. In this study, we used different versions to calculate the contributions of QED corrections, depending on the calculation results with which our data were compared.

Table 12 contains the calculated self-energy corrections for neutral alkali atoms. DFS data (columns 3–6) were obtained for different values of the parameter x_α.

These data were found as expectation values of the nonlocal radiative potential (12.27), because specifically this technique for calculating the self-energy correc-

Table 12: Self-energy corrections F(Zα) to the energies of valence levels in alkali atoms. PW (present work).

		DFS $x_\alpha = 0$	DFS $x_\alpha = 1/3$	DFS $x_\alpha = 2/3$	DFS $x_\alpha = 1$	DF
Li $2s_{1/2}$	PW	1.64	1.53	1.47	1.52	1.17
		1.56[a]	1.49[a]	1.44[a]	1.51[a]	1.13[b]
Na $3s_{1/2}$	PW	0.173	0.170	0.185	0.225	0.156
		0.169[a]	0.167[a]	0.181[a]	0.223[a]	0.155[b]
K $4s_{1/2}$	PW	0.0729	0.0729	0.0832	0.110	0.0732
		0.0720[a]	0.0721[a]	0.0829[a]	0.110[a]	0.0719[b]
Rb $5s_{1/2}$	PW	0.0230	0.0238	0.0285	0.0398	0.0264
		0.0228[a]	0.0236[a]	0.0283[a]	0.0396[a]	0.0244[b]
Cs $6s_{1/2}$	PW	0.0127	0.0133	0.0164	0.0237	0.0159
		0.0126[a]	0.0132[a]	0.0162[a]	0.0235[a]	0.0151[b]
Fr $7s_{1/2}$	PW	0.0070	0.0077	0.0101	0.0154	0.0115
		0.0068[a]	0.0075[a]	0.0098[a]	0.0150[a]	0.0107[b]

[a] - from [28]

[b] - from [30]

tions corresponds to the results of [28]. As can be seen in the table, the data that we obtained are in very good agreement with the results of [28]. Our data obtained by the DF method are also in good agreement with the results of [30] (Table 12, column 7). In this case, the self-energy corrections were also calculated as the expectation values of nonlocal radiative potential $\hat{V}_{\rm SE}$ (12.27) with DF wave functions. All data in Table 12 are presented in terms of dimensionless function $F(\alpha Z)$ (12.1).

The results of calculating the self-energy correction for the 2s-, $2p_{1/2}$- and $2p_{3/2}$-states of Li-like ions are listed in Table refLi-like. The table contains corrections caused by screening rather than directly QED contributions. These screening corrections were determined as differences in the self-energy contributions to the energy levels of Li-like ions and the corresponding contributions to the energies of

Table 13: Screening corrections to the contributions of self-energy to the ionization potentials of Li-like ions (in eV).

	Z	Level	DFS[a]	DF	[29]
Ca	20	$2s_{1/2}$	-0.0430	-0.0453	-0.0444
Sn	50	$2s_{1/2}$	-0.463	-0.484	-0.478
Bi	83	$2s_{1/2}$	-2.18	-2.25	-2.32
Ca	20	$2p_{1/2}$	-0.0078	-0.0085	-0.0083
Sn	50	$2p_{1/2}$	-0.109	-0.115	-0.124
Bi	83	$2p_{1/2}$	-0.979	-0.948	-1.069
Ca	20	$2p_{3/2}$	-0.0109	-0.0117	-0.0126
Sn	50	$2p_{3/2}$	-0.137	-0.145	-0.160
Bi	83	$2p_{3/2}$	-0.625	-0.653	-0.752

[a] - Calculated with $x_\alpha = 2/3$.

hydrogen-like ions. Our data, which are listed in columns 3 and 4 of Table 13, were obtained by the DFS method with parameter $x_\alpha = 2/3$ and by the DF method, respectively. The self-energy corrections were calculated as the differences between the total energies, taking into account radiative potential $\hat{V}_{\rm SE}$ (12.27) and disregarding it. Consideration of radiative potential $\hat{V}_{\rm SE}$ means that it was involved in the self-consistency procedure. The data obtained can be compared with the results of [29] (the last column of the table). On the whole, there is good agreement between the data obtained by different methods,despite the fact that, in [29], in contrast to our study, the electron–electron interaction was taken into account in the calculations of QED corrections based on the $1/Z$ perturbation theory

12.5 Conclusion

We proposed a new nonlocal single-particle potential to take into account the self-energy radiative corrections in calculations of the electric structure of many-electron ions and neutral atoms. A specific feature of this potential is that its addition to the Hamiltonian of a hydrogen-like ion causes shifts in the single-electron energies by values exactly coinciding with the self-energy corrections for H-like ions. The thus constructed nonlocal potential was used to calculate the self-energy corrections for a number of alkali atoms and Li-like ions by the single-configuration DF method and the DFS method. Furthermore, we plan to use the nonlocal potential proposed in this study, along with the Uehling potential [15] (which makes it possible to take into account the contribution of vacuum polarization), to calculate the electronic structure of neutral atoms and ions by the multiconfiguration DF method.

12.6 Bibliography

References

[1] T.A. Welton, Phys.Rev. **74**, 1157 (1948).

[2] V.A. Dzuba, V.V. Flambaum and O.P. Sushkov, Phys. Lett. A, **95**, 230 (1983).

[3] K.G. Dyall, I.P. Grant, C.T. Johnson, F.A. Parpia, E.P. Plummer. Comp. Phys. Comm, **55**, 425 (1989).

[4] P. Indelicato, J.P. Desclaux, Phys. Rev. A, **42**, 5139-5149 (1990).

[5] P. Pyykkö, M. Tokman, L.N. Labzowsky, Phys. Rev. A **57**, R689 (1999).

[6] I. I. Tupitsyn, V. M. Shabaev, J. R. Crespo López-Urrutia, I. Draganić, R. Soria Orts, and J. Ullrich, Phys.Rev. A, **68**, 022511 (2003).

[7] P. Pyykkö, L.B. Zhao, J.Phys.B, **36**, 1469 (2003).

[8] P. Pyykkö, Chem. Rev. **112** (1), 371 (2012)

[9] A. Pais, Verh. Kon. ned. Akad. Wet., **19** 1, Section 1 (1947).

[10] H.A. Bethe and E.E. Salpeter Quantum Mechanics of One- and Two-Electron Systems (Berlin: Springer) p. 103, (1947).

[11] B. Fricke and J.T. Waber, J.Chem.Phys. **57**, 371 (1972).

[12] M.V. Pak, A.V. Tulub, V.F. Brattsev, Opt. Spektr., **80**, 570 (1996), Engl. Transl. Opt.Spectr. **80**, 507 (1996).

[13] M.I. Eides, H. Grotch, V.A. Shelyuto, Phys. Reports, **342**, 63 (2001)

[14] V.V. Flambaum and J.S.M. Ginges, Phys. Rev. A **72**, 052115 (2005).

[15] E.A. Uehling, Phys. Rev. **48**, 55 (1935).

[16] W.R. Johnson, G. Soff, At. Data Nucl. Data Tables **33**, 405-446 (1985).

[17] P.J. Mohr, Yong-Ki. Kim, Phys.Rev.A, **45**, 2727 (1985).

[18] L.N. Labzowsky, G.L. Klimchitskaya and Y.Y. Dmitriev, Relativistic Effects in the Spectra of Atomic Systems, Bristol: Institute of Physics Publishing, p 66 (1993).

[19] T.H. Dinh, V.A. Dzuba, V.V. Flambaum, and J.S.M. Ginges, Phys. Rev. A, **78**, 022507, (2010).

[20] C. Thierfelder, P. Schwerdtfeger, Phys. Rev. A, **82**, 062503 (2010).

[21] V.B. Berestetskii, E.M. Lifschitz, and L.P. Pitaevskii, Relativistische Quantentheorie (Akademie Verlag, Berlin, 1991).

[22] M. Abramovitz and I.Stegun, Handbook of Mathematical Functions, NBS, 830, (1964).

[23] S. Kotochigova, P.J. Mohr, and B.N. Taylor, Can. J. Phys. **80**, 1373 (2002).

[24] V.F. Brattsev, G.B. Deyneka, and I.I. Tupitsyn, Bull.Acad.Sci. USSR, Phys. Ser. **41**, 173 (1977).

[25] J. C. Slater, Phys. Rev. **81**, 385 (1951).

[26] W. Kohn and L.J. Sham, Phys. Rev. **140**, A1133 (1965).

[27] R. Latter, Phys. Rev. **99**, 510 (1955).

[28] J. Sapirstein, Phys.Rev A. **66**, 042501 (2002).

[29] Y.S. Kozhedub, A.V. Volotka, A.N. Artemyev, D.A. Glazov, G. Plunien, V.M. Shabaev, I.I. Tupitsyn, and Th. Stöhlker, Phys.Rev. **81**, 042513 (2010).

[30] L. Labzowsky and I. Goidenko, M. Tokman and P. Pyykkö, Phys.Rev.A, **59**, 2707 (1999).

[31] A.V. Tulub, M.V. Pak, V.F. Brattsev, Opt. Spektr. v82, 533-535 (1997), Engl. Transl. Opt. Spectr. v82, 491-493 (1997).

[32] S.Boucard, P.Indelicato, Eur.Phys. J. D, v8, 59-73 (2000)

[33] V.A. Yerokhin, V.A. Shabaev, Phys. Rev. A, v64, 012506 (2001)

[34] V.V. Flambaum, J.S.M. Ginges, Phys. Rev. A, v72, 052115 (2005), See Table II. Further values for Fr and E119 given in private communication to P. Pyykko om January 27, 2011

[35] M.E.Rose,Relativistic Electron Theory, NY-London, John-Wiley & Sons (1960), 302p.

13 Hyperfine structure of laser-cooling transitions in fermionic Erbium-167

We have measured and analyzed the hyperfine structure of two lines, one at 583 nm and one at 401 nm, of the only stable fermionic isotope of atomic erbium as well as determined its isotope shift relative to the four most-abundant bosonic isotopes. Our work focuses on the $J \rightarrow J+1$ laser cooling transitions from the $[\mathrm{Xe}]4\mathrm{f}^{12}6\mathrm{s}^2(^3\mathrm{H}_6)$ ground state to two levels of the excited $[\mathrm{Xe}]4\mathrm{f}^{12}6\mathrm{s}6\mathrm{p}$ configuration, which are of major interest for experiments on quantum degenerate dipolar Fermi gases. From a fit to the observed spectra of the strong optical transition at $401\,\mathrm{nm}$ we find that the magnetic dipole and electric quadrupole hyperfine constants for the excited state are $A_e/h = -100.1(3)\,\mathrm{MHz}$ and $B_e/h = -3079(30)\,\mathrm{MHz}$, respectively. The hyperfine spectrum of the narrow transition at $583\,\mathrm{nm}$, was previously observed and accurate A_e and B_e coefficients are available. A simulated spectrum based on these coefficients agrees well with our measurements. We have also determined the hyperfine constants using relativistic configuration-interaction *ab-initio* calculations. The agreement between the *ab initio* and fitted data for the ground state is better than 0.1% , while for the two excited states the agreement is 1% and 11% for the A_e and B_e constants, respectively.

13.1 Introduction

The field of ultracold quantum gases has historically heavily relied on alkali-metal atoms. Only recently, the use of non-alkali-metal atoms has gained attention as a means to explore fascinating quantum phases of matter that are not accessible with alkali-metal species. Species with multiple unpaired valence electrons have rich atomic energy spectra and exhibit various types of coupling between the electronic angular momentum $\boldsymbol{J}$ and the nuclear spin $\boldsymbol{I}$ of the atom. For instance, fermionic

alkaline-earth-metal atoms have $J=0$ and $I\neq 0$ and the electronic and nuclear angular momenta decouple. This decoupling is at the center of proposals for efficient quantum simulation [1–3] and quantum magnetism [4–7]. Recently, degenerate Bose and Fermi gases of Ca [8], Sr [9–11], and the alkaline-earth-metal-like Yb atoms [12, 13] have been realized.

Lanthanides with submerged 4f-shell electrons are a novel class of atoms that attract attention in the field of ultracold quantum physics. Lanthanide atoms can have an exceptionally large electronic angular momentum $\boldsymbol{J}$ resulting from the alignment of the angular momenta of the submerged electrons. Consequently, these species can have strong magnetic moments μ as large as $10\,\mu_B$, where μ_B is the Bohr magneton. The mutual interaction is dominated by long-range magnetic dipole-dipole forces. Their dipolar character can be one hundred times larger than that for alkali-metal atoms. This key property makes lanthanides prime candidates for the study of atomic dipolar physics [14–16]. Dy [17, 18] and Er [19], with $\mu = 10\,\mu_{\mathrm{B}}$ and $7\,\mu_{\mathrm{B}}$, respectively, have been recently brought to quantum degeneracy while others are under investigation [20–22].

The success of quantum-degenerate-gas experiments relies on a precise understanding of the atomic properties, such as energy levels, hyperfine structures, and atomic polarizabilities. However, for unconventional atomic species, such as lanthanides, the available knowledge is in many instances insufficient for laser cooling and trapping purposes. Therefore, dedicated experiments need to be conducted en route to quantum degeneracy [21, 23–25].

In this paper, we present a combined experimental and theoretical investigation of the hyperfine structure of the only stable fermionic erbium isotope, ^{167}Er. In particular, we obtain the magnetic dipole, A, and electric quadrupole, B, hyperfine structure constants for the ground and two electronically excited states of ^{167} Er, which are relevant for laser cooling experiments [23, 26]. The two elec-

tronic excited states investigated are the one at a wavelength of $582.67\,\mathrm{nm}$ (corresponding to photon energy $E/(hc) = 17157.307\,\mathrm{cm}^{-1}$) and one at $400.796\,\mathrm{nm}$ ($E/(hc) = 24943.272\,\mathrm{cm}^{-1}$) from the ground state [27]. Here h is Planck's constant and c is the speed of light. In addition to the study of the hyperfine constants, we also obtained the isotope shift of ^{167}Er relative to the most-abundant bosonic isotopes. Our work provides important information for future experiments on quantum-degenerate Fermi gases of strongly dipolar Er atoms.

In a previous work, we used the optical transitions at about $401\,\mathrm{nm}$ and $583\,\mathrm{nm}$ for Zeeman slowing (ZS) and magneto-optical trapping (MOT) applications [26]. We demonstrated efficient laser cooling for five Er isotopes, including the fermionic one. However, the realization of a MOT of fermionic Er isotope was challenging since only the hyperfine structure of the ground and the $583\,\mathrm{nm}$-excited state were known [28, 29], while the one of the state at $401\,\mathrm{nm}$ was unknown prior to this work. To operate the Zeeman slower and the transversal cooling stage we had in fact to proceed empirically and try different locking points for the light at $401\,\mathrm{nm}$ before being able to produce a MOT of Fermions.

Figure 3 shows the atomic level scheme of Er. The electronic ground state belongs to the $[\mathrm{Xe}]4\mathrm{f}^{12}6\mathrm{s}^2$ configuration and has a large orbital angular momentum quantum number $L = 5$ (H state) and a total electronic angular momentum quantum number $J = 6$. The excited states at $401\,\mathrm{nm}$ and $583\,\mathrm{nm}$ belong to the $[\mathrm{Xe}]4\mathrm{f}^{12}6\mathrm{s}6\mathrm{p}$ configuration and have singlet $^1\mathrm{P}_1$ and triplet $^3\mathrm{P}_1$ character for the outer two valence electrons, respectively. Both excited states have a total electron angular momentum $J = 7$.

Erbium has six stable isotopes with natural abundance being 33.6 % for ^{166}Er, 26.8 % for ^{168}Er, 23.0 % for ^{167}Er , 14.9 % for ^{170}Er, 1.61 % for ^{164}Er, and 0.14 % for ^{162}Er. ^{167}Er is the only stable fermonic isotope. The bosonic isotopes have zero nuclear spin ($I = 0$) while the fermonic one has $I = 7/2$ and shows hyperfine

structure. All three electronic states of ^{167}Er have eight hyperfine levels ranging from $F = J - 7/2$ to $F = J + 7/2$, where $\boldsymbol{F} = \boldsymbol{J} + \boldsymbol{I}$.

13.2 Atomic spectroscopy

We measure the hyperfine structure of the ^{167}Er isotope using modulation-transfer spectroscopy [31]. The spectroscopy is performed on an atomic Er vapor created with a hollow cathode discharge lamp (HCL). The HCL, based on a sputtering process, has the advantage of providing atomic vapors without the need of a high-temperature atomic source.

We use a commercially available HCL, which is filled with an argon gas at a fixed pressure of $4\,\mathrm{mbar}$ [32]. By applying a high voltage on the electrodes, the argon gas is ionized and accelerated into the center of the Er-coated cathode. When hitting the surface the kinetic energy of the Ar-ions is high enough to free neutral erbium atoms by sputtering processes [33]. We typically operate the HCL with a voltage of $110\,\mathrm{V}$, giving a discharge current of $9.2\,\mathrm{mA}$.

We perform a Doppler-free modulation-transfer spectroscopy in the HCL [34, 35]. The laser beam is split into a pump and a probe beam, as shown in Fig. 4(a). The pump light is modulated with an electro-optical modulator (EOM) driven by a local oscillator (LO) at a frequency of $14.2\,\mathrm{MHz}$ and with a power of $23\,\mathrm{dBm}$ [36]. A four-wave mixing process transfers the sidebands from the modulated pump beam onto the counter-propagating probe beam [37]. We acquire the spectroscopy signal by mixing the LO signal with the probe beam signal detected by a photodiode (PD). By setting the LO and the signal either in-phase or shifted by π, one can obtain a signal proportional to the dispersion or to the absorption of the atomic sample, respectively. In our setup we use the dispersion signal.

In a first set of experiments, we measure the hyperfine structure and the isotope shift of the excited state at $401\,\mathrm{nm}$, with a natural linewidth of $2\pi \times 29.7(5)\,\mathrm{MHz}$

[38–40]. A frequency-doubled diode laser is used for the spectroscopy. Figure 4(b) shows the dispersive spectroscopy signal for this transition. The signal is averaged over 16 scans with a scanning speed of $2.4\,\mathrm{GHz/s}$ [41].

Our measurement reveals the full hyperfine structure for the fermionic ^{167}Er. The discussion and the assignment of the observed spectral features are given in Sec. 13.3. In addition, we determine the isotope shifts for the bosonic isotopes relative to ^{166}Er. We measure a shift of $-1681(14)\,\mathrm{MHz}$ for ^{170}Er, $-840(14)\,\mathrm{MHz}$ for ^{168}Er, and $+849(17)\,\mathrm{MHz}$ for ^{164}Er, which is in good agreement with Ref. [42]. The linewidths are extracted by fitting the derivative of a Lorentzian curve to the data. This gives an averaged value of $2\pi \times 88(8)\,\mathrm{MHz}$, corresponding to about three times the natural linewidth. This broadening of the transition can be explained as a combined effect of collisional and power broadening. For a number density of about $10^{17}\,\mathrm{cm}^{-3}$ and an argon background pressure of $4\,\mathrm{mbar}$, we calculate a collisional broadening of $2\pi \times 8.2\,\mathrm{MHz}$. Considering a total intensity of the pump and probe beams of $\mathscr{I} = 250\,\mathrm{mW/cm^2}$, we estimate a power broadening of a factor of $\sqrt{1 + \mathscr{I}/\mathscr{I}_0} = 2.3$ with $\mathscr{I}_0 = 60.3\,\mathrm{mW/cm^2}$ being the saturation intensity. Combining the two contributions, we estimate a broadened linewidth of $2\pi \times 81\,\mathrm{MHz}$, which is in agreement with the observed value.

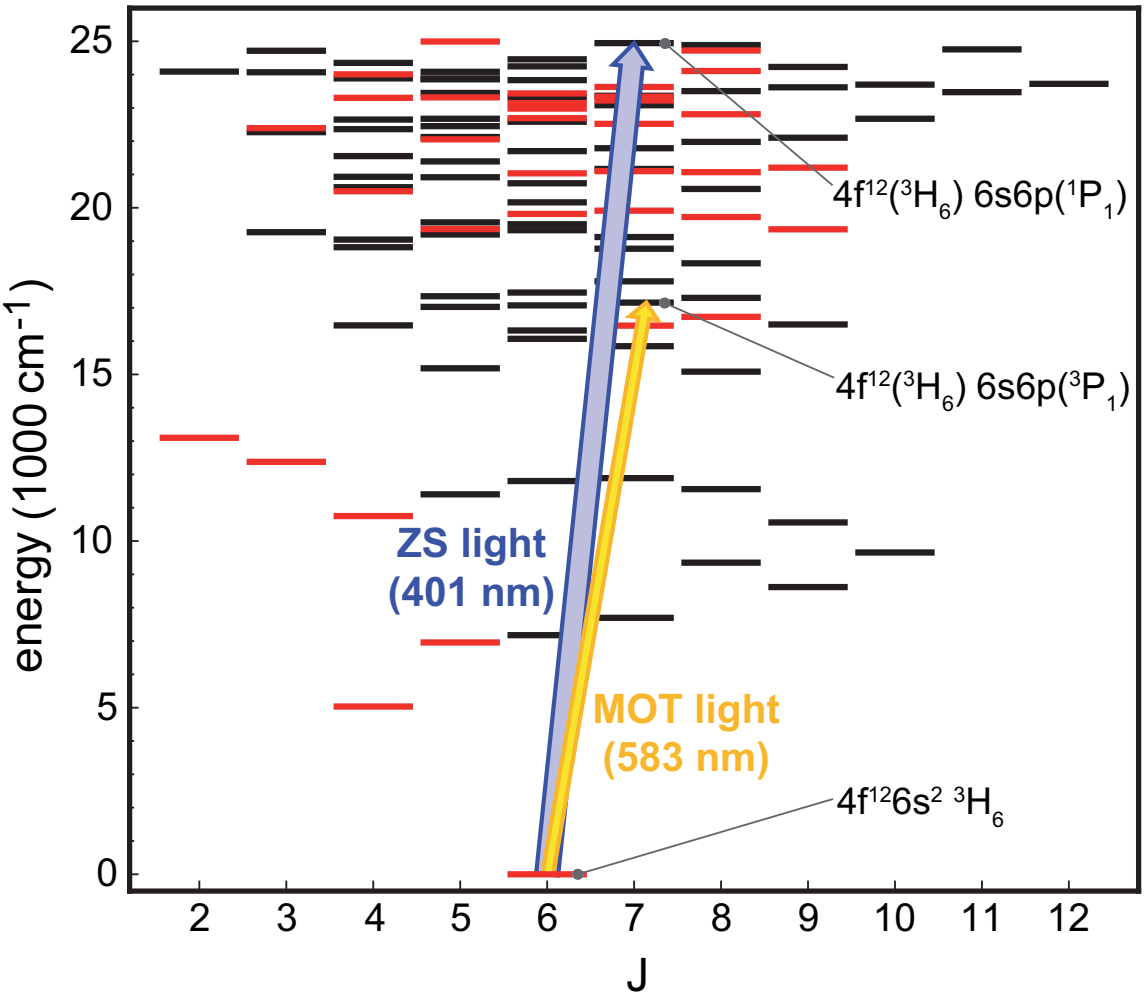

Figure 3: (Color online) Energy levels of atomic Er up to $E/(hc) = 25000\,\mathrm{cm}^{-1}$ for different electronic angular momentum quantum numbers J [27, 30]. States with odd (even) parity are indicated by black (red) horizontal lines. The two relevant laser-cooling transitions at $401\,\mathrm{nm}$ and $583\,\mathrm{nm}$ are indicated by arrows.

In a second set of measurements, we focus on the hyperfine structure of the excited state at $583\,\mathrm{nm}$, with a linewidth of $2\pi \times 186\,\mathrm{kHz}$ [43]. The spectroscopy is performed with a dye laser, which is frequency-stabilized to an ultra-low expansion cavity within 30 kHz [26]. We use a spectroscopy setup similar to the one described above for the 401 nm transition. Figure 4(c) shows the corresponding spectroscopy signal.

Despite the narrow-line nature of the transition, we could observe five features related to the hyperfine structure of the fermionic isotope and three features for the bosonic ones. The discussion of the hyperfine structure is given in Sec. 13.3. We measure an isotope shift of $-975(15)\,\mathrm{MHz}$ for ^{168}Er and $-1966(14)\,\mathrm{MHz}$ for ^{170}Er relative to ^{166}Er, respectively. These values are in good agreement with Ref. [29].

For this transition, we extract an averaged value for the linewidth of $2\pi \times 23(5)\,\mathrm{MHz}$, corresponding to about 120 times the natural linewidth. This large broadening can again be explained in term of collisional and power broadening. Considering the saturation intensity of $\mathscr{I}_0 = 0.13\,\mathrm{mW/cm^2}$ and our total intensity of $\mathscr{I} = 1.3 \times 10^3\,\mathrm{mW/cm^2}$, we calculate a power broadening of a factor of 100. Adding the effect of collisional broadening, we obtain an overall linewidth of $2\pi \times 19.3\,\mathrm{MHz}$, which is in agreement with the measured value. Because of this large broadening, we could operate the modulation-transfer spectroscopy at the same LO frequency as the one used for the 401 nm transition.

13.3 Analysis of hyperfine structure

In this section we describe our fitting procedure to the observed spectra of the five most abundant Er isotopes and we present the resulting hyperfine-structure constants A_e and B_e for ^{167}Er. The bosonic features are easily assigned as shown in Fig. 4. The remaining weaker features, which sometimes overlap with those from the bosonic isotopes, are due to ^{167}Er.

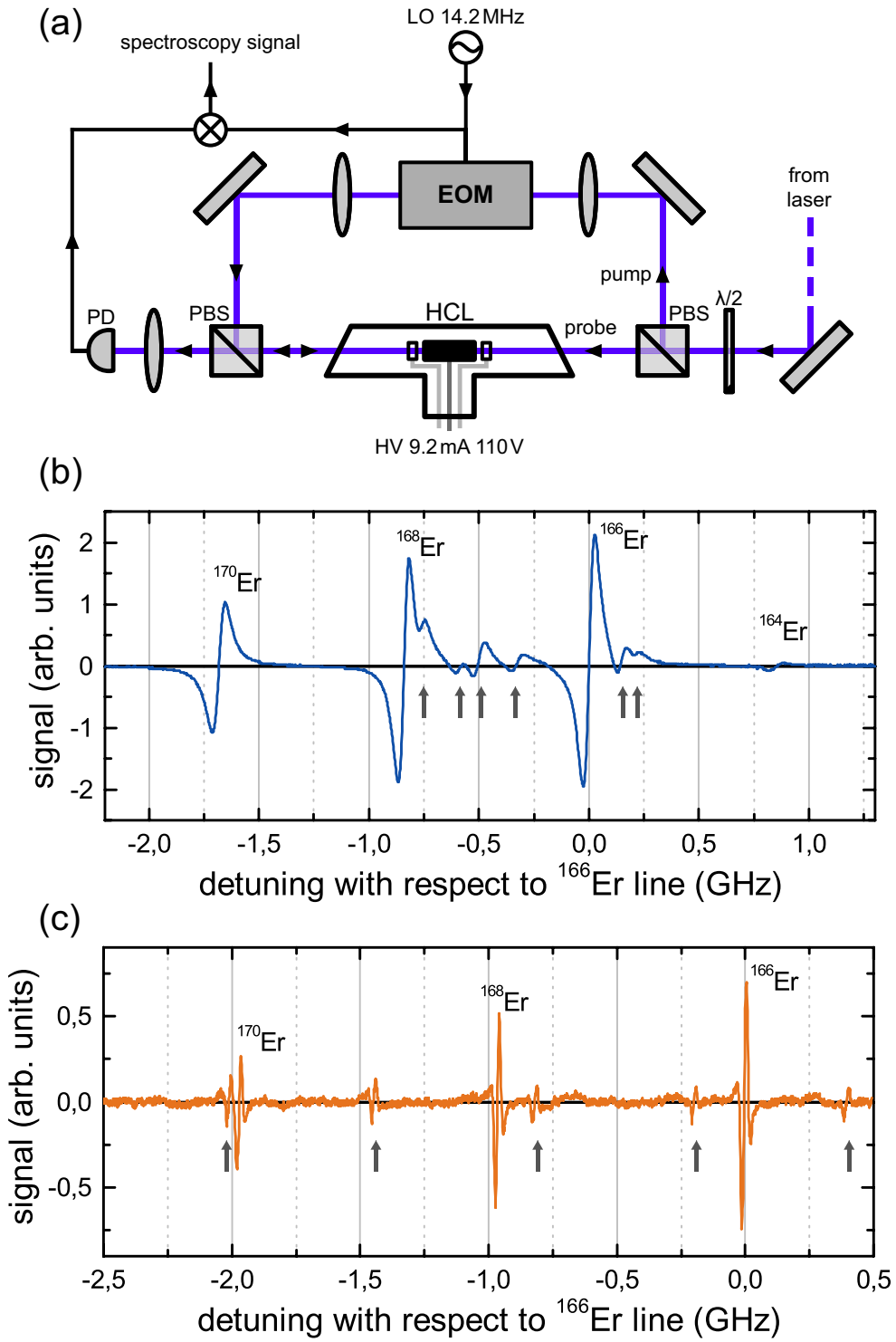

Figure 4: (Color online) Modulation transfer spectroscopy of Er for the 401 nm and 583 nm transitions. (a) Laser setup for spectroscopy on a hollow cathode discharge lamp (HCL); see text. The pump (probe) light has a power of 3.3 mW (0.6 mW) for the 401 nm transition and 20 mW (1 mW) for the 583 nm transition. (b), (c) Obtained spectroscopy signals for the 401 nm and the 583 nm transitions of different isotopes. Signals related to the hyperfine structure of ^{167}Er are indicated by arrows. The relative amplitudes of the observed signals reflect the natural isotope abundances.

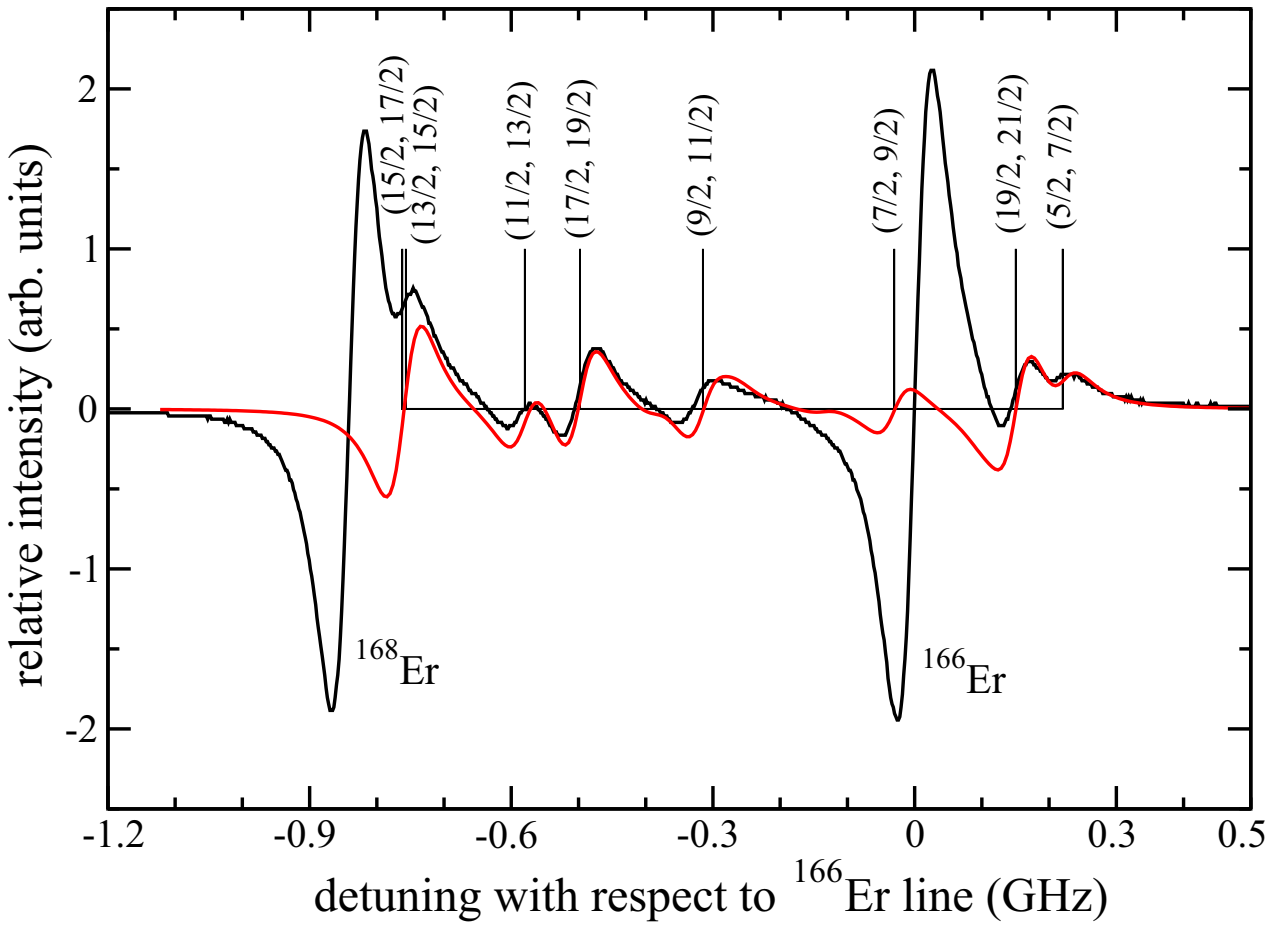

Figure 5: (Color online) Spectroscopy signal and hyperfine assignment of the 401 nm transition of the fermionic ^{167}Er. The black solid line is the recorded line. The red line is a simulated line shape obtained using a nonlinear fit to the line positions and a linewidth of $\gamma/(2\pi) = 90\,\mathrm{MHz}$. The simulated line shape is a sum of the first derivative of several Lorentzians, one for each hyperfine transition, whose relative strength is given by a theoretical estimate of the line strength. We scaled the overall size of the simulated lineshape to fit to the experiment. The assignment of the P-branch transitions ($F_g \rightarrow F_e = F_g + 1$) is shown by vertical lines and pairs (F_g, F_e). The hyperfine coefficients of the excited state are $A_e/h = -100.1\,\mathrm{MHz}$ and $B_e/h = -3079\,\mathrm{MHz}$.

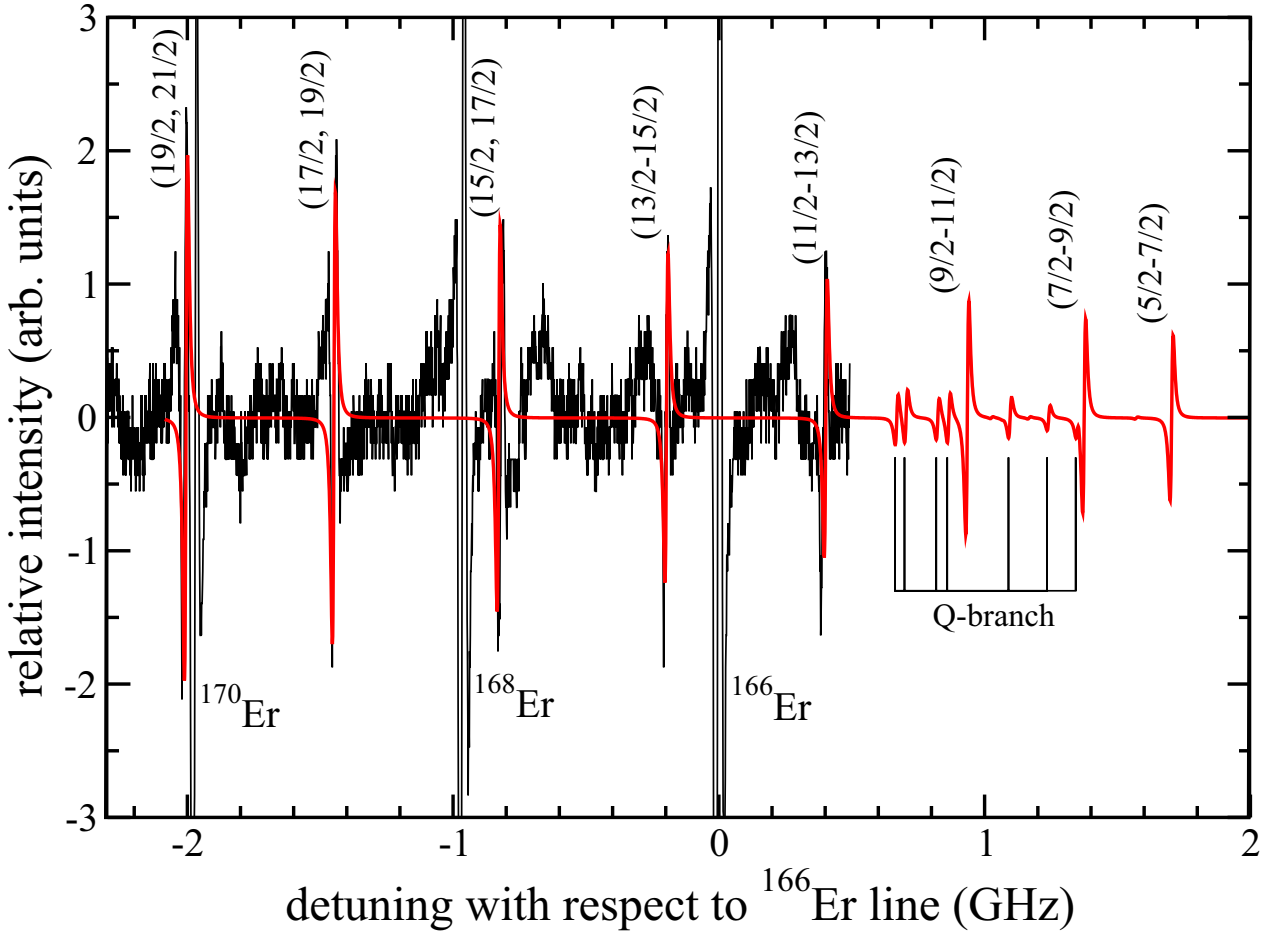

Figure 6: (Color online) Spectroscopy signal and hyperfine assignment of the 583 nm transition of the fermionic ^{167}Er. The solid black line is the experimental spectrum while the red line is a simulated line shape using a linewidth of $\gamma/(2\pi) = 20\,\mathrm{MHz}$. The P-branch transitions ($F_g \to F_e = F_g + 1$) are assigned by pairs (F_g, F_e). Three P-branch resonances and several Q-branch ($F_g \to F_e = F_g$) resonances are predicted to lie outside of the measurement range. The simulated line-shape is a sum of the first derivative of several Lorentzians, one for each hyperfine transition, whose relative strength is given by a theoretical estimate of the line strength. We scaled the overall size of the simulated line shape to fit to the experiment. The hyperfine coefficients of the excited state are $A_e/h = -172.7\,\mathrm{MHz}$ and $B_e/h = -4457.2\,\mathrm{MHz}$.

We start with the definition of the transition energies between the ground and an excited state of ^{167}Er including hyperfine interactions [44]

$$\hbar\omega_{F_eF_g} = \Delta_{167} + \hbar\omega_{166} + E_e(F_e, J_e, I) - E_g(F_g, J_g, I)\,, \tag{13.1}$$

where Δ_{167} is the ^{167}Er isotope shift relative to the transition energy $\hbar\omega_{166}$ of the bosonic ^{166}Er atom, the most abundant isotope, and $E_e(F_e, J_e, I)$ and $E_g(F_g, J_g, I)$ are hyperfine energies of the excited and ground state, respectively. The quantum numbers F_i and J_i with $i = e$ or g are the total atomic and electronic angular momentum of the excited and ground state, respectively, and

$$\begin{aligned} E_i(F_i, J_i, I) = &\frac{1}{2}A_i\,C_i \\ &+\frac{1}{2}B_i\frac{3C_i(C_i+1) - 4I(I+1)J_i(J_i+1)}{2I(2I-1)2J_i(2J_i-1)}\,, \end{aligned} \tag{13.2}$$

where $C_i = F_i(F_i+1) - J_i(J_i+1) - I(I+1)$. Finally, the transition energies $\Delta_A + \hbar\omega_{166}$ define the isotope shift for bosonic Er isotopes with atomic number A.

In addition to the resonance positions, we can calculate the line shape of the fermionic spectral features $S(\omega)$ by noting that the signal is well approximated by

$$S(\omega) \propto -\sum_{F_eF_g} Q_{F_e,F_g}\frac{d}{d\omega}\mathcal{L}(\omega - \omega_{F_eF_g}, \gamma) \tag{13.3}$$

as a function of laser frequency ω, where the sum is over all (F_g, F_e) hyperfine lines, and $\mathcal{L}(\omega, \gamma)$ is a Lorentzian centered around zero with linewidth γ [45]. Consequently, for an isolated line the resonance occurs when the signal is zero. The

fluorescence line strength Q_{F_e,F_g} is

$$\begin{aligned} Q_{F_e,F_g} &= \sum_{M_e M_g q} |\langle (J_g I) F_g M_g | d_{1q} | (J_e I) F_e M_e \rangle|^2 \\ &= \hat{F}_g \hat{F}_e \hat{J}_g \begin{pmatrix} F_g & F_e & 1 \\ J_e & J_g & I \end{pmatrix}^2 |\langle J_g || d || J_e \rangle|^2 , \end{aligned} \tag{13.4}$$

where the M_i are magnetic quantum numbers, d_{1q} is the electric dipole-moment operator, and we have assumed equal population for all hyperfine states $F_e M_e$ of the electronic excited state. Finally, $\hat{F} = 2F + 1$, $\begin{pmatrix} \cdots \\ \cdots \end{pmatrix}$ is a six-j symbol, and $\langle J_g || d || J_e \rangle$ is a reduced dipole matrix element independent of F_g and F_e.

We use a nonlinear least-squares fit to the experimental spectra to determine the hyperfine constants and isotope shift Δ_{167} of the excited states. The fit is based on six resolved hyperfine features for the 401 nm line and five resolved features for the narrow 583 nm line. In our analysis, we hold the hyperfine constants for the ground state to the literature values of $A_g/h = -120.487(1)$ MHz and $B_g/h = -4552.984(10)$ MHz [28], which have significantly lower uncertainties than those for the excited states.

Figure 5 and 6 are the results of our fit for the 401 nm and 583 nm line, respectively. We observe remarkable agreements between the simulated and experimental spectra. For the excited 401 nm level, we extract the best value for the hyperfine coefficients to be $A_e/h = -100.1(3)$ MHz and $B_e/h = -3079(30)$ MHz. Using these coefficients and those for the ground state, we obtain resonance positions that agree to better than 11 MHz with the experimental values. For the excited 583 nm level, we fit the line shape of the spectral features while the resonance positions are calculated by using the hyperfine constants of the excited states, $A_e/h = -172.7$ MHz and $B_e/h = -4457.2$ MHz, from Ref. [29]. We note that the additional structure in the experimental data, which is not fitting to the theoreti-

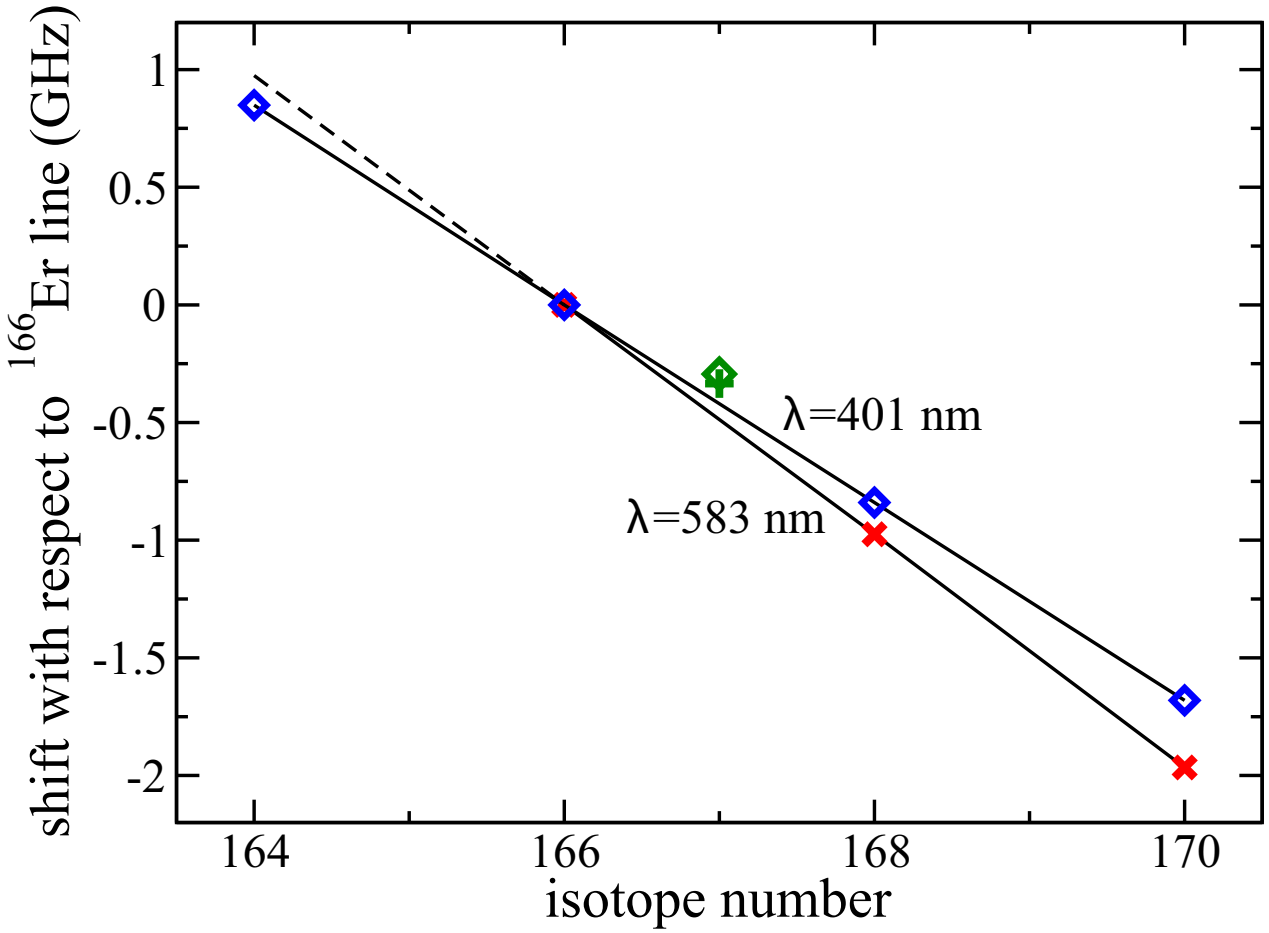

Figure 7: (color online). Isotope shifts for the 583 nm and 401 nm lines of the isotopes ^{164}Er up to ^{170}Er as a function of mass number where the transition energy for the bosonic isotope ^{166}Er is taken as energy reference. The isotope shift of the bosonic isotopes falls on a single straight line, with the isotope shift of the center of gravity of the fermionic ^{167}Er isotope, green cross and green square, is slightly displaced from this linear dependence.

cal curve, originates from a slightly misadjusted phase of the local oscillator in the spectroscopy setup. Table 14 compares the theoretical and experimental hyperfine energies $\Delta_{167} + E_e(F_e, J_e, I) + E_e(F_g, J_g, I)$ for the 583 nm and 401 nm transitions in ^{167}Er and lists the corresponding quantum numbers of F_g and F_e. Table 15 and Fig. 7 show the resulting isotope shifts Δ_A as a function of the mass number A relative to the energy of the ^{166}Er isotope.

Table 14: The observed and calculated hyperfine energies $\Delta_{167} + E_e(F_e, J_e, I) + E_e(F_g, J_g, I)$ for the 583 nm and 401 nm lines in ^{167}Er. The theoretical values are based on the hyperfine coefficients $A_e/h = -172.7$ MHz and $B_e/h = -4457.2$ MHz [29] for the 583 nm line and our values $A_e/h = -100.1$ MHz and $B_e/h = -3079$ MHz for the 401 nm line.

Obs. Energy (MHz)	Calc. Energy (MHz)	(F_g, F_e)	Obs. Energy (MHz)	Calc. Energy (MHz)	(F_g, F_e)
583 nm			401 nm		
−2011	−2011	(19/2, 21/2)	−761	−762	(15/2, 17/2)
−1449	−1454	(17/2, 19/2)	-	−757	(13/2, 15/2)
−820	−834	(15/2, 17/2)	−589	−580	(11/2, 13/2)
−200	−203	(13/2, 15/2)	−498	−498	(17/2, 19/2)
393	396	(11/2, 13/2)	−325	−315	(9/2, 11/2)
-	941	(9/2, 11/2)	-	−31	(7/2, 9/2)
-	1369	(7/2, 9/2)	150	150	(19/2, 21/2)
-	1709	(5/2, 7/2)	220	220	(5/2, 7/2)

13.4 *ab initio hyperfine constants*

In conjunction with the experimental measurements and fits, we have performed extensive *ab initio* electronic structure calculations of the magnetic dipole A and electric quadrupole B hyperfine constants. They describe the coupling of the nuclear spin $\boldsymbol{I}$ to the total electron angular momentum $\boldsymbol{J}$, due to the magnetic dipole and electric quadrupole interaction, respectively. The latter originates from the electric field gradient created by the electrons at the nuclear location. We were interested to reproduce the known constants for the Er ground state as well as those of the excited state at the 583 nm line obtained by Ref. [28, 29]. We can then confirm our measurement of the unknown constants of the excited level at the 401 nm line.

The *ab initio* calculations of the hyperfine structure constants have been performed using a relativistic multiconfiguration Dirac-Fock (MCDF) method [46]. In this method we perform an all-electron calculation of the wave function leading to an accurate description of the electron-spin density near the nucleus. The eigen-

Table 15: Observed isotope shift of the Er isotopes for the 583 nm and 401 nm lines. The transition energy for the bosonic isotope ^{166}Er is taken as energy reference. The isotope shift of the center of gravity of fermionic ^{167}Er was obtained from fitting.

Isotope	Obs. Energy (MHz)	Calc. Energy (MHz)	Obs. Energy (MHz)	Calc. Energy (MHz)
	583 nm		401 nm	
170	−1966(14)		−1681(14)	
168	−975(15)		−840(14)	
167		−337(11)		−297(6)
166	0		0	
164	-		+849(17)	

functions are superpositions of non orthogonal many-electron determinants of one-electron Dirac-Fock functions for the core and valence orbitals and Sturm functions for virtual orbitals. Both types of one-electron orbitals are optimized for either the $4f^{12}6s^2$ ground or $4f^{12}6s6p$ excited-state reference configurations.

The hyperfine splittings of atomic levels are due to interactions between electrons and nuclear multipole moments. In the configuration interaction picture and using atomic units the A and B constants are given by

$$A(J) = \frac{g_I \mu_N}{M_J} \langle \Psi, JM_J | \sum_i \frac{[\boldsymbol{r}_i \times \boldsymbol{\alpha}_i]_{00}}{r_i^3} | \Psi, JM_J \rangle \,, \tag{13.5}$$

$$B(J) = \frac{2Q}{M_J} \sqrt{\frac{2J(2J-1)(2J+1)}{(2J+2)(2J+3)}} \times \langle \Psi, JM_J | \sum_i \frac{Y_{20}(\hat{r}_i)}{r_i^3} | \Psi, JM_J \rangle \,, \tag{13.6}$$

where the sum i is over all electrons with positions $\boldsymbol{r}_i$ with respect to the nucleus, $Y_{\ell m}(\hat{r})$ are spherical harmonics, and $\boldsymbol{\alpha}_i$ is the Dirac matrix for electron i. Furthermore, g_I is the nuclear g-factor, μ_N is the nuclear magneton in atomic units, and Q is the nuclear quadrupole moment. The relativistic electronic eigenfunctions $|\Psi, JM_J\rangle = \sum_\beta c_\beta |\phi_\beta, JM_J\rangle$, obtained from the configuration-interaction calcu-

lations with relativistic determinants $|\phi_\beta, JM_J\rangle$ and CI coefficients c_β, have total angular momentum J and projection M_J.

When an atom has open or unfilled electron shells, it leads to an unbalanced electron-spin density near the location of the nucleus. As hyperfine constants are proportional to the difference in electron-spin densities this leads to nonzero A and B coefficients. To account for this effect we use a model, where the single-electron orbitals differ for each spin direction or more precisely for each spinor of the Dirac-Fock equation. Alternatively, this implies different exchange potentials for electrons with spin up or down.

We use three restricted active spaces (RAS) to classify the electron Dirac-Fock and Sturm orbitals, ensuring an efficient and compact CI expansion that, nevertheless, remains accurate. The first group of orbitals, RAS1, contains the occupied spinors of the relevant reference configuration. We have studied convergence of the hyperfine structure constants as the active set of orbitals was systematically increased. For our most-precise Er atom calculation RAS1 includes the occupied $1s^2, 2s^2, 2p_{1/2}^2, 2p_{3/2}^4$, ..., and $4f_{5/2}^6$ shell electrons. We allow up to one electron to be excited out of RAS1 into the two other active spaces. The second group, RAS2, contains the open-shell $4f_{7/2}^6$, $6s_{1/2}^2$, and $6p_{1/2}, 6p_{3/2}$ spinors, while the third group, RAS3, contains spinors that are unoccupied in the reference configuration. These latter virtual Sturm orbitals are the high-lying s-wave spinors from $7s$ up to $13s$, p-wave spinors from $7p$ up to $11p$, and the $5d$-spinor. For both RAS2 and RAS3 we allow up to two electrons to enter or leave.

With this basis our finite-nuclear-size and finite-nuclear mass corrected *ab initio* values of the A and B hyperfine constants are -120.42 MHz and -4554 MHz for the ground state level, -174 MHz and -4057 MHz for the excited level at 583 nm, and -100 MHz and -3424 MHz for the excited level at 401 nm, respectively. Consequently, the *ab initio* A constants agree with experimentally determined values to

better than 1%, whereas the B constants differ by up to 11% for the two excited states. For the ground state the agreement for the B constant is also better than 1%.

13.5 Conclusion

We have used laser modulation-transfer spectroscopy on atomic Er as well as performed *ab initio* electronic structure calculations of Er to obtain the magnetic dipole and electric quadrupole constants for the only stable fermionic isotope, ^{167}Er. We focused on transitions from the $4f^{12}6s^2$ ($J = 6$) ground state to two $J = 7$ levels within the excited $4f^{12}6s6p$ configuration. A least-squares algorithm applied to the experimentally-measured hyperfine-structure energies gives accurate values for the two constants as well as values for the isotope shift of five isotopes. The *ab initio* calculation is based on a multiconfiguration Dirac-Fock method where we allow no more than two electrons to be excited from and between the active spaces. The method has no further adjustable parameters.

Our results are summarized in Table 16 and Fig. 8. We find that the *ab initio* A coefficients for all three states and the B coefficient for the ground state agree to better than 1% with the experimental values, which is in a surprisingly good agreement considering the complex electron-shell structure of the Er atom. We note that the *ab initio* electric quadrupole constants B for the two excited states exhibit a larger deviation from the experimental values. This might be a consequence of missing key configurations: the excited states have three open shells, $4f^{12}$, $6s$, and $6p$, from which more than two electrons might need to be excited. In addition, Sternheimer shielding (e.g., distortions in the electron shells by the nuclear quadrupole moment), which is not considered in our MCDF theory, might cause significant corrections.

Table 16: A summary of the relevant hyperfine A and B constants for ground and excited states (e.s.) usable for laser-cooling of ^{167}Er.

state	J	A/h (MHz)	B/h (MHz)	Ref.
ground state	6	−120.487(1)	−4552.984(10)	[28]
ab initio		−120.42	−4554	this work
583-nm e.s.	7	−172.70(7)	−4457.2(29)	[29]
ab initio		−174	−4057	this work
401-nm e.s.	7	−100.1(3)	−3079(30)	this work
ab initio		−100	−3424	this work

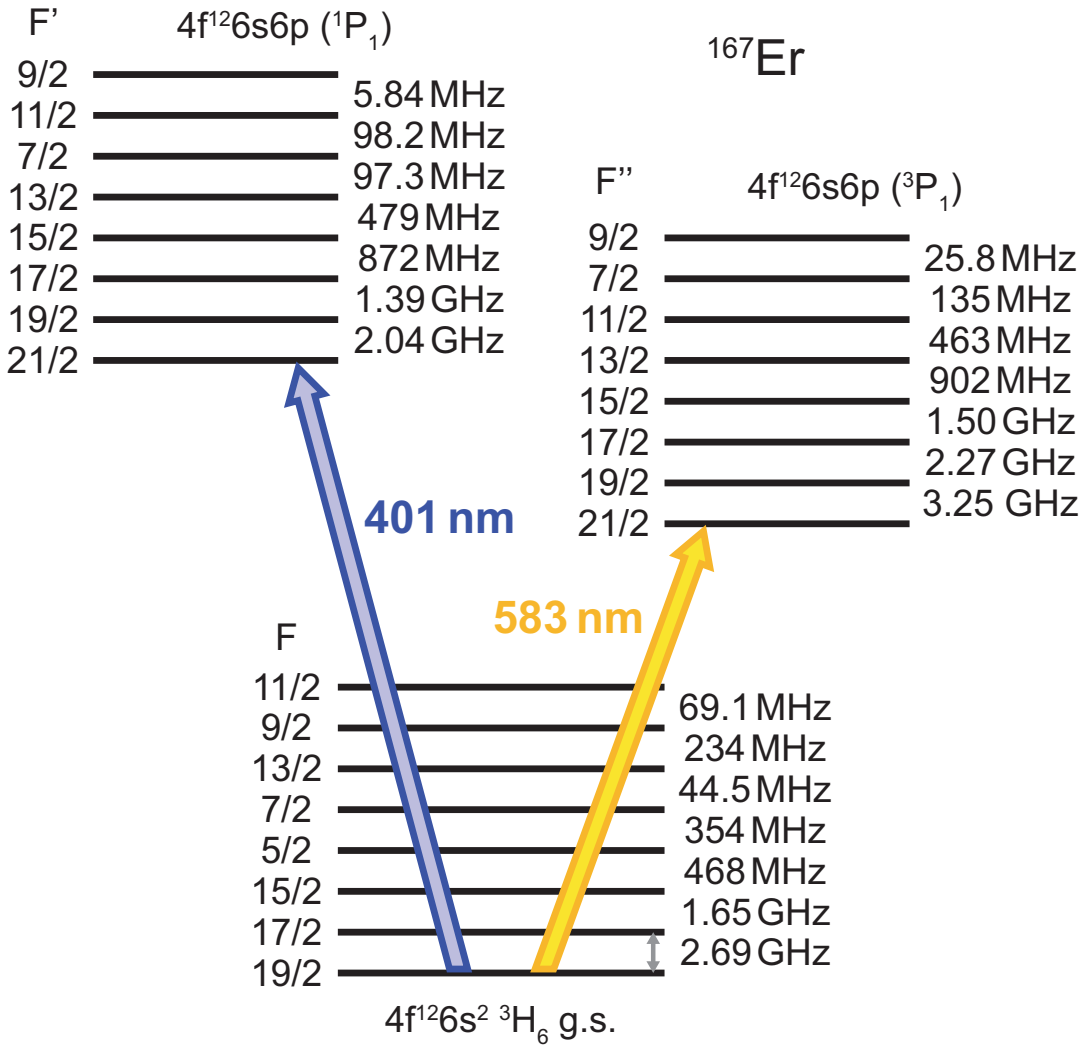

Figure 8: (Color online) Hyperfine levels of the ground (g.s.) and two excited states of ^{167}Er with particular interest for laser cooling. The level splitting was calculated using A and B constants given in Table 16 for the respective transitions. The arrows depict two laser-cooling transitions. The transition at 401 nm used for Zeeman slowing is shown in blue and the transition used for magneto-optical trapping at 583 nm is shown in yellow.

References

[1] A. J. Daley, M. M. Boyd, J. Ye, and P. Zoller, Phys. Rev. Lett. **101**, 170504 (2008).

[2] R. Stock, N. S. Babcock, M. G. Raizen, and B. C. Sanders, Phys. Rev. A **78**, 022301 (2008).

[3] A. V. Gorshkov, A. M. Rey, A. J. Daley, M. M. Boyd, J. Ye, P. Zoller, and M. D. Lukin, Phys. Rev. Lett. **102**, 110503 (2009).

[4] M. Hermele, V. Gurarie, and A. M. Rey, Phys. Rev. Lett. **103**, 135301 (2009).

[5] A. Gorshkov, M. Hermele, V. Gurarie, C. Xu, P. Julienne, J. Ye, P. Zoller, E. Demler, M. D. Lukin, and A. M. Rey, Nature Phys. **6**, 289 (2010).

[6] M. Foss-Feig, M. Hermele, V. Gurarie, and A. M. Rey, Phys. Rev. A **82**, 053624 (2010).

[7] H.-H. Hung, Y. Wang, and C. Wu, Phys. Rev. B **84**, 054406 (2011).

[8] S. Kraft, F. Vogt, O. Appel, F. Riehle, and U. Sterr, Phys. Rev. Lett. **103**, 130401 (2009).

[9] S. Stellmer, M. K. Tey, B. Huang, R. Grimm, and F. Schreck, Phys. Rev. Lett. **103**, 200401 (2009).

[10] Y. N. Martinez de Escobar, P. G. Mickelson, M. Yan, B. J. DeSalvo, S. B. Nagel, and T. C. Killian, Phys. Rev. Lett. **103**, 200402 (2009).

[11] S. Stellmer, R. Grimm, and F. Schreck, Phys. Rev. A **84**, 043611 (2011).

[12] Y. Takasu, K. Maki, K. Komori, T. Takano, K. Honda, M. Kumakura, T. Yabuzaki, and Y. Takahashi, Phys. Rev. Lett. **91**, 040404 (2003).

[13] T. Fukuhara, Y. Takasu, M. Kumakura, and Y. Takahashi, Phys. Rev. Lett. **98**, 030401 (2007).

[14] M. A. Baranov, Physics Reports **464**, 71 (2008).

[15] T. Lahaye, C. Menotti, L. Santos, M. Lewenstein, and T. Pfau, Rep. Prog. Phys. **72**, 126401 (2009).

[16] M. A. Baranov, M. Dalmonte, G. Pupillo, and P. Zoller, Chem. Rev. **112**, 5012 (2012).

[17] M. Lu, N. Q. Burdick, S. H. Youn, and B. L. Lev, Phys. Rev. Lett. **107**, 190401 (2011).

[18] M. Lu, N. Q. Burdick, and B. L. Lev, Phys. Rev. Lett. **108**, 215301 (2012).

[19] K. Aikawa, A. Frisch, M. Mark, S. Baier, A. Rietzler, R. Grimm, and F. Ferlaino, Phys. Rev. Lett. **108**, 210401 (2012).

[20] M. Saffman and K. Mølmer, Phys. Rev. A **78**, 012336 (2008).

[21] D. Sukachev, A. Sokolov, K. Chebakov, A. Akimov, S. Kanorsky, N. Kolachevsky, and V. Sorokin, Phys. Rev. A **82**, 011405 (2010).

[22] D. Sukachev, K. Chebakov, A. Sokolov, A. Akimov, N. Kolachevsky, and V. Sorokin, Opt. Spectrosc. **111**, 633 (2011).

[23] J. J. McClelland and J. L. Hanssen, Phys. Rev. Lett. **96**, 143005 (2006).

[24] S. H. Youn, M. Lu, U. Ray, and B. L. Lev, Phys. Rev. A **82**, 043425 (2010).

[25] V. A. Dzuba, V. V. Flambaum, and B. L. Lev, Phys. Rev. A **83**, 032502 (2011).

[26] A. Frisch, K. Aikawa, M. Mark, A. Rietzler, J. Schindler, E. Zupanic, R. Grimm, and F. Ferlaino, Phys. Rev. A **85**, 051401 (2012).

[27] Y. Ralchenko, A. Kramida, J. Reader, and N. A. Team, NIST Atomic Spectra Database (2011).

[28] W. J. Childs, L. S. Goodman, and V. Pfeufer, Phys. Rev. A **28**, 3402 (1983).

[29] W. G. Jin, T. Horiguchi, M. Wakasugi, and Y. Yoshizawa, J. Phys. Soc. Jpn. **59**, 3148 (1990).

[30] H. Y. Ban, M. Jacka, J. L. Hanssen, J. Reader, and J. J. McClelland, Opt. Exp. **13**, 3185 (2005).

[31] J. H. Shirley, Opt. Lett. **7**, 537 (1982).

[32] Manufacturer Heraeus Noblelight GmbH, model number 3QQAYEr.

[33] T. Musha, J. Phys. Soc. Jpn. **17**, 1440 (1962).

[34] J. E. Lawler, A. Siegel, B. Couillaud, and T. W. Hansch, J. Appl. Phys. **52**, 4375 (1981).

[35] H. Brammer, J. Ulitzsch, R. Bourouis, and M. Weitz, Appl. Phys. B **106**, 405 (2012).

[36] The modulation frequency is chosen such that the steepness of the spectroscopy signal is maximized, according to [37].

[37] D. J. McCarron, S. A. King, and S. L. Cornish, Meas. Sci. Technol. **19**, 105601 (2008).

[38] Prior to our work on ultracold atoms, two values of the natural linewidth were available in literature, $2\pi \times 35.6(1.2)\,\mathrm{MHz}$ [39] and $2\pi \times 29.5(1.6)\,\mathrm{MHz}$ [40]. Our measurement is based on absorption imaging experiments on magneto-optically trapped atoms of three bosonic isotopes. Our value of

$2\pi \times 29.7(5)\,\mathrm{MHz}$ confirms the findings of Ref. [40]. We note that our previous value of $2\pi \times 27.5(4)\,\mathrm{MHz}$ [26] was affected by calibration issues.

[39] J. J. McClelland, Phys. Rev. A **73**, 064502 (2006).

[40] J. E. Lawler, J.-F. Wyart, and E. A. D. Hartog, J. Phys. B: At. Mol. Opt. Phys. **43**, 235001 (2010).

[41] The frequency is monitored during recording the spectroscopy signal and the systematic uncertainty due to nonlinear scanning is estimated to be $12\,\mathrm{MHz}$.

[42] C. B. Connolly, Y. S. Au, S. C. Doret, W. Ketterle, and J. M. Doyle, Phys. Rev. A **81**, 010702 (2010).

[43] E. A. D. Hartog, J. P. Chisholm, and J. E. Lawler, J. Phys. B **43**, 155004 (2010).

[44] E. Arimondo, M. Inguscio, and P. Violini, Rev. Mod. Phys. **49**, 37 (1977).

[45] Pressure broadening, giving a Gaussian contribution to the full profile, is small and can thus be neglected.

[46] P. Villemoes, R. van Leeuwen, A. Arnesen, F. Heijkenskjöld, A. Kastberg, M. O. Larsson, and S.A. Kotochigova, Phys. Rev. A **45**, 6241 (1992).

14 Weighted difference of g-factors of light Li-like and H-like ions for an improved determination of the fine-structure constant

A weighted difference of the g-factors of the Li- and H-like ion of the same element is studied and optimized in order to maximize the cancellation of nuclear effects. To this end, a detailed theoretical investigation is performed for the finite nuclear size correction to the one-electron g-factor, the one- and two-photon exchange effects, and the QED effects. The coefficients of the $Z\alpha$ expansion of these corrections are determined, which allows us to set up the optimal definition of the weighted difference. It is demonstrated that, for moderately light elements, such weighted difference is nearly free from uncertainties associated with nuclear effects and can be utilized to extract the fine-structure constant from bound-electron g-factor experiments with an accuracy competitive with or better than its current literature value.

14.1 Introduction

Modern measurements of the bound-electron g-factor in H-like ions have reached the level of fractional accuracy of 3×10^{-11} [43]. Experiments have also been performed with Li-like ions [44]. In future it shall be possible to conduct similar experiments not only with a single ion in the trap, but also with several ions simultaneously. Such a setup would allow one to directly access differences of the g-factors of different ions, thus largely reducing systematic uncertainties and possibly gaining about two orders of magnitude in experimental accuracy [46]. So, experimental investigations of differences of the bound-electron g factors on a sub-10^{-12} level look feasible in the future. Such measurements would become sensitive to the uncertainty of the fine-structure constant α, which is presently known up to

the fractional accuracy of 3×10^{-10} [36]. It might be tempting to use such future experiments as a tool for an independent determination of α.

In order to accomplish a competitive determination of α from the bound-electron g-factor experiments, one has to complete theoretical calculations to a matching accuracy, which is a challenging task. One of the important problems on the way is the uncertainty due to nuclear effects, which cannot be well understood at present. These uncertainties set a limitation on the ultimate accuracy of the theoretical description and, therefore, on the determination of α.

There is a way to reduce the nuclear effects and the associated uncertainties, by forming differences of different charge states of the same element. In Ref. [37], it was suggested to use a weighted difference of the g-factors of the H- and Li-like ions of the same element in order to suppress the nuclear size effects by about two orders of magnitude for high-Z ions. In Ref. [38], a weighted difference of the g-factors of B-like and H-like charge states of the same element was proposed. It was shown that the theoretical uncertainty of the nuclear size effect for ions around Pb can be reduced to 4×10^{-10}, which was several times smaller than the uncertainty due to the fine-structure constant at the time of publication of Ref. [38]. Since then, however, the uncertainty of α was decreased by an order of magnitude [40–42], thus making it more difficult to access it in the bound-electron g-factor experiments. In our recent Letter [10] we proposed a weighted difference of the g-factors of low-Z Li-like and H-like ions, for which a more significant cancellation of nuclear effects can be achieved. In the present paper we describe details of the underlying calculations and report extended numerical results for the finite nuclear size corrections.

In our approach, the weight Ξ of the specific difference of the g-factors is determined on the basis of studying the $Z\alpha$ and $1/Z$ expansions of various finite nuclear size (fns) corrections, in such a way that the cancellation of these undesirable contributions is maximized. We introduce the following Ξ-weighted difference of the

bound-electron g-factors of the Li-like and H-like charge states of the same element,

$$\delta_{\Xi} g = g(2s) - \Xi\, g(1s)\,, \tag{14.1}$$

where $g(2s)$ is the g-factor of the Li-like ion, $g(1s)$ is the g-factor of the H-like ion, and the parameter Ξ is defined as

$$\Xi = 2^{-2\gamma-1}\left[1+\frac{3}{16}(Z\alpha)^2\right]\left(1-\frac{2851}{1000}\frac{1}{Z}+\frac{107}{100}\frac{1}{Z^2}\right)\,, \tag{14.2}$$

with the notation $\gamma = \sqrt{1-(Z\alpha)^2}$. The justification of this choice of Ξ will be given later, after studying the contributions of individual physical terms to the fns effect.

This article is organized as follows. In Section 14.2 we describe our calculations of various fns contributions, namely, the leading one-electron fns effect, the fns correction from the one-electron QED effects, and the two- and three-electron fns corrections due to the exchange of one or more photons between the electrons. The resulting weighted difference of the g-factors and its utility in determining the fine-structure constant are discussed in Section 14.3, which is followed by a short conclusion.

14.2 Finite nuclear size corrections

14.2.1 One-electron finite nuclear size

The leading one-electron fns correction to the bound-electron g-factor is defined as follows:

$$\delta g_{\rm N}^{(0)} = g_{\rm ext}^{(0)} - g_{\rm pnt}^{(0)}\,, \tag{14.3}$$

where $g^{(0)}_{\rm ext}$ and $g^{(0)}_{\rm pnt}$ are the leading-order bound-electron g factor values calculated assuming the extended and the point-like nuclear models, respectively. The leading-order bound-electron g factor is obtained for ns states as

$$g^{(0)} = -\frac{8}{3}\int_0^\infty dr\, r^3\, g_a(r)\, f_a(r)\,, \tag{14.4}$$

where g_a and f_a are the upper and the lower radial components of the ns Dirac wave function, respectively [11].

The fns correction $\delta g^{(0)}_{\rm N}$ has an approximate relation to the corresponding correction to the Dirac energy, which reads [12] for ns states as

$$\delta g^{(0)}_{\rm N} = \frac{4}{3}\,(2\gamma+1)\,\frac{\delta E_{\rm N}}{m}\,, \tag{14.5}$$

where $\delta E_{\rm N}$ is the nuclear-size correction to the Dirac energy. Eq. (14.5) is exact in the nonrelativistic limit and also holds with a reasonable accuracy in the whole region of nuclear charge numbers Z. Using Eq. (14.5) and the result of Ref. [13] for $\delta E_{\rm N}$, the leading one-electron fns effect for ns states can be parameterized as

$$\delta g^{(0)}_{\rm N} = \frac{2}{5}\left(\frac{2\,Z\alpha\,R_{\rm sph}}{n}\right)^{2\gamma}\,\frac{(Za)^2}{n}\,\left[1+(Za)^2\,H_n^{(0,2+)}\right]\,, \tag{14.6}$$

where $R_{\rm sph} = \sqrt{5/3}\,R$ is the radius of the nuclear sphere with the root-mean-square (rms) charge radius R and $H_n^{(0,2+)}$ is the remainder due to relativistic effects. The superscript $(0,2+)$ indicates that its contribution is of zeroth order in $1/Z$ and of second and higher orders in $Z\alpha$. The nonrelativistic limit of Eq. (14.6) agrees with the well-known result of Refs. [47, 48].

The leading relativistic correction $H_n^{(0,2)}$ has been given in a closed analytical form in Ref. [48]. We deduce from it that the difference of the relativistic corrections of relative order $(Za)^2$ for $2s$ and $1s$ states does not depend on the nuclear charge

radius nor on the nuclear charge distribution model, and is just a constant:

$$H_{21}^{(0,2)} \equiv H_2^{(0,2)} - H_1^{(0,2)} = \frac{3}{16}\,. \tag{14.7}$$

In the present work we calculate the nuclear-size correction $\delta g_{\rm N}^{(0)}$ numerically. For the extended nucleus, the radial Dirac equation is solved with the Dual Kinetic Balance (DKB) method [49], which allows us to determine $g_{\rm ext}^{(0)}$ with a very high accuracy. The nuclear-size correction is obtained by subtracting the analytical point-nucleus result. In order to avoid loss of numerical accuracy in the low-Z region, we used the DKB method implemented in the quadruple (about 32 digits) arithmetics.

In our calculations, we used three models of the nuclear charge distribution. The two-parameter Fermi model is given by

$$\rho_{\rm Fer}(r) = \frac{N}{1+\exp[(r-r_0)/a]}\,, \tag{14.8}$$

where r_0 and a are the parameters of the Fermi distribution, and N is the normalization factor. The parameter a was fixed by the standard choice of $a = 2.3/(4\ln 3) \approx 0.52$ fm. The homogeneously charged sphere distribution of the nuclear charge is given by

$$\rho_{\rm Sph}(r) = \frac{3}{4\pi R_{\rm sph}^3}\,\theta(R_{\rm Sph}-r)\,, \tag{14.9}$$

where θ is the Heaviside step function. The Gauss distribution of the nuclear charge reads

$$\rho_{\rm Gauss}(r) = \left(\frac{3}{2\pi R^2}\right)^{3/2} \exp\left(-\frac{3\,r^2}{2R^2}\right)\,. \tag{14.10}$$

The results of our calculations for the $2s$ and $1s$ states are presented in Table 17,

expressed in terms of the function $H_n^{(0,2+)}$. Experimental values of the rms nuclear charge radii R are taken from Ref. [17]. For ions with $Z \geq 10$, we perform calculations with the Fermi and the homogeneously charged sphere models. The difference of the values obtained with these two models is taken as an estimation of the model dependence of the results. For ions with $Z < 10$, the Fermi model is no longer adequate and we use the Gauss model instead.

We observe that the model dependence of the relativistic fns correction $H_n^{(0,2+)}$ is generally not negligible; it varies from 1% in the medium-Z region to 5% in the low-Z region. However, the model dependence of the difference $H_2^{(0,2+)} - H_1^{(0,2+)}$ is tiny. According to Eq. (14.7), it is suppressed by a small factor of $(Za)^2$. Our calculations show that in addition it is suppressed by a small numerical coefficient.

We conclude that both the model dependence and the R uncertainty of the one-electron fns correction can be cancelled up to a very high accuracy by forming a suitably chosen difference. The following weighted difference of the $2s$ and $1s$ one-electron g-factors cancels the one-electron fns contributions of relative orders $(Za)^0$ and $(Za)^2$,

$$\delta_{\Xi_0} g = g^{(0)}(2s) - \Xi_0\, g^{(0)}(1s)\,, \tag{14.11}$$

with the weight

$$\Xi_0 = 2^{-2\gamma-1}\left[1 + \frac{3}{16}(Z\alpha)^2\right]. \tag{14.12}$$

The one-electron fns effects in the difference $\delta_{\Xi_0} g$ arise only in the relative order $(Za)^4$, with a numerically small coefficient.

Table 17: The relativistic fns correction, in terms of function $H_n^{(0,2+)}$ defined by Eq. (14.6), for the $2s$ state ($n = 2$) and the $1s$ state ($n = 1$), for different models of the nuclear charge distribution. The rms charge radii R and their errors are taken from the compilation of Ref. [17].

Z	R [fm]	Model	$H_2^{(0,2+)}$	$H_1^{(0,2+)}$	$H_2^{(0,2+)} - H_1^{(0,2+)} - 3/16$
6	2.4702(22)	Gauss	0.9296(3)	0.7421(3)	0.00003
		Sphere	0.9827(3)	0.7951(3)	0.00007
8	2.6991(52)	Gauss	0.9912(6)	0.8035(5)	0.0001
		Sphere	1.0408(5)	0.8531(5)	0.0002
10	3.0055(21)	Fermi	1.0248	0.8370	0.0003
		Sphere	1.0700(2)	0.8822(2)	0.0003
12	3.0570(16)	Fermi	1.0690	0.8810	0.0005
		Sphere	1.1067(1)	0.9186(1)	0.0006
14	3.1224(24)	Fermi	1.1001(1)	0.9118(1)	0.0008
		Sphere	1.1327(1)	0.9443(1)	0.0009
20	3.4776(19)	Fermi	1.1542(1)	0.9647(1)	0.0020
		Sphere	1.1764(1)	0.9868(1)	0.0021
25	3.7057(22)	Fermi	1.1843	0.9934	0.0034
		Sphere	1.2030(1)	1.0119(1)	0.0035
30	3.9283(15)	Fermi	1.2085	1.0159	0.0051
		Sphere	1.2246	1.0319(1)	0.0053
35	4.1629(21)	Fermi	1.2297(1)	1.0350	0.0071
		Sphere	1.2438	1.0490(1)	0.0073
40	4.2694(10)	Fermi	1.2518	1.0548	0.0095
		Sphere	1.2652(1)	1.0679	0.0098
45	4.4945(23)	Fermi	1.2714(1)	1.0718	0.0121
		Sphere	1.2834(1)	1.0836(1)	0.0123
50	4.6519(21)	Fermi	1.2920	1.0897	0.0148
		Sphere	1.3033(1)	1.1006	0.0151
55	4.8041(46)	Fermi	1.3129(1)	1.1077	0.0177
		Sphere	1.3235(1)	1.1180(1)	0.0180
60	4.9123(25)	Fermi	1.3346(1)	1.1265	0.0206
		Sphere	1.3447	1.1363(1)	0.0209

14.2.2 One-electron QED fns correction

The one-electron QED fns correction $\delta g^{(0)}_{\rm NQED}$ to the bound-electron g factor can be conveniently parameterized by means of the dimensionless function $G^{(0)}_{\rm NQED}$ [50],

$$\delta g^{(0)}_{\rm NQED} = \delta g^{(0)}_{\rm N}\,\frac{\alpha}{\pi}\,G^{(0)}_{\rm NQED}(Z\alpha, R)\,, \tag{14.13}$$

where $\delta g^{(0)}_{\rm N}$ is the leading-order fns correction discussed in Sec. 14.2.1, and $G^{(0)}_{\rm NQED}$ is a slowly varying function. The correction can be divided into four parts,

$$G^{(0)}_{\rm NQED} = G_{\rm NSE} + G_{\rm NUe,el} + G_{\rm NWK,el} + G_{\rm NVP,ml}\,, \tag{14.14}$$

where $G_{\rm NSE}$ is the contribution of the electron self-energy, $G_{\rm NUe,el}$ is induced by the insertion of the Uehling potential into the electron line, $G_{\rm NWK,el}$ is the analogous correction by the Wichmann-Kroll potential, and $G_{\rm NVP,ml}$ is the so-called magnetic-loop vacuum-polarization correction.

The QED fns correction was studied in detail in our previous investigation [50], where we reported numerical results for the $1s$ state of H-like ions. In the present work, we extend our calculations to the $2s$ state, which is required for describing the Li-like ions. The numerical results obtained for the $2s$ state are listed in Table 18. The results for the $1s$ state are taken from Ref. [50]. We observe that the QED fns corrections for the $1s$ and $2s$ states, expressed in terms of the function $G^{(0)}_{\rm NQED}$, are very close to each other. Therefore, they largely cancel in the weighted difference $\delta_{\Xi_0} g$ introduced in Eq. (14.11).

14.2.3 One-photon exchange fns correction

The one-photon exchange fns correction is the dominant two-electron contribution to the total fns effect. It is suppressed by the factor of $1/Z$ with respect to the leading

Table 18: One-electron QED fns corrections to the bound-electron g factor, expressed in terms of $G^{(0)}_{\rm NQED}$ defined by Eq. (14.13). The abbreviations are as follows: "NSE" denotes the self-energy contribution, "NUe,el" denotes the Uehling electric-loop vacuum-polarization correction, "NWK,el" stands for the Wichmann-Kroll electric-loop vacuum-polarization correction, and "NVP,ml" denotes the magnetic-loop vacuum-polarization contribution.

Z	NSE	NUe,el	NWK,el	NVP,ml	Total, $2s$	Total, $1s$
6	$-0.54\,(20)$	0.179	-0.011	$-0.010\,(1)$	$-0.38\,(20)$	$-0.60\,(1)$
8	$-0.77\,(10)$	0.256	-0.019	$-0.010\,(1)$	$-0.55\,(10)$	$-0.70\,(1)$
10	$-0.94\,(4)$	0.337	-0.028	$-0.013\,(1)$	$-0.65\,(4)$	$-0.807\,(9)$
12	$-1.14\,(4)$	0.430	-0.040	$-0.017\,(2)$	$-0.77\,(4)$	$-0.905\,(8)$
14	$-1.32\,(4)$	0.530	-0.053	$-0.018\,(2)$	$-0.86\,(4)$	$-0.996\,(5)$
20	$-1.86\,(4)$	0.863	-0.098	$-0.025\,(4)$	$-1.12\,(4)$	$-1.237\,(3)$
25	$-2.36\,(4)$	1.185	-0.143	$-0.030\,(4)$	$-1.35\,(4)$	$-1.404\,(2)$
30	$-2.82\,(4)$	1.543	-0.191	$-0.035\,(6)$	$-1.50\,(4)$	$-1.542\,(2)$
35	$-3.27\,(2)$	1.933	-0.240	$-0.039\,(8)$	$-1.62\,(4)$	$-1.655\,(1)$
40	$-3.75\,(2)$	2.376	-0.295	$-0.044\,(8)$	$-1.71\,(2)$	$-1.733\,(1)$
45	$-4.23\,(1)$	2.837	-0.345	$-0.047\,(10)$	$-1.79\,(2)$	$-1.793\,(1)$
50	$-4.73\,(1)$	3.348	-0.398	$-0.050\,(12)$	$-1.83\,(1)$	$-1.821\,(1)$
55	$-5.25\,(1)$	3.902	-0.450	$-0.053\,(12)$	$-1.85\,(1)$	$-1.819\,(1)$
60	$-5.79\,(2)$	4.515	$-0.502\,(1)$	$-0.055\,(14)$	$-1.83\,(2)$	$-1.780\,(1)$

one-electron fns contribution $\delta g^{(0)}_{\rm N}$. The one-photon exchange fns correction can be obtained as a difference of the one-photon exchange contributions to the g-factor evaluated with the extended nuclear charge distribution and with the point nucleus,

$$\delta g^{(1)}_{\rm N} = \delta g^{(1)}_{\rm ext} - \delta g^{(1)}_{\rm pnt}\,. \tag{14.15}$$

The one-photon exchange correction to the g-factor of the ground and valence-

excited states of Li-like ions is given by [37]

$$\begin{aligned}\delta g^{(1)} = 2\sum_{\mu_c}\sum_{P}(-1)^P\Big[&\langle Pv\,Pc|I(\Delta_{Pc\,c})|\delta_V^{(1)}v\,c\rangle \\ &+\langle Pv\,Pc|I(\Delta_{Pc\,c})|v\,\delta_V^{(1)}c\rangle\Big] \\ &-\sum_{\mu_c}\big[\langle v|V_g|v\rangle-\langle c|V_g|c\rangle\big]\,\langle cv|I'(\Delta_{vc})|vc\rangle\,,\end{aligned} \tag{14.16}$$

where v and c denote the valence and the core electron states, respectively, μ_c is the momentum projection of the core electron, P is the permutation operator, $(PvPc) = (vc)$ or (cv), $(-1)^P$ is the sign of the permutation, $\Delta_{ab} = \varepsilon_a - \varepsilon_b$, $I(\omega)$ is the relativistic operator of the electron-electron interaction defined below, and $I'(\omega_0) = dI(\omega)/(d\omega)$ at $\omega = \omega_0$. Further notations used in Eq. (14.16) are as follows: $\delta_V^{(1)}a$ stands for the first-order perturbation of the wave function a by the potential V_g,

$$|\delta_V^{(1)}a\rangle = \sum_{n}^{\varepsilon_a\neq\varepsilon_n}\frac{|n\rangle\,\langle n|V_g|a\rangle}{\epsilon_a-\epsilon_n}\,, \tag{14.17}$$

and V_g is the effective g-factor potential (see, e.g., Eq. (14) of Ref. [19]),

$$V_g(\boldsymbol{r}) = 2\,m\,[\boldsymbol{r}\times\boldsymbol{\alpha}]_z\,, \tag{14.18}$$

where $\boldsymbol{\alpha}$ is the vector of Dirac matrices in the standard representation. The above form of the potential $V_g(\boldsymbol{r})$ assumes that the momentum projection of the valence state v in Eq. (14.16) is fixed as $\mu_v = 1/2$.

The relativistic electron-electron interaction operator $I(\omega)$ in the Feynman gauge reads

$$I(\omega,\boldsymbol{r}_1,\boldsymbol{r}_2) = \alpha\,(1-\boldsymbol{\alpha}_1\cdot\boldsymbol{\alpha}_2)\,\frac{\exp\left[i|\omega|r_{12}\right]}{r_{12}}\,, \tag{14.19}$$

where $r_{12} = |\boldsymbol{r}_1 - \boldsymbol{r}_2|$ is the distance between the two electrons and ω is the frequency of the photon exchanged between them.

The calculation of the one-photon exchange contribution with the extended and the point nuclear models was reported in Ref. [37]. In the present work, we redo these calculations with an enhanced precision, which is necessary for an accurate identification of the fns effect. The one-photon exchange fns correction $\delta g_N^{(1)}$ can be parameterized as

$$\delta g_N^{(1)} = \delta g_N^{(0)} \frac{1}{Z} H^{(1)}(Za, R)\,, \tag{14.20}$$

where $\delta g_N^{(0)}$ is the one-electron nuclear-size correction introduced earlier, and $H^{(1)}$ is a slowly varying function. The Za expansion of $H^{(1)}$ reads

$$H^{(1)} = H^{(1,0)} + (Za)^2\, H^{(1,2+)}\,, \tag{14.21}$$

where $H^{(1,0)}$ is the leading nonrelativistic contribution and $H^{(1,2+)}$ is the higher-order remainder.

The nuclear-size correction is evaluated in this work as the difference of Eq. (14.16) calculated with the extended vs. point-like nuclear models. The numerical evaluation of Eq. (14.16) with the extended nucleus is performed by using the DKB method [49]. For the point nucleus, we use the analytical expressions for the reference-state wave functions and for the diagonal (in κ) g-factor perturbed wave function [20], and the standard implementation of the B-splines method [21] for the non-diagonal in κ part of the perturbed wave function. In order to avoid loss of numerical accuracy in the low-Z region, we employ the DKB and the B-splines methods implemented in the quadruple arithmetics.

The accuracy of the obtained numerical results is checked as follows. We observe that the leading term of the $Z\alpha$ expansion of Eq. (14.21), $H^{(1,0)}$, should not

Table 19: The one-photon exchange fns correction to the bound-electron g factor of the ground state of Li-like ions, in terms of the function $H^{(1)}$ defined by Eq. (14.20). The column (R, c) contains results obtained with the actual values of the nuclear charge radii R and the speed of light c. The column $(4R, c)$ presents results obtained with the nuclear charge radii multiplied by a factor of 4. The column $(40R, 10c)$ contains results obtained with the nuclear charge radii multiplied by a factor of 40 and the speed of light multiplied by 10.

Z	(R, c)	$(4R, c)$	$(40R, 10c)$
6	-2.8529	-2.8529	-2.8527
8	-2.8538	-2.8539	-2.8533
10	-2.8550	-2.8552	-2.8539
12	-2.8566	-2.8568	-2.8545
14	-2.8584	-2.8586	-2.8550
20	-2.8654	-2.8658	-2.8569
25	-2.8731	-2.8735	-2.8585
30	-2.8824	-2.8828	-2.8601
35	-2.8933	-2.8936	-2.8616
40	-2.9057	-2.9057	-2.8629
45	-2.9194	-2.9191	-2.8642
50	-2.9346	-2.9336	-2.8653
55	-2.9510	-2.9491	-2.8663
60	-2.9686	-2.9655	-2.8670

depend on the nuclear charge radius R. It also cannot depend on the speed of light c. All dependence of $H^{(1,0+)}$ on R and c comes only through the relativistic effects, which are small corrections in the low-Z region. Therefore, numerical calculations of $H^{(1,0+)}$ performed with different choices of R and c should have the same low-Z limit.

The numerical results for the nuclear-size correction to the one-photon exchange are presented in Table 19 and shown graphically on Fig. 9. We observe that the results obtained with different values of R and c are in very good agreement for low Z. This agreement also indicates that the results for $H^{(1)}$ are practically independent of the nuclear model.

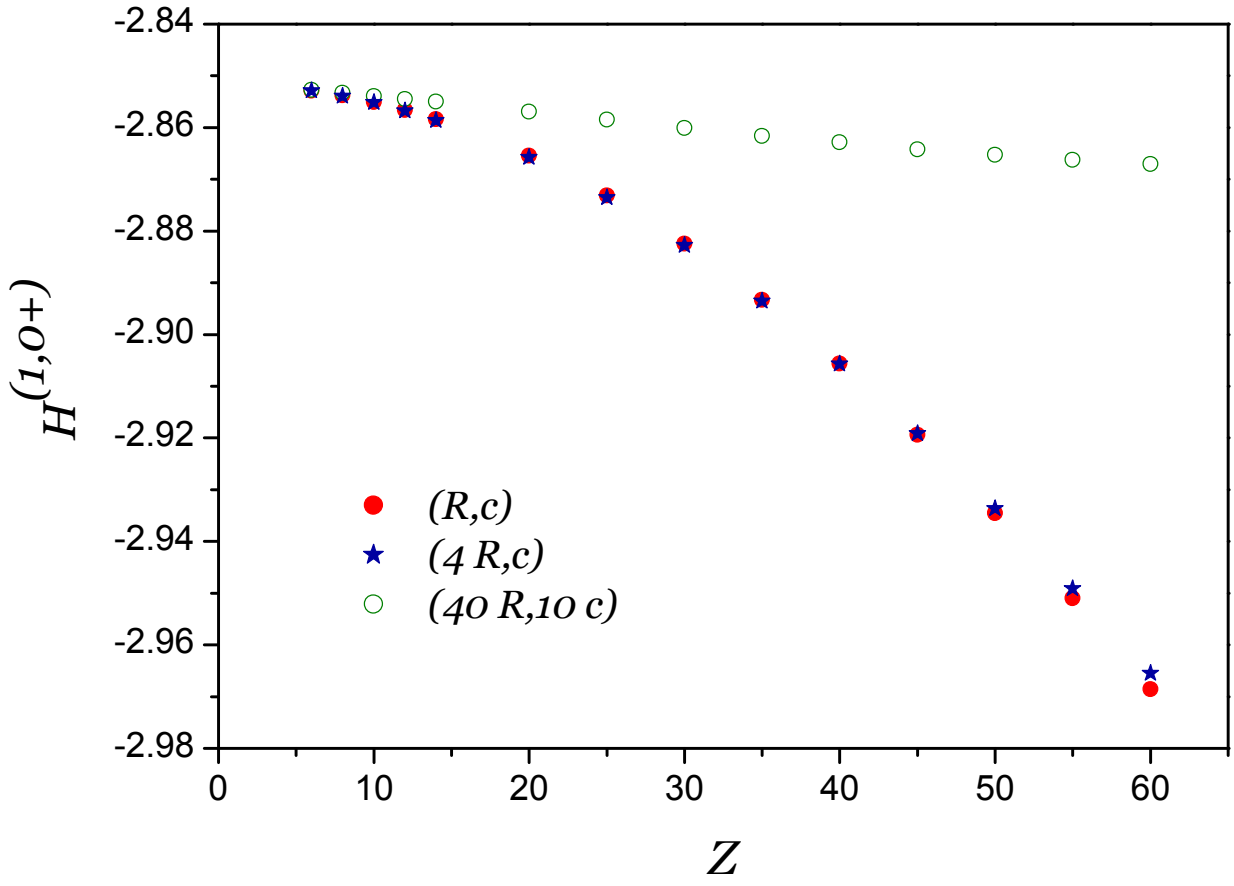

Figure 9: (Color online) The one-photon exchange fns correction to the bound-electron g factor of the ground state of Li-like ions, in terms of the function $H^{(1)}$ defined by Eq. (14.20). Numerical results for the actual values the nuclear charge radii and the speed of light (R, c) (filled dots, red) are compared with the results obtained with with the nuclear charge radii multiplied by a factor of 4 $(4R, c)$ (filled stars, blue) and with the results obtained with the nuclear charge radii multiplied by a factor of 40 and the speed of light multiplied by 10 $(40R, 10c)$ (open dots, green).

The results obtained with enlarged speed of light show very weak Z dependence, which might have been anticipated since the Z dependence of $H^{(1)}$ comes through the relativistic corrections only. These results can be easily extrapolated to $Z \to 0$, yielding

$$H^{(1,0)} = -2.8512\,(10)\,. \tag{14.22}$$

On the basis of this result, we conclude that the following weighted difference of the $2s$ and $1s$ g-factors cancels most of the fns contribution of order $1/Z$ for light ions,

$$\delta_{\Xi_1} g = \delta g^{(1)}(2s) - \Xi_0 \left(-\frac{2851}{1000} \frac{1}{Z} \right) g^{(0)}(1s) \,. \tag{14.23}$$

14.2.4 Two and more photon exchange fns correction

The fns correction with two and more photon exchanges between the electrons is suppressed by the factor of $1/Z^2$ with respect to the leading fns contributions. A parametrization of this term can be given as

$$\delta g_N^{(2+)} = \delta g_N^{(0)} \, \frac{1}{Z^2} \, H^{(2+)}(Za, R) \,, \tag{14.24}$$

where $\delta g_N^{(0)}$ is the one-electron nuclear-size correction defined in Eq. (14.3), and $H^{(2+)}$ is a slowly varying function of its arguments.

In order to compute the fns correction, we need to calculate the two and more photon exchange correction for the extended and the point nucleus and take the difference,

$$\delta g_N^{(2+)} = \delta g_{\rm ext}^{(2+)} - \delta g_{\rm pnt}^{(2+)} \,. \tag{14.25}$$

In this work, we calculate $\delta g_{\rm ext}^{(2+)}$ and $\delta g_{\rm pnt}^{(2+)}$ within the Breit approximation. The whole calculation is performed in three steps. In the first step, we solve the no-pair Dirac-Coulomb-Breit Hamiltonian by the Configuration-Interaction Dirac-Fock-Sturm (CI-DFS) method [51]. In the second step, we subtract the leading-order terms of orders $1/Z^0$ and $1/Z^1$, thus identifying the contribution of order $1/Z^2$ and higher. The subtraction terms of order $1/Z^0$ and $1/Z^1$ were calculated separately by perturbation theory. In the third step, we repeat the calculation for the extended and the

point nuclear models and, by taking the difference, obtain the fns correction.

The fns effect is very small in the low-Z region, which makes it very difficult to obtain reliable predictions for this correction. In order to be able to monitor the numerical accuracy, we performed three sets of calculations. The first set (R, c) was obtained with the actual values of the nuclear charge radii R and the speed of light c; the second set $(4R, c)$ was obtained with the nuclear charge radii multiplied by a factor of 4; the third set $(40R, 10c)$ was obtained with the nuclear charge radii multiplied by a factor of 40 and the speed of light multiplied by 10. The obtained results are listed in Table 20 and presented in Fig. 10.

Similarly to the one-photon exchange fns correction, we assume that the low-Z limit of $H^{(2+)}$, denoted as $H^{(2,0)}$, does not depend either on R or on c. By extrapolating our numerical results in Table 20 to $Z \to 0$, we obtain the nonrelativistic value of the $1/Z^2$ correction as

$$H^{(2,0)} = 1.070\,(25)\,. \tag{14.26}$$

Based on this result, we conclude that for light ions, the following weighted difference of the $2s$ and $1s$ g-factors cancels most of the $1/Z^2$ fns contribution:

$$\delta_{\Xi_2} g = \delta g^{(2+)}(2s) - \Xi_0 \left(\frac{107}{100}\frac{1}{Z^2}\right) g^{(0)}(1s)\,. \tag{14.27}$$

14.3 The weighted difference of the $2s$ and $1s$ g factors

Combining the results obtained in the previous section, we introduce the total Ξ-weighted difference as follows

$$\delta_{\Xi} g = g(2s) - \Xi\, g(1s)\,, \tag{14.28}$$

Table 20: The two and more photon exchange fns correction to the bound-electron g factor of the ground state of Li-like ions, in terms of the function $H^{(2+)}$ defined by Eq. (14.24). Notations are the same as in Table 19.

Z	(R,c)	$(4R,c)$	$(40R,10c)$
10		1.059 (20)	1.081 (20)
14		1.073 (20)	1.075 (20)
20	1.102 (20)	1.110 (20)	1.075 (20)
25	1.157 (20)	1.149 (20)	1.074 (20)
30	1.198 (20)	1.195 (20)	1.074 (20)
35	1.255 (20)	1.249 (20)	1.073 (20)
40	1.321 (20)	1.312 (20)	1.072 (20)
50	1.481 (20)	1.466 (20)	1.068 (20)
55	1.579 (20)	1.560 (20)	1.067 (20)
60	1.690 (20)	1.672 (20)	1.064 (20)

where $g(2s)$ is the g factor of the ground state of the Li-like ion, $g(1s)$ is the g factor of the ground state of the H-like ion, and the weight parameter Ξ is defined by Eq. (14.2). Basing on the analysis of the preceding Section, we claim that in the Ξ-weighted difference $\delta_\Xi g$, the nonrelativistic fns corrections to order $1/Z^0$, $1/Z^1$, and $1/Z^2$ and, in addition, the relativistic contribution to order $(Z\alpha)^2/Z^0$ are cancelled. A small remaining fns correction to $\delta_\Xi g$ is calculated numerically. The definition of $\delta_\Xi g$ is based on the $Z\alpha$ expansion of the fns corrections. Because of this, it is applicable for low- and medium-Z ions. For heavy systems, the $Z\alpha$ expansion is no longer useful. In this case, the cancellation of the fns effect in the weighted difference is still possible but should be achieved differently [37, 38].

In Table 21 we present the individual fns contributions to the g-factor of the ground state of Li-like ions $g(2s)$, H-like ions $g(1s)$ and for the weighted difference $\delta_\Xi g$. We observe that the uncertainty of the fns corrections for $g(2s)$ and $g(1s)$ is dominated by the nuclear-model and nuclear-radii errors, which means they cannot be significantly improved. On the contrary, the fns effect for $\delta_\Xi g$ is much smaller,

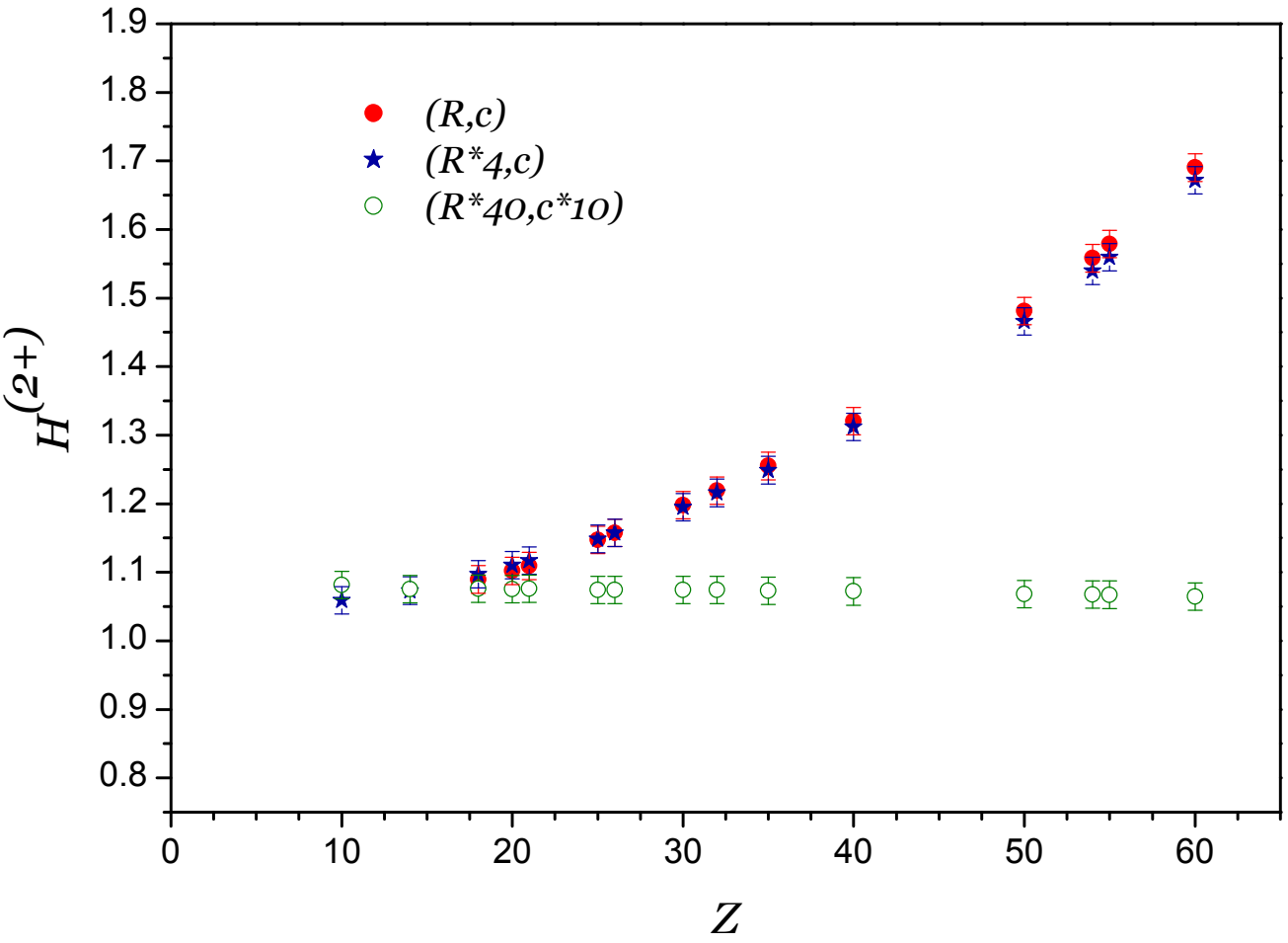

Figure 10: (Color online) The two and more photon exchange fns correction to the bound-electron g factor of the ground state of Li-like ions, in terms of the function $H^{(2+)}$ defined by Eq. (14.24). Notations are the same as in Fig. 9.

and its uncertainty is mainly numerical, meaning that it can be improved further.

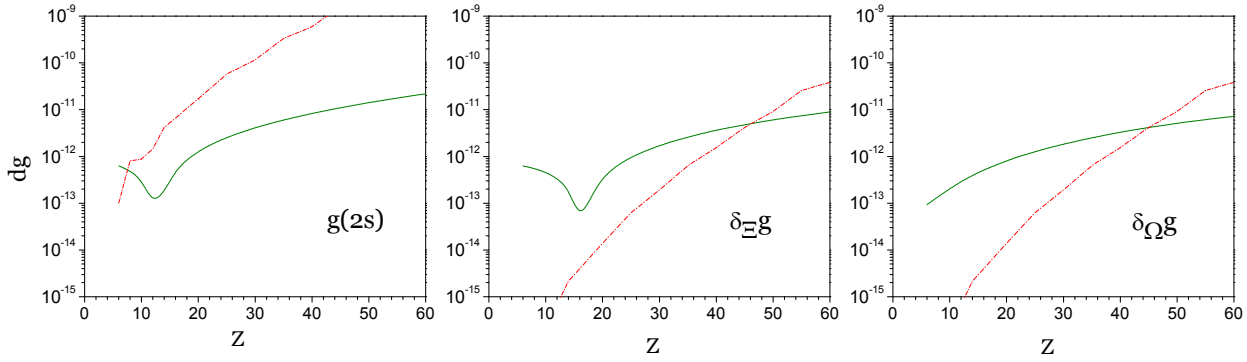

Figure 11: (Color online) Comparison of the error $\delta g = (\partial g/\partial\alpha)\,\delta\alpha$ due to the uncertainty of the fine-structure constant $\delta\alpha/\alpha = 3.2\times10^{-10}$ (solid line, green) and the error due to the finite nuclear size effect (dashed-dot line, red), for the g-factor of the ground state of Li-like ions $g(2s)$ (left panel); for the weighted difference $\delta_\Xi g(Z)$ (middle panel); and for the weighted difference $\delta_\Omega g = \delta_\Xi g(Z) - \delta_\Xi g([Z/2])$ (right panel).

Table 21: The fns corrections to the bound-electron g fac-tor of the ground state of Li-like and H-like ions and their weighted difference, multiplied by a factor of 10^6. The num-bers in the parentheses denote the uncertainty in the last fig-ure. When three uncertainties are specified, the first one is the numerical error, the second one the model-dependence error, and the third one the uncertainty induced by the error of the nuclear charge radius. In the case only one uncertainty is specified, it is the numerical error (whereas the other errors are significantly smaller and are not indicated).

Z	Term	$\delta g_{\rm N}(2s)$	$\Xi_i/Z^i\,\delta g_{\rm N}(1s)$	$\delta g_{\rm N}(2s) - \Xi_i/Z^i\,\delta g_{\rm N}(1s)$
6	$1/Z^0$	0.000 050 99 (0)(1)(9)	0.000 050 99 (0)(1)(9)	0.
	α/Z^0	-0.000 000 05 (2)	-0.000 000 071 (2)	0.000 000 03 (2)
	$1/Z^1$	-0.000 024 24 (0)(0)(4)	-0.000 024 23 (0)(0)(4)	-0.000 000 016 (1)(0)(0)
	$1/Z^{2+}$	0.000 001 52 (4)	0.000 001 515	0.000 000 00 (4)
	Total	0.000 028 2 (0)(0)(1)	0.000 0282 (0)(0)(1)	0.000 000 01 (4)(0)(0)
8	$1/Z^0$	0.000 194 7 (0)(0)(7)	0.000 194 7 (0)(0)(7)	0.

	α/Z^0	-0.000 000 25 (3)	-0.000 000 317 (5)	0.000 000 07 (3)
	$1/Z^1$	-0.000 069 5 (0)(0)(3)	-0.000 069 4 (0)(0)(3)	-0.000 000 068 (1)(0)(0)
	$1/Z^{2+}$	0.000 003 26 (8)	0.000 003 256	0.000 000 00 (8)
	Total	0.000 128 3 (1)(0)(8)	0.000 128 3 (0)(0)(8)	0.000 000 00 (8)(0)(0)
10	$1/Z^0$	0.000 598 3 (0)(1)(8)	0.000 598 3 (0)(1)(8)	-0.000 000 002
	α/Z^0	-0.000 000 90 (8)	-0.000 001 12 (1)	0.000 000 22 (8)
	$1/Z^1$	-0.000 170 8 (0)(0)(2)	-0.000 170 6 (0)(0)(2)	-0.000 000 241 (1)(0)(0)
	$1/Z^{2+}$	0.000 006 4 (1)	0.000 006 40	0.000 000 0 (1)
	Total	0.000 433 0 (2)(1)(9)	0.000 433 0 (0)(1)(9)	0.000 000 0 (2)(0)(0)
12	$1/Z^0$	0.001 307 (0)(0)(1)	0.001 307 (0)(0)(1)	-0.000 000 007
	α/Z^0	-0.000 002 3 (2)	-0.000 002 74 (2)	0.000 000 4 (2)
	$1/Z^1$	-0.000 311 1 (0)(1)(3)	-0.000 310 5 (0)(1)(3)	-0.000 000 604 (1)(0)(1)
	$1/Z^{2+}$	0.000 009 7 (2)	0.000 009 71	0.000 000 0 (2)
	Total	0.001 003 (0)(0)(1)	0.001 003 (0)(0)(1)	-0.000 000 2 (3)(0)(0)
14	$1/Z^0$	0.002 580 (0)(1)(4)	0.002 580 (0)(1)(4)	-0.000 000 026 (0)(1)(0)
	α/Z^0	-0.000 005 1 (3)	-0.000 005 96 (3)	0.000 000 8 (3)
	$1/Z^1$	-0.000 5267 (0)(2)(8)	-0.000 525 3 (0)(2)(8)	-0.000 001 353 (1)(0)(2)
	$1/Z^{2+}$	0.000 014 1 (3)	0.000 014 1	0.000 000 0 (3)
	Total	0.002 062 (0)(1)(4)	0.002 062 (0)(1)(4)	-0.000 000 6 (4)(0)(0)
20	$1/Z^0$	0.014 41 (0)(1)(2)	0.014 41 (0)(1)(2)	-0.000 000 554 (0)(7)(1)
	α/Z^0	-0.000 038 (2)	-0.000 041 4 (1)	0.000 004 (2)
	$1/Z^1$	-0.002 064 (0)(1)(2)	-0.002 054 (0)(1)(2)	-0.000 010 31 (0)(0)(1)
	$1/Z^{2+}$	0.000 040 0 (7)	0.000 038 5	0.000 001 4 (7)
	Total	0.012 34 (0)(1)(2)	0.012 35 (0)(1)(2)	-0.000 006 (2)(0)(0)
25	$1/Z^0$	0.043 36 (0)(3)(5)	0.043 36 (0)(3)(5)	-0.000 003 90 (0)(4)(1)
	α/Z^0	-0.000 136 (5)	-0.000 141 4 (2)	0.000 005 (5)
	$1/Z^1$	-0.004 983 (0)(3)(6)	-0.004 945 (0)(3)(6)	-0.000 037 92 (0)(2)(4)
	$1/Z^{2+}$	0.000 080 (1)	0.000 074	0.000 006 (1)

	Total	0.038 32 (1)(3)(5)	0.038 35 (0)(3)(5)	-0.000 031 (5)(0)(0)
30	$1/Z^0$	0.111 34 (0)(8)(8)	0.111 36 (0)(8)(8)	-0.000 020 3 (0)(1)(0)
	α/Z^0	-0.000 39 (1)	-0.000 398 9 (5)	0.000 01 (1)
	$1/Z^1$	-0.010 697 (0)(8)(8)	-0.010 583 (0)(8)(8)	-0.000 114 72 (0)(9)(9)
	$1/Z^{2+}$	0.000 148 (2)	0.000 132	0.000 016 (2)
	Total	0.100 40 (1)(8)(8)	0.100 51 (0)(8)(8)	-0.000 11 (1)(0)(0)
35	$1/Z^0$	0.258 8 (0)(2)(3)	0.258 9 (0)(2)(3)	-0.000 086 4 (0)(5)(1)
	α/Z^0	-0.000 97 (2)	-0.000 995 4 (6)	0.000 02 (2)
	$1/Z^1$	-0.021 40 (0)(2)(2)	-0.021 09 (0)(2)(2)	-0.000 305 7 (0)(3)(3)
	$1/Z^{2+}$	0.000 265 (4)	0.000 226	0.000 039 (4)
	Total	0.236 7 (0)(2)(3)	0.237 1 (0)(2)(3)	-0.000 33 (2)(0)(0)
40	$1/Z^0$	0.527 6 (0)(5)(2)	0.527 9 (0)(5)(2)	-0.000 298 (0)(1)(0)
	α/Z^0	-0.002 10 (3)	-0.002 125 (1)	0.000 03 (3)
	$1/Z^1$	-0.038 33 (0)(4)(2)	-0.037 63 (0)(4)(2)	-0.000 699 6 (0)(8)(3)
	$1/Z^{2+}$	0.000 436 (7)	0.000 353	0.000 083 (7)
	Total	0.487 6 (0)(5)(2)	0.488 5 (0)(5)(2)	-0.000 89 (3)(0)(0)
45	$1/Z^0$	1.076 (0)(1)(1)	1.077 (0)(1)(1)	-0.000 982 (0)(3)(1)
	α/Z^0	-0.004 47 (3)	-0.004 486 (3)	0.000 02 (4)
	$1/Z^1$	-0.069 81 (0)(8)(7)	-0.068 24 (0)(8)(7)	-0.001 574 (0)(2)(2)
	$1/Z^{2+}$	0.000 74 (1)	0.000 569	0.000 17 (1)
	Total	1.003 (0)(1)(1)	1.005 (0)(1)(1)	-0.002 37 (4)(0)(0)
50	$1/Z^0$	2.050 (0)(3)(2)	2.053 (0)(3)(2)	-0.002 885 (0)(7)(3)
	α/Z^0	-0.008 73 (5)	-0.008 684 (5)	-0.000 05 (5)
	$1/Z^1$	-0.120 3 (0)(2)(1)	-0.117 1 (0)(1)(1)	-0.003 262 (0)(5)(3)
	$1/Z^{2+}$	0.001 21 (2)	0.000 878	0.000 34 (2)
	Total	1.922 (0)(3)(2)	1.928 (0)(3)(2)	-0.005 86 (5)(1)(0)
55	$1/Z^0$	3.788 (0)(5)(7)	3.796 (0)(5)(7)	-0.007 95 (0)(1)(2)

	α/Z^0	-0.016 29 (9)	-0.016 037 (9)	-0.000 26 (9)
	$1/Z^1$	-0.203 2 (0)(3)(4)	-0.196 8 (0)(3)(3)	-0.006 47 (0)(1)(1)
	$1/Z^{2+}$	0.001 98 (3)	0.001 342	0.000 63 (3)
	Total	3.570 (0)(5)(7)	3.584 (0)(5)(7)	-0.014 05 (9)(2)(2)
60	$1/Z^0$	6.74 (0)(1)(1)	6.76 (0)(1)(1)	-0.020 51 (0)(2)(2)
	α/Z^0	-0.028 7 (2)	-0.027 96 (2)	-0.000 8 (2)
	$1/Z^1$	-0.333 6 (0)(5)(3)	-0.321 4 (0)(5)(3)	-0.012 24 (0)(2)(1)
	$1/Z^{2+}$	0.003 17 (4)	0.002 010	0.001 16 (4)
	Total	6.38 (0)(1)(1)	6.42 (0)(1)(1)	-0.032 4 (2)(0)(0)

We would like now to address the question whether the weighted difference $\delta_\Xi g$ might be useful for the determination of the fine-structure constant α. The leading dependence of $\delta_\Xi g$ on α is given by the expansion

$$\delta_\Xi g = 2\,(1-\Xi) - \frac{2}{3}(Za)^2\left(\frac{1}{4}-\Xi\right) + \frac{\alpha}{\pi}(1-\Xi) + \dots\,, \tag{14.29}$$

where the second term in the right-hand-side stems from the binding corrections, whereas the third term is due to the one-loop free-electron QED effect. In the above equation, we keep Ξ fixed, ignoring its dependence on α, since it does not contribute to the sensitivity of $\delta_\Xi g$ on α (the same value of Ξ should be used when comparing the experimental and theoretical values of $\delta_\Xi g$). By varying α in Eq. (14.29) within its current error bars of $\delta\alpha/\alpha = 3.2 \times 10^{-10}$ [36], the corresponding error of $\delta_\Xi g$ can be obtained.

In Fig. 11 we compare the uncertainty due to α and the uncertainty due to the nuclear model and radius, keeping in mind that the latter defines the ultimate limit of the accuracy of theoretical calculations. The left panel of Fig. 11 shows this comparison for the g-factor of the ground state of Li-like ions $g(2s)$, whereas the middle panel gives the same comparison for the Ξ-weighted difference $\delta_\Xi g$. The dip of the α-sensitivity curve around $Z = 16$ is caused by the fact that the dependence

of the binding and the free-QED effects on α in Eq. (14.29) (second and third terms) have different signs, and thus cancel each other in this Z region. From Fig. 11 we can conclude that up to $Z \approx 45$, the weighted difference $\delta_{\Xi} g$ yields possibilities for an improved determination of α.

The determination of α from $\delta_{\Xi} g$ has two drawbacks. The first one is the cancellation of α dependence of $\delta_{\Xi} g$ around $Z = 16$, leading to a loss of sensitivity to α in this Z region. The second one is that $\delta_{\Xi} g$ contains the same free-QED part which is used for the determination of α from the free-electron g factor, which means that these two determinations cannot be regarded as fully independent. Both drawbacks can be avoided by introducing another difference,

$$\delta_{\Omega} g = \delta_{\Xi} g(Z) - \delta_{\Xi} g([Z/2])\,, \tag{14.30}$$

with $\delta_{\Xi} g(Z)$ being the weighted difference (14.28) for the nuclear charge Z, and $\delta_{\Xi} g([Z/2])$ is the corresponding difference for the nuclear charge $[Z/2]$, where $[\ldots]$ stands for the upper or the lower integer part. In the difference $\delta_{\Omega} g$, most free-QED contributions vanish. So, by a small sacrifice of the sensitivity of the binding effects to α, we removed the dip around $Z = 16$ and made the theory of the weighted difference (almost) independent on the theory of the free-electron g-factor.

The right panel of Fig 11 presents the comparison of the uncertainty due to α with the error of the fns effect for the weighted difference $\delta_{\Omega} g$. One finds a smooth dependence of the sensitivity to α on Z, without any dip in the region around $Z = 16$. We observe that in the region $Z = 10 - 20$, the weighted difference $\delta_{\Omega} g$ offers better possibilities for determining α than $\delta_{\Xi} g$.

Employing the difference $\delta_{\Omega} g$ can be also advantageous from the experimental

point of view. It can be rewritten as

$$\begin{aligned}\delta_\Omega g &= g(2s,Z) - g(2s,Z_2) \\ &- \Xi(Z)\,[g(1s,Z) - g(1s,Z_2)] \\ &- g(1s,Z_2)\,[\Xi(Z) - \Xi(Z_2)]\ ,\end{aligned} \tag{14.31}$$

with $Z_2 = [Z/2]$. We thus observe that $\delta_\Omega g$ can be effectively determined in an experiment by measuring two equal-weight g-factor differences (namely, the ones in the first and second rows of the above equation) and $g(1s, Z_2)$. The equal-weight differences may be measured with largely suppressed systematic errors and thus can be determined in near-future experiments much more accurately than the g-factors of individual ions. The last term in Eq. (14.31) is suppressed by a small factor of $[\Xi(Z) - \Xi(Z_2)] \approx 0.02 - 0.04$ in the region of interest. Therefore, the experimental error of $\delta_\Omega g$ can be significantly improved as compared to that of the absolute g-factors.

Let us now turn to the experimental consequences of the present calculations. So far, the only element for which g-factors in both the H-like and Li-like charge states have been measured is silicon. In Table 22 we collect the individual theoretical contributions to $\delta_\Xi g(^{28}\mathrm{Si})$ and compare the result with the experimental value. Theoretical results for various effects were taken from the literature, Refs. [42, 52–56, 64]. The total theoretical value is compared to the experimental result [44, 45, 58]. The errors of the Dirac value and of the one-loop free QED ($\sim \alpha(Z\alpha)^0$) result specified in the table are due to the uncertainty of the current value of $\alpha^{-1} = 137.035\,999\,074\,(44)$ [36]. The uncertainty of the fns effect specified in the table is 6×10^{-13}, which is already smaller than the uncertainty of the Dirac value due to α. The fns uncertainty is of purely numerical origin, i.e. it does not influenced by the errors due to the rms charge radius and the nuclear charge distribution, and thus it can be further improved in future calculations.

Table 22 illustrates another advantage of the Ξ-weighted difference: the contributions of one-electron binding QED effects to $\delta_\Xi g$ are much smaller than those to $g(2s)$. This is explained by the fact that these effects largely originate from short distances, similarly to the fns effect, and thus are significantly canceled in the difference. In particular, the uncertainty of $\delta_\Xi g(\mathrm{Si})$ due to three-loop binding QED effects is on the 10^{-12} level, implying that these effects do not need to be known to a high degree of accuracy for the determination of α.

Table 22 shows that the present experimental and theoretical precision of $\delta_\Xi g(\mathrm{Si})$ is on the level of few parts in 10^{-9}, which is significantly worse than the precision achieved for other systems (in particular, H-like carbon, where the present experimental and theoretical uncertainties are, correspondingly, 6×10^{-11} and 6×10^{-12} [43]). This underperformance is, however, more due to a lack of motivation than due to principal obstacles.

On the experimental side, the same precision as for H-like carbon can be also obtained for $\delta_\Xi g(\mathrm{C})$, with an existing ion trap [46]. Further experimental advance is anticipated that could bring one or two orders of magnitude of improvement [46]. On the theoretical side, the modern nonrelativistic quantum electrodynamics (NRQED) approach (see, e.g., [59]) can apparently provide a theoretical result for Li-like carbon with the same accuracy as obtained for its H-like counterpart [60]. Moreover, further theoretical advance is possible: the two-loop QED corrections of order $\alpha^2(Za)^5$ and the three-loop QED corrections of order $\alpha^3(Za)^4$ can be calculated, both for H-like and Li-like ions [60].

As we are presently interested in light ions, the best way for the advancement of theory would be a combination of two complementary methods. The first one is the NRQED method (used, e.g., in [62]) that accounts for the nonrelativistic electron-electron interactions to all orders in $1/Z$, but expands the QED and relativistic effects in powers of α and Za. The second approach (used, e.g., in [53, 55, 56, 64])

accounts for the relativistic effects to all orders in $Z\alpha$ but employs perturbation expansions in α (QED effects) and in $1/Z$ (electron-electron interaction). Matching the coefficients of the $Z\alpha$ and $1/Z$ expansions from the two methods allows one to combine them together, as it was done for energy levels in Ref. [34]. As a result of this procedure, only higher-order corrections in $Z\alpha$ will be expanded in $1/Z$ and only higher-order corrections in $1/Z$ will be expanded in $Z\alpha$. This approach should allow one to advance theory to the level required for a determination of α.

The principal limitation for the theory is set by the non-trivial nuclear structural effects, such as the nuclear deformation, nuclear polarization, etc. For light ions, the leading nuclear effects are described by effective operators proportional to the Dirac delta function $\delta(\boldsymbol{r})$. Such effects are canceled in the weighted difference $\delta_\Xi g$. We estimate that the uncertainty due to the remaining nuclear effects in $\delta_\Xi g$ should be of the same order as the nuclear-model dependence error of the fns effect. From the breakdown in Table 21 we deduce that for silicon, this error is by about two orders of magnitude smaller than the uncertainty due to α. We thus conclude that the nuclear effects do not represent any obstacles for the determination of α from $\delta_\Xi g$ and $\delta_\Omega g$.

14.4 Conclusion

In this work we investigated specific weighted differences of the g-factors of H- and Li-like ions of the same element. An accurate formula was obtained for the weight parameter Ξ, determined by requiring cancellation of the nonrelativistic finite nuclear size corrections to orders $1/Z^0$, $1/Z^1$, and $1/Z^2$ and, in addition, the relativistic contribution to order $(Z\alpha)^2/Z^0$. The coefficients of the $Z\alpha$ expansion of the finite nuclear size corrections were obtained by performing accurate numerical calculations and fitting the results to the known expansion form. It was demonstrated that the Ξ- and Ω-weighted differences, as given by Eqs. (14.28) and (14.30),

Table 22: Individual contributions to the weighted difference $\delta_{\Xi} g$ for ^{28}Si, $M/m = 50984.833$, $\Xi = 0.101136233077060$.

Contribution	Order	Value
Dirac		1.796 687 854 216 5 (7)
1-loop QED	$\alpha(Za)^0$	0.002 087 898 255 0 (7)
	$\alpha(Za)^2$	0.000 000 601 506 0
	$\alpha(Za)^4$	0.000 000 014 797 0
	$\alpha(Za)^{5+}$	0.000 000 015 48 (52)
2-loop QED	$\alpha^2(Za)^0$	−0.000 003 186 116 6
	$\alpha^2(Za)^2$	−0.000 000 000 917 9
	$\alpha^2(Za)^4$	−0.000 000 000 084 4
	$\alpha^2(Za)^{5+}$	0.000 000 000 00 (13)
$\geq$ 3-loop QED	$\alpha^{3+}(Za)^0$	0.000 000 026 514 9 (1)
	$\alpha^{3+}(Za)^2$	0.000 000 000 007 6
	$\alpha^{3+}(Za)^{4+}$	0.000 000 000 000 0 (11)
Recoil	$m/M(Z\alpha)^{2+}$	0.000 000 030 5 (11)
1-photon exchange	$(1/Z)(Za)^{2+}$	0.000 321 590 803 3
2-photon exchange	$(1/Z^2)(Za)^{2+}$	−0.000 006 876 0 (5)
$\geq$ 3-photon exchange	$(1/Z^{3+})(Za)^{2+}$	0.000 000 093 0 (60)
2-electron QED	$(\alpha/Z)(Za)^{2+}$	−0.000 000 236 0 (50)
2-electron Recoil	$(m/M)(1/Z)(Za)^{2+}$	−0.000 000 012 1 (7)
Finite nuclear size		−0.000 000 000 000 6 (4)
Total theory		1.799 087 813 9 (80)
Experiment [44, 58]		1.799 087 812 5 (21)

can be used for an efficient suppression of nuclear effects. The residual uncertainty due to nuclear effects is smaller than the uncertainty due to the currently accepted value of the fine-structure constant α. The Ξ- and Ω-weighted differences may be used in future to determine α from a comparison of theoretical and experimental bound-electron g-factors with an accuracy competitive with or better than the present literature value.

References

[1] S. Sturm, F. Köhler, J. Zatorski, A. Wagner, Z. Harman, G. Werth, W. Quint, C. H. Keitel, and K. Blaum, Nature **506**, 467-470 (2014).

[2] A. Wagner, S. Sturm, F. Köhler, D. A. Glazov, A. V. Volotka, G. Plunien, W. Quint, G. Werth, V. M. Shabaev, and K. Blaum, Phys. Rev. Lett. **110**, 033003 (2013).

[3] S. Sturm, Private communication, 2015.

[4] P. J. Mohr, B. N. Taylor, and D. B. Newell, Rev. Mod. Phys. **84**, 1527 (2012).

[5] V. M. Shabaev, D. A. Glazov, M. B. Shabaeva, V. A. Yerokhin, G. Plunien, and G. Soff, Phys. Rev. A **65**, 062104 (2002).

[6] V. M. Shabaev, D. A. Glazov, N. S. Oreshkina, A. V. Volotka, G. Plunien, H.-J. Kluge, and W. Quint, Phys. Rev. Lett. **96**, 253002 (2006).

[7] R. Bouchendira, P. Cladé, S. Guellati-Khélifa, F. m. c. Nez, and F. m. c. Biraben, Phys. Rev. Lett. **106**, 080801 (2011).

[8] T. Aoyama, M. Hayakawa, T. Kinoshita, and M. Nio, Phys. Rev. Lett. **109**, 111807 (2012).

[9] T. Aoyama, M. Hayakawa, T. Kinoshita, and M. Nio, Phys. Rev. D **91**, 033006 (2015).

[10] V. A. Yerokhin, E. Berseneva, Z. Harman, I. I. Tupitsyn, and C. H. Keitel, Phys. Rev. Lett. **116**, 100801 (2016).

[11] M. E. Rose, *Relativistic Electron Theory*, John Wiley & Sons, NY, 1961.

[12] S. G. Karshenboim, R. N. Lee, and A. I. Milstein, Phys. Rev. A **72**, 042101 (2005).

[13] V. M. Shabaev, J. Phys. B **26**, 1103 (1993).

[14] S. G. Karshenboim, Phys. Lett. **A 266**, 380 (2000).

[15] D. A. Glazov and V. M. Shabaev, Phys. Lett. A **297**, 408 (2002).

[16] V. M. Shabaev, I. I. Tupitsyn, V. A. Yerokhin, G. Plunien, and G. Soff, Phys. Rev. Lett. **93**, 130405 (2004).

[17] I. Angeli and K. Marinova, At. Data Nucl. Data Tabl. **99**, 69 (2013).

[18] V. A. Yerokhin, C. H. Keitel, and Z. Harman, J. Phys. B **46**, 245002 (2013).

[19] V. A. Yerokhin and U. D. Jentschura, Phys. Rev. A **81**, 012502 (2010).

[20] V. Shabaev, in *Precision Physics of Simple Atomic Systems*, ed. S. G. Karshenboim and V. B. Smirnov, (Lecture Notes in Physics, Berlin, 2003, Springer), p. 97.

[21] W. R. Johnson, S. A. Blundell, and J. Sapirstein, Phys. Rev. A **37**, 307 (1988).

[22] I. I. Tupitsyn, V. M. Shabaev, J. R. Crespo López-Urrutia, I. Draganić, R. Soria Orts, and J. Ullrich, Phys. Rev. A **68**, 022511 (2003).

[23] V. A. Yerokhin, P. Indelicato, and V. M. Shabaev, Phys. Rev. A **69**, 052503 (2004).

[24] D. A. Glazov, V. M. Shabaev, I. I. Tupitsyn, A. V. Volotka, V. A. Yerokhin, G. Plunien, and G. Soff, Phys. Rev. A **70**, 062104 (2004).

[25] K. Pachucki, A. Czarnecki, U. D. Jentschura, and V. A. Yerokhin, Phys. Rev. A **72**, 022108 (2005).

[26] A. V. Volotka, D. A. Glazov, V. M. Shabaev, I. I. Tupitsyn, and G. Plunien, Phys. Rev. Lett. **103**, 033005 (2009).

[27] D. A. Glazov, A. V. Volotka, V. M. Shabaev, I. I. Tupitsyn, and G. Plunien, Phys. Rev. A **81**, 062112 (2010).

[28] A. V. Volotka, D. A. Glazov, V. M. Shabaev, I. I. Tupitsyn, and G. Plunien, Phys. Rev. Lett. **112**, 253004 (2014).

[29] S. Sturm, A. Wagner, M. Kretzschmar, W. Quint, G. Werth, and K. Blaum, Phys. Rev. A **87**, 030501 (2013).

[30] S. Sturm, A. Wagner, B. Schabinger, J. Zatorski, Z. Harman, W. Quint, G. Werth, C. H. Keitel, and K. Blaum, Phys. Rev. Lett. **107**, 023002 (2011).

[31] M. Puchalski and K. Pachucki, Phys. Rev. Lett. **113**, 073004 (2014).

[32] K. Pachucki, Private communication, 2015.

[33] Z.-C. Yan, Phys. Rev. Lett. **86**, 5683 (2001).

[34] V. A. Yerokhin and K. Pachucki, Phys. Rev. A **81**, 022507 (2010).

[35] D. Hanneke, S. Fogwell, and G. Gabrielse, Phys. Rev. Lett. **100**, 120801 (2008).

[36] P. J. Mohr, B. N. Taylor, and D. B. Newell, Rev. Mod. Phys. **84**, 1527 (2012).

[37] V. M. Shabaev, D. A. Glazov, M. B. Shabaeva, V. A. Yerokhin, G. Plunien, and G. Soff, Phys. Rev. A **65**, 062104 (2002).

[38] V. M. Shabaev, D. A. Glazov, N. S. Oreshkina, A. V. Volotka, G. Plunien, H.-J. Kluge, and W. Quint, Phys. Rev. Lett. **96**, 253002 (2006).

[39] H.-J. Kluge, T. Beier, K. Blaum, L. Dahl, S. Eliseev, F. Herfurth, B. Hofmann, O. Kester, S. Koszudowski, C. Kozhuharov, *et al.*, Adv. Quantum Chem. **53**, 83 (2008).

[40] R. Bouchendira, P. Cladé, S. Guellati-Khélifa, F. Nez, and F. Biraben, Phys. Rev. Lett. **106**, 080801 (2011).

[41] T. Aoyama, M. Hayakawa, T. Kinoshita, and M. Nio, Phys. Rev. Lett. **109**, 111807 (2012).

[42] T. Aoyama, M. Hayakawa, T. Kinoshita, and M. Nio, Phys. Rev. D **91**, 033006 (2015).

[43] S. Sturm, F. Köhler, J. Zatorski, A. Wagner, Z. Harman, G. Werth, W. Quint, C. H. Keitel, and K. Blaum, Nature **506**, 467 (2014).

[44] A. Wagner, S. Sturm, F. Köhler, D. A. Glazov, A. V. Volotka, G. Plunien, W. Quint, G. Werth, V. M. Shabaev, and K. Blaum, Phys. Rev. Lett. **110**, 033003 (2013).

[45] S. Sturm, A. Wagner, B. Schabinger, J. Zatorski, Z. Harman, W. Quint, G. Werth, C. H. Keitel, and K. Blaum, Phys. Rev. Lett. **107**, 023002 (2011).

[46] S. Sturm, Private communication (2015).

[47] S. G. Karshenboim, Phys. Lett. **A 266**, 380 (2000).

[48] D. A. Glazov and V. M. Shabaev, Phys. Lett. A **297**, 408 (2002).

[49] V. M. Shabaev, I. I. Tupitsyn, V. A. Yerokhin, G. Plunien, and G. Soff, Phys. Rev. Lett. **93**, 130405 (2004).

[50] V. A. Yerokhin, C. H. Keitel, and Z. Harman, J. Phys. B **46**, 245002 (2013).

[51] I. I. Tupitsyn, V. M. Shabaev, J. R. Crespo López-Urrutia, I. Draganić, R. Soria Orts, and J. Ullrich, Phys. Rev. A **68**, 022511 (2003).

[52] V. A. Yerokhin, P. Indelicato, V. M. Shabaev, Phys. Rev. A **69**, 052503 (2004).

[53] D. A. Glazov, V. M. Shabaev, I. I. Tupitsyn, A. V. Volotka, V. A. Yerokhin, G. Plunien, and G. Soff, Phys. Rev. A **70**, 062104 (2004).

[54] K. P. Pachucki, A. Czarnecki, U. D. Jentschura, and V. A. Yerokhin, Phys. Rev. A **72**, 022108 (2005).

[55] A. V. Volotka, D. A. Glazov, V. M. Shabaev, I. I. Tupitsyn, and G. Plunien, Phys. Rev. Lett. **103**, 033005 (2009).

[56] D. A. Glazov, A. V. Volotka, V. M. Shabaev, I. I. Tupitsyn, and G. Plunien, Phys. Rev. A **81**, 062112 (2010).

[57] A. V. Volotka, D. A. Glazov, V. M. Shabaev, I. I. Tupitsyn, and G. Plunien, Phys. Rev. Lett. **112**, 253004 (2014).

[58] S. Sturm, A. Wagner, M. Kretzschmar, W. Quint, G. Werth, and K. Blaum, Phys. Rev. A **87**, 030501 (2013).

[59] M. Puchalski and K. Pachucki, Phys. Rev. Lett. **113**, 073004 (2014).

[60] K. Pachucki, Private communication (2015).

[61] V. A. Yerohin and K. Pachucki, Phys. Rev. A **81**, 022507 (2010).

[62] Z.-C. Yan, Phys. Rev. Lett. **86**, 5683 (2001).

[63] J. Zatorski, N. Oreshkina, C. H. Keitel, and Z. Harman, Phys. Rev. Lett. **108**, 63005 (2012).

[64] A. V. Volotka and G. Plunien, Phys. Rev. Lett. **113**, 023002 (2014).

15 Summary

The aim of this thesis was to develop a concept for the high precision calculations for various QED effects, mostly for the G-factor and Hyperfine structure splitting of different elements. By considering the existing results and literature, we performed the high accuracy calculations on H-like, Li-like and B-like elements. Moreover working closely with experimental groups we performed calculations on lanthanide atoms.

In the first part of these thesis we have elaborated a new nonlocal single-particle potential, that allows to significantly improve the self-energy radiative corrections in calculations of the electric structure of many-electron ions and neutral atoms. Its addition to the Hamiltonian of a hydrogen-like ion causes shifts in the single-electron energies by values exactly coinciding with the self-energy corrections for H-like ions.

In the second part we investigated the experimental results and ab initio calculations approach for the Hyperfine structure splitting calculations used in laser-cooling transitions in fermionic Erbium-167. These calculations provided with data for the magnetic dipole and electric quadrupole constants for the only stable fermionic isotope, 167Er. We obtained the magnetic dipole and electric quadrupole hyperfine structure constants for the ground and two electronically excited states of the only stable fermionic erbium isotope ^{167} Er, which are relevant for laser cooling experiments.

In this paper, we present a combined experimental and theoretical investigation of the hyperfine structure of the only stable fermionic erbium isotope, ^{167}Er. In particular,

Further we demonstrated the implementation of the high accuracy MCDFS computational method for the calculations of the weighted difference of the g-factors of H-and Li-like ions of the same element. We showed that this weighted difference

and its combination for two different elements can be used to extract a value for the fine-structure constant from near-future bound-electron g-factor experiments with an accuracy competitive with the highest accuracy reported to date.

16 Appendix I

Bessel and Neuman functions and its derivative

16.0.1 Bessel functions $j_k(x)$

Consider Bessel function $j_k(x)$ where $x = r \cdot \omega$

1. $\mathbf{j_0(x)}$

$$j_0(x) = \frac{\sin(x)}{x}\,, \qquad j_0'(x) = \frac{d}{dx} j_0(x) = \frac{\cos(x)}{x} - \frac{\sin(x)}{x^2}\,.$$

$$\frac{\partial}{\partial \omega}\, j_0(x) = \frac{1}{\omega}\left\{\cos(x) - \frac{\sin(x)}{x}\right\}$$

2. $\mathbf{j_1(x)/\omega}$

$$j_1(x) = \left\{\frac{\sin(x)}{x^2} - \frac{\cos(x)}{x}\right\}$$

$$j_1'(x) = j_0(x) - \frac{2}{x}\, j_1(x) = \left\{\frac{\sin(x)}{x} + \frac{2\cos(x)}{x^2} - \frac{2\sin(x)}{x^3}\right\}$$

$$\frac{\partial}{\partial \omega}\left(\frac{1}{\omega}\, j_1(x)\right) = \frac{1}{\omega^2}\,\left[x\, j_0(x) - 3\, j_1(x)\right] = \frac{1}{\omega^2}\left[\sin(x) + \frac{3\cos(x)}{x} - \frac{3\sin(x)}{x^2}\right] \tag{16.1}$$

3. $\mathbf{j_k(x)/\omega^k}$

Recurrence relations for large $x > 0.5\,(k+1)$

$$j_k(x) = \frac{(2k-1)}{x}\, j_{k-1}(x) - j_{k-2}(x)\,, \qquad j_k'(x) = j_{k-1}(x) - \frac{k+1}{x}\, j_k(x)\,.$$

$$\frac{\partial}{\partial \omega}\left(\frac{1}{\omega^k}\, j_k(x)\right) = \frac{1}{\omega^{k+1}}\,\left[x\, j_{k-1}(x) - (2k+1)\, j_k(x)\right]$$

Taylor expansions for small $x \leq 0.5\,(k+1)$

$$\begin{aligned} j_k(x) &= \frac{x^k}{(2k+1)!!}\left\{1 - \frac{\frac{1}{2}x^2}{1!(2k+3)} + \frac{(\frac{1}{2}x^2)^2}{2!(2k+3)(2k+5)} - ...\right\} \\ &= \frac{x^k}{(2k+1)!!}\sum_{n=0}\frac{(-x^2/2)^n\,(2k+1)}{n!\,(2k+n+1)!!} \end{aligned}$$

$$j'_k(x) = \frac{x^{k-1}}{(2k+1)!!}\sum_{n=1}\frac{(-x^2/2)^n\,(2n+k)\,(2k+1)}{n!\,(2k+n+1)!!}$$

$$\frac{\partial}{\partial\omega}\left(\frac{1}{\omega^k}\,j_k(x)\right) = \frac{x^k}{(2k+1)!!}\,\frac{2}{\omega^{k+1}}\sum_{n=1}\frac{(-x^2/2)^n\,(2k+1)}{(n-1)!\,(2k+n+1)!!}$$

16.0.2 Neuman functions $n_k(x)$

Consider Neuman function $n_k(x)$ where $x = r\cdot\omega$

1. $\mathbf{n_0(x)}$

$$n_0(x) = -\frac{\cos(x)}{x}\,, \qquad n'_0(x) = \frac{\sin(x)}{x} + \frac{\cos(x)}{x^2}$$

what we further use in program is

$$\bar{n}_0(x) = -\frac{\cos(x)}{x}\cdot\omega$$

$$\frac{\partial}{\partial\omega}\left(\omega\,n_0(x)\right) = \omega^k\,\left[x\,n'_0(x) + (k+1)n_0(x)\right] = \sin(x)\,.$$

2. $\mathbf{n_1(x)}$

$$n_1(x) = -\left\{\frac{\cos(x)}{x^2} + \frac{\sin(x)}{x}\right\}\,, \qquad n'_1(x) = \frac{2\sin(x)}{x^2} + \frac{2\cos(x)}{x^3} - \frac{\cos(x)}{x}$$

what we use in program is

$$\bar{n}_1(x) = -\left\{\frac{\cos(x)}{x^2} + \frac{\sin(x)}{x}\right\}\cdot\omega^2$$

$$\frac{\partial}{\partial\omega}\left(\omega^2\, n_1(x)\right) = \omega^k\ \left[x\, n_1'(x) + (k+1)n_1(x)\right] = -\omega\cos(x)$$

3. $\mathbf{n_k(x)\,\omega^{k+1}}$

Taylor expansions for small $x \le 0.5\,(k+1)$

$$n_k(x) = -\frac{(2k-1)!!}{x^{k+1}}\left\{1 + \frac{(-x^2/2)}{1!(1-2k)} + \frac{(-x^2/2)^2}{2!(1-2k)(3-2k)} - ...\right\}$$

$$n_k'(x) = -\frac{2(2k-1)!!}{x^{k+2}}\left\{1 + \frac{(-x^2/2)}{1!(1-2k)} + \frac{2(-x^2/2)^2}{2!(1-2k)(3-2k)} + ...\right\}$$

$$\frac{\partial}{\partial\omega}\left(\omega^{k+1}\, n_k(x)\right) = -\frac{2(2k-1)!!\,\omega^k}{x^{k+1}}\ \left\{\frac{(-x^2/2)}{1!(1-2k)} + \frac{2(-x^2/2)^2}{2!(1-2k)(3-2k)} - ...\right\}$$

Recurrence relations for large $x > 0.5\cdot(k+1)$

$$n_k(x) = \frac{(2k-1)}{x}\, n_{k-1}(x) - n_{k-2}(x)\,, \qquad n_k'(x) = n_{k-1}(x) - \frac{k+1}{x}\, n_k(x)\,.$$

$$\frac{\partial}{\partial\omega}\left(\omega^{k+1}\, n_k(x)\right) = \omega^k\left[x\, n_k'(x) + (k+1)\, n_k(x)\right] = \omega^k x\, n_{k-1}(x)$$

where $n_k(x)$ is a real Bessel function from the Abramovitz book

16.0.3 Second derivative of Neuman function as in program

1. $\mathbf{n_k(x)\,\omega^{k+1}}$

$$\frac{\partial}{\partial\omega}\frac{\partial}{\partial\omega}\left(\omega^{k+1}\, n_k(x)\right) = \frac{\partial}{\partial\omega}\left(\omega^k x\, n_{k-1}(x)\right)$$

where

$$\omega^k \, n_{k-1}(x) = \bar{n}_{k-1}(x)$$

then

$$\frac{\partial}{\partial \omega} \left(\omega^k x \, n_{k-1}(x) \right) = \frac{\partial}{\partial \omega} \left(x \, \bar{n}_{k-1}(x) \right) = r \, \left(\bar{n}_{k-1}(x) + \omega \bar{n}'_{k-1}(x) \right)$$

where $x = \omega \, r$ and
$\omega \bar{n}'_{k-1}(x) = r \omega \bar{n}_{k-2}(x)$ so

$$\frac{\partial}{\partial \omega} \left(\omega^k x \, n_{k-1}(x) \right) = r \, \bar{n}_{k-1}(x) + r^2 \, \omega^2 \, \bar{n}_{k-2}(x)$$

2. $\mathbf{n_{k-1}(x) \, \omega^k}$

let's remind that

$$\omega^{k+1} \, n_k(x) = \bar{n}_k(x)$$

$$\bar{n}_{k-1}(x) = n_{k-1}(x) \, \omega^k$$

let's derive formulas for $k = 0$

$$\omega^0 \, n_{-1}(x) = \bar{n}_{-1}(x)$$

$$\frac{\partial}{\partial \omega} \left(\omega^1 \, n_0(x) \right) = \omega^0 x \, n_{-1}(x) = x \, n_{-1}(x) = x \, \bar{n}_{-1}(x)$$

we know that

$$\frac{\partial}{\partial \omega} \left(\omega \, n_0(x) \right) = \sin(x)$$

so

$$x\,\bar{n}_{-1}(x) = \sin(x)$$

therefore

$$\bar{n}_{-1}(x) = \frac{\sin(x)}{x}$$

3. $\mathbf{n_{k-2}(x)\,\omega^k}$

let's remind that

$$\omega^{k+1}\,n_k(x) = \bar{n}_k(x)$$

$$\bar{n}_{k-2}(x) = n_{k-2}(x)\,\omega^{k-1}$$

let's derive formulas for $k = -1$

$$\bar{n}_{-2}(x) = \omega^{-1}\,n_{-2}(x)$$

$$\frac{\partial}{\partial\omega}\left(\omega^0\,n_{-1}(x)\right) = \omega^{-1}x\,n_{-2}(x)$$

$$\frac{\partial}{\partial\omega}\left(\omega^0\,n_{-1}(x)\right) = \frac{\partial}{\partial\omega}\left(n_{-1}(x)\right) = \frac{\partial}{\partial\omega}\left(\bar{n}_{-1}(x)\right) = \frac{\partial}{\partial\omega}\left(\frac{\sin(x)}{x}\right) = \frac{\partial}{\partial\omega}\left(\frac{\sin(r\,\omega)}{r\,\omega}\right)$$
$$= \frac{r\,x\,\cos x - r\,\sin(x)}{x^2}$$

so

$$\omega^{-1}x\,n_{-2}(x) = \frac{r\,x\,\cos x - r\,\sin(x)}{x^2}\,, \qquad n_{-2}(x) = \frac{x\,\cos x - \sin(x)}{x^2}$$

if

$$\bar{n}_{-2}(x) = \omega^{-1}\, n_{-2}(x) = \left[\frac{x\, \cos x - \sin(x)}{x^2}\right] \frac{1}{\omega}$$

we know that

16.0.4 Second derivative of Bessel function as in program

1. $\mathbf{j_k(x)\,/\omega^k}$

we remember that

$$\frac{\partial}{\partial\omega}\left[\frac{1}{\omega^k}\, j_k(x)\right] = \frac{1}{\omega^{k+1}}\left[x\, j_{k-1}(x) - (2k+1)\, j_k(x)\right]$$

then for the second derivativ over ω we have

$$\begin{aligned}
&\frac{\partial}{\partial\omega}\frac{\partial}{\partial\omega}\left[\frac{1}{\omega^k}\, j_k(x)\right] = \frac{\partial}{\partial\omega}\left(\frac{1}{\omega^{k+1}}\left[x\, j_{k-1}(x) - (2k+1)\, j_k(x)\right]\right)\\
&\frac{\partial}{\partial\omega} = \frac{\partial}{\partial\omega}\left[\frac{1}{\omega^{k+1}}\left[x\, j_{k-1}(x) - (2k+1)\, j_k(x)\right]\right]\\
&= \left(\frac{1}{\omega^{k+1}}\right)'\left[x\, j_{k-1}(x) - (2k+1)\, j_k(x)\right] +\\
&+ \frac{1}{\omega^{k+1}}\left[x\, j_{k-1}(x) - (2k+1)\, j_k(x)\right]'
\end{aligned}$$

let's call it like

$$\frac{\partial}{\partial\omega}\left[\frac{1}{\omega^k}\, j_k(x)\right] = A + B$$

then

$$B = \frac{1}{\omega^{k+1}} \left[x\, j_{k-1}(x) - (2k+1)\, j_k(x) \right]' =$$
$$\frac{1}{\omega^{k+1}} \left[r\, j_{k-1}(x) + x\, j'_{k-1}(x) - -(2k+1) j'_k(x) \right] =$$
$$\frac{1}{\omega^{k+1}} \left[r\, j_{k-1}(x) + x[r\, j_{k-2}(x) - \frac{k}{x}\, j_{k-1}(x)] - (2k+1)[j_{k-1}(x) - \frac{k+1}{x} j_k(x)] \right] =$$
$$\frac{1}{\omega^{k+1}} \left[j_{k-1}(x)[r - 3k - 1] + x\, j_{k-2}(x) + \frac{2k^2+3k+1}{x} j_k(x) \right]$$

$$A = \left(\frac{1}{\omega^{k+1}} \right)' \left[x\, j_{k-1}(x) - (2k+1)\, j_k(x) \right] =$$
$$- \frac{k+1}{\omega^{k+2}} \left[x\, j_{k-1}(x) - (2k+1)\, j_k(x) \right]$$

it is easy to write like that

$$\frac{\partial}{\partial \omega} \left[\frac{1}{\omega^k}\, j_k(x) \right] =$$
$$j_{k-1}(x) \left[\frac{1}{\omega^{k+1}} [r - 3k - 1] - \frac{k+1}{\omega^{k+2}}\, x \right] +$$
$$+ j_{k-2}(x)\, x\, \frac{1}{\omega^{k+1}} +$$
$$+ j_k(x) \left[\frac{1}{\omega^{k+1}} \frac{2k^2+3k+1}{x} + \frac{2k^2+3k+1}{\omega^{k+2}} \right]$$

2. $\mathbf{j_{k-1}(x)\,/\omega^k}$

first of all

$$\bar{j}_{k-1}(x) = \frac{j_{k-1}(x)}{\omega^{k-1}}$$

for $k = 0$

$$\bar{j}_{-1}(x) = \frac{j_{-1}(x)}{\omega^{-1}} = j_{-1}(x)\, \omega$$

$$\frac{\partial}{\partial\omega}\left(\frac{1}{\omega^0}\,j_0(x)\right)=\frac{\partial}{\partial\omega}\bar{j}_0(x)=\frac{1}{\omega}\left[x\,j_{-1}(x)-(2k+1)\,j_0(x)\right]$$

$$\frac{1}{\omega}\left[x\,j_{-1}(x)-(2k+1)\,j_0(x)\right]=\frac{1}{\omega}\left[\cos x-\frac{\sin x}{x}\right]$$

So

$$j_{-1}(x)=\frac{\cos x}{x}\,,\qquad \bar{j}_{-1}(x)=\frac{\cos x}{x}\,\omega$$

3. $\mathbf{j_{k-2}(x)\,/\omega^k}$

first of all

$$\bar{j}_{k-2}(x)=\frac{j_{k-2}(x)}{\omega^{k-2}}$$

for $k=-1$

$$\bar{j}_{-2}(x)=\frac{j_{-2}(x)}{\omega^{-2}}\omega^2$$

$$\frac{\partial}{\partial\omega}\left(\frac{1}{\omega^{-1}}\,j_{-1}(x)\right)=\frac{\partial}{\partial\omega}\bar{j}_{-1}(x)=\frac{1}{\omega^0}\left[x\,j_{-2}(x)-(2k+1)\,j_{-1}(x)\right]$$

where

$$\frac{\partial}{\partial\omega}\bar{j}_{-1}(x)=\frac{\partial}{\partial\omega}\left(\frac{\cos x}{x}\,\omega\right)=-\sin x$$

$$-\sin x=x\,j_{-2}(x)+\frac{\cos x}{x}$$

finally we have

$$j_{-2}(x)=-\frac{\cos x}{x^2}-\frac{\sin x}{x}\,,\qquad \bar{j}_{-2}(x)=-\left(\frac{\cos x}{x^2}+\frac{\sin x}{x}\right)\omega^2$$

16.0.5 Second derivative

1. $\mathbf{n_k(x)\,\omega^{k+1}}$

$$\frac{\partial}{\partial\omega}\frac{\partial}{\partial\omega}\left(\omega^{k+1}\,n_k(x)\right) = \frac{\partial}{\partial\omega}\left((k+1)\,\omega^k\,n_k(x) + \omega^{k+1}\,n_k'(x)\right)$$
$$= (k+1)\,k\,\omega^{k-1}\,n_k(x) + (k+1)\,\omega^k\,n_k'(x) + (k+1)\,\omega^k\,n_k'(x) + \omega^{k+1}\,n_k''(x)$$

worth noting that

$$f(x(\omega)) = f' \cdot \frac{dx}{d\omega}$$

where

$$\frac{dx}{d\omega} = r$$

so then we have the following

$$\omega^{k-1}\,k\,(k+1)n_k(x) + 2(k+1)\,\omega^k\,n_k'(x)\,r + \omega^{k+1}\,n_k''(x)\,r^2$$

where $n_k(x)$ is a real Bessel function from the Abramovitz book

2. $\mathbf{n_k(x)}$

we should start with the know formula from the Abramovitz book

$$n_k'(x) = n_{k-1}(x) - \frac{k+1}{x}\,n_k(x)$$

then

$$n_k''(x) = (n_{k-1}(x) - \frac{k+1}{x}\,n_k(x))'$$

$$n'_{k-1}(x) - \left(\frac{k+1}{x}\right)' n_k(x) - \frac{k+1}{x} n'_k(x)$$

$$= n_{k-2}(x) - \frac{k}{x} n_{k-1}(x) + \frac{2(k+1)}{x^2} n_k(x) - \frac{k+1}{x}\left[n_{k-1}(x) - \frac{k+1}{x} n_k(x)\right] =$$

$$= n_{k-2}(x) - \frac{2k+1}{x} n_{k-1}(x) + n_k(x)\left[\frac{k^2+4k+2}{x^2}\right]$$

where $n_k(x)$ is a real Bessel function from the Abramovitz book

16.0.6 Integral

$$\bar{j_k}(x) = \frac{j_k(x)}{\omega^k}$$

$$\bar{n_k}(x) = \omega^{k+1} n_k(x)$$

Integral as a function Y_b^k

$$Y_b^k = \int_0^\infty V_k(r, r')\rho(r')dr'$$

$$V_k(r, r') = \bar{j_k}(\omega r_<)\, \bar{n_k}(\omega r_>)$$

$$\int_0^\infty dr' = \int_0^r dr' + \int_r^\infty dr' = Z_b^k(r) + X_b^k(r)$$

1. $\mathbf{Z_b^k(r)}$

$$Z_b^k(r) = \bar{n_k}(\omega r') \int_0^r \bar{j_k}(\omega r')\, \rho(r')dr'$$

$$Z_b^k(r_{i+1}) = \bar{n_k}(\omega r_{i+1}) \int_0^{r_{i+1}} \bar{j_k}(\omega r')\, \rho(r')$$

$$Z_b^k(r_{i+1}) = \bar{n_k}(\omega r_{i+1}) \left[\int_0^{r_i} \bar{j_k}(\omega r')\, \rho(r') + \int_{r_i}^{r_{i+1}} \bar{j_k}(\omega r')\, \rho(r')\right]$$

$$Z_b^k(r_{i+1}) = \bar{n_k}(\omega r_{i+1}) \left[\frac{Z_b^k(r)}{\bar{n_k}(\omega r_i)} + \int_{r_i}^{r_{i+1}} \bar{j_k}(\omega r')\, \rho(r')\right]$$

$$Z_b^k(r_{i+1}) = \bar{n_k}(\omega r_{i+1}) \left[\frac{Z_b^k(r_i)}{\bar{n_k}(\omega r_i)} + \int_{r_i}^{r_{i+1}} \bar{j_k}(\omega r') \, \rho(r') \right]$$

let's apply $f_1(t) = \bar{j_k}(\omega r') \, V_k(r') \, \rho(r')$ then

$$\int_{r_i}^{r_{i+1}} f(t)dt = \frac{h}{2} \left[f(r_i) + f(r_{i+1}) \right] + \frac{h^2}{12} \left[f'(r_i) - f'(r_{i+1}) \right] + O(h^5)$$

where $f' = \frac{d}{dt} f$. Then we could derive the following equation:

$$\frac{Z_b^k(r_{i+1})}{\bar{n_k}(\omega r_{i+1})} = \frac{Z_b^k(r_i)}{\bar{n_k}(\omega r_i)} + \frac{h}{2} f_1(r_i) + \frac{h}{2} f_1(r_{i+1}) + \frac{h^2}{12} f_1'(r_i) - \frac{h^2}{12} f_1'(r_{i+1})$$

Taking into account previously derived equations we obtain:

$$\frac{Z_b^k(r_{i+1})}{\bar{n_k}(\omega r_{i+1})} + \frac{h}{2} f_1(r_{i+1}) + \frac{h^2}{12} f_1'(r_{i+1}) = \frac{Z_b^k(r_i)}{\bar{n_k}(\omega r_i)} + \frac{h}{2} f_1(r_i) + \frac{h^2}{12} f_1'(r_i) + h f_1(r_{i+1})$$

After cancelling equal terms on the right and left-hand side of the equation, we obtain:

$$\bar{Z}_b^k(r_{i+1}) = \frac{Z_b^k(r_{i+1})}{\bar{n_k}(\omega r_{i+1})} + \frac{h}{2} f_1(r_{i+1}) + \frac{h^2}{12} f_1'(r_{i+1})$$

$$\bar{Z}_b^k(r_{i+1}) = \frac{Z_b^k(r_i)}{\bar{n_k}(\omega r_i)} + \frac{h}{2} f_1(r_i) + \frac{h^2}{12} f_1'(r_i)$$

Finally, we derive:

$$\bar{Z}_b^k(r_{i+1}) = \bar{Z}_b^k(r_i) + h f_1(r_{i+1})$$

1. $\mathbf{X_b^k(r)}$

$$X_b^k(r_i) = \bar{j_k}(\omega r_i) \int_{r_i}^{\infty} \bar{n_k}(\omega r_i) \, \rho(r_i) dr_i$$

$$X_b^k(r_i) = \bar{j_k}(\omega r_i) \int_{r_i+1}^{\infty} \bar{n_k}(\omega r_i)\, \rho(r_i) dr_i + \bar{j_k}(\omega r_i) \int_{r_i}^{r_i+1} \bar{n_k}(\omega r_i)\, \rho(r_i) dr_i$$

$$\frac{X_b^k(r_i)}{\bar{j_k}(\omega r_i)} = \int_{r_i+1}^{\infty} \bar{n_k}(\omega r_i)\, \rho(r_i) dr_i + \int_{r_i}^{r_i+1} \bar{n_k}(\omega r_i)\, \rho(r_i) dr_i$$

$$\frac{X_b^k(r_i)}{\bar{j_k}(\omega r_i)} = \frac{X_b^k(r_{i+1})}{\bar{j_k}(\omega r_{i+1})} + \int_{r_i}^{r_i+1} \bar{n_k}(\omega r_i)\, \rho(r_i) dr_i$$

let's apply $f_2(t) = \bar{n_k}(\omega r')\, V_k(r')\, \rho(r')$ and

$$\int_{r_i}^{r_{i+1}} f(t)dt = \frac{h}{2}\left[f(r_i) + f(r_{i+1})\right] + \frac{h^2}{12}\left[f'(r_i) - f'(r_{i+1})\right] + O(h^5)$$

then, after the substitution we rewrite the above equation:

$$\frac{X_b^k(r_i)}{\bar{j_k}(\omega r_i)} = \frac{X_b^k(r_{i+1})}{\bar{j_k}(\omega r_{i+1})} + \frac{h}{2} f_2(r_i) + \frac{h}{2} f_2(r_{i+1}) + \frac{h^2}{12} f_2'(r_i) - \frac{h^2}{12} f_2'(r_{i+1})$$

$$\frac{X_b^k(r_i)}{\bar{j_k}(\omega r_i)} - \frac{h}{2} f_2(r_i) - \frac{h^2}{12} f_2'(r_i) = \frac{X_b^k(r_{i+1})}{\bar{j_k}(\omega r_{i+1})} - \frac{h}{2} f_2(r_{i+1}) - \frac{h^2}{12} f_2'(r_{i+1}) + h f_2(r_{i+1})$$

$$\bar{X}_b^k(r_i) = \frac{X_b^k(r_i)}{\bar{j_k}(\omega r_i)} - \frac{h}{2} f_2(r_i) - \frac{h^2}{12} f_2'(r_i)$$

Consequently, we obtain:

$$\bar{X}_b^k(r_i) = X_b^k(r_{i+1}) + h f_2(r_{i+1})$$

3. $\mathbf{Y_b^k}$

$$Y_b^k = X_b^k(r_i) + Z_b^k(r_i)$$

We can derive the following equation:

$$\begin{aligned}
Y_b^k =& \bar{j}_k(\omega r_i)\left[\bar{X}_b^k(r_i) + \frac{h}{2}f_2(r_i) + \frac{h^2}{12}f_2'(r_i)\right] + \\
&+ \bar{n}_k(\omega r_i)\left[\bar{Z}_b^k(r_{i+1}) - \frac{h}{2}f_1(r_i) - \frac{h^2}{12}f_1'(r_i)\right] = \\
&= \bar{j}_k(\omega r_i)\bar{X}_b^k(r_i) + \frac{h}{2}\bar{j}_k(\omega r_i)\bar{n_k}(\omega r_i)\, V_k(r_i)\,\rho(r_i) + \bar{j}_k(\omega r_i)\frac{h^2}{12}f_2'(r_i) \\
&+ \bar{n}_k(\omega r_i)\bar{Z}_b^k(r_i) - \frac{h}{2}\bar{n}_k(\omega r_i)\bar{j_k}(\omega r_i)\, V_k(r_i)\,\rho(r_i) - \bar{n}_k(\omega r_i)\frac{h^2}{12}f_1'(r_i) = \\
&= \bar{j}_k(\omega r_i)\bar{X}_b^k(r_i) + \bar{n}_k(\omega r_i)\bar{Z}_b^k(r_i) + \bar{j}_k(\omega r_i)\frac{h^2}{12}f_2'(r_i) - \bar{n}_k(\omega r_i)\frac{h^2}{12}f_1'(r_i)
\end{aligned}$$

Where:

$$\begin{aligned}
&\bar{j}_k(\omega r_i)\frac{h^2}{12}f_2'(r_i) = \frac{h^2}{12}\bar{j}_k(\omega r_i)\frac{\partial}{\partial t}\bar{n_k}(\omega r_i)\, V_k(r_i)\,\rho(r_i) + \\
&+ \frac{h^2}{12}\bar{j}_k(\omega r_i)\bar{n_k}(\omega r_i)\frac{\partial}{\partial t}\, V_k(r_i)\,\rho(r_i) + \frac{h^2}{12}\bar{j}_k(\omega r_i)\bar{n_k}(\omega r_i)\, V_k(r_i)\,\frac{\partial}{\partial t}\rho(r_i)
\end{aligned}$$

And:

$$\begin{aligned}
&\bar{n}_k(\omega r_i)\frac{h^2}{12}f_1'(r_i) = \frac{h^2}{12}\bar{n}_k(\omega r_i)\frac{\partial}{\partial t}\bar{j}_k(\omega r_i)\, V_k(r_i)\,\rho(r_i) + \\
&+ \frac{h^2}{12}\bar{n}_k(\omega r_i)\bar{j}_k(\omega r_i)\frac{\partial}{\partial t}\, V_k(r_i)\,\rho(r_i) + \frac{h^2}{12}\bar{n}_k(\omega r_i)\bar{j}_k(\omega r_i)\, V_k(r_i)\,\frac{\partial}{\partial t}\rho(r_i)
\end{aligned}$$

So

$$\begin{aligned}
&\bar{j}_k(\omega r_i)\frac{h^2}{12}f_2'(r_i) - \bar{n}_k(\omega r_i)\frac{h^2}{12}f_1'(r_i) = \\
&\frac{h^2}{12}\bar{n}_k(\omega r_i)\frac{\partial}{\partial t}\bar{j}_k(\omega r_i)\, V_k(r_i)\,\rho(r_i) + \frac{h^2}{12}\bar{j}_k(\omega r_i)\frac{\partial}{\partial t}\bar{n}_k(\omega r_i)\, V_k(r_i)\,\rho(r_i)
\end{aligned}$$

Finally we obtain the following equation:

$$\begin{aligned}
&Y_b^k = \bar{j}_k(\omega r_i)\bar{X}_b^k(r_i) + \bar{n}_k(\omega r_i)\bar{Z}_b^k(r_i) + \\
&+ \frac{h^2}{12}\, V_k(r_i)\,\rho(r_i)\left[\bar{j}_k(\omega r_i)\frac{\partial}{\partial t}\bar{n}_k(\omega r_i) - \bar{n}_k(\omega r_i)\frac{\partial}{\partial t}\bar{j}_k(\omega r_i)\right]
\end{aligned}$$

where $W = \bar{j}_k(\omega r_i)\frac{\partial}{\partial t}\bar{n}_k(\omega r_i) - \bar{n}_k(\omega r_i)\frac{\partial}{\partial t}\bar{j}_k(\omega r_i)$ - Wronskian

note - $W\left[j_k(x), n_k(x)\right] = \frac{1}{x^2}$

$$\left[\bar{j}_k(\omega r_i)\frac{\partial}{\partial t}\bar{n}_k(\omega r_i) - \bar{n}_k(\omega r_i)\frac{\partial}{\partial t}\bar{j}_k(\omega r_i)\right]$$
$$= \left[\bar{j}_k(\omega r_i)\frac{\partial}{\partial t}\bar{n}_k(\omega r_i)\right] - \left[\bar{n}_k(\omega r_i)\frac{\partial}{\partial t}\bar{j}_k(\omega r_i)\right] = M - L$$

and $t = r\,\omega$

let's derive by parts

$$M = j_k\,\omega^{-k}\omega^{k+1}\frac{\partial}{\partial(\omega r_i)}\;(n_k\,) + j_k\,\omega^{-k}\,n_k\frac{\partial}{\partial(\omega r_i)}\left(\frac{x}{r}\right)^{k+1}$$
$$= \omega j_k\frac{\partial}{\partial(\omega r_i)}\,n_k + \;\frac{k+1}{r}\,j_k n_k$$

$$L = n_k\,\omega^{k+1}\omega^{-k}\frac{\partial}{\partial(\omega r_i)}\;(j_k\,) + n_k\,\omega^{k+1}\,j_k\frac{\partial}{\partial(\omega r_i)}\left(\frac{x}{r}\right)^{-k}$$
$$= \omega n_k\frac{\partial}{\partial(\omega r_i)}\,j_k - \;\frac{k}{r}\,j_k n_k$$

then $M - L$

$$\omega\left(j_k\frac{\partial}{\partial(\omega r_i)} - n_k\frac{\partial}{\partial(\omega r_i)}\right) + j_k\,n_k = \omega\,W + j_k\,n_k = \frac{\omega}{x^2} + j_k\,n_k$$

then we apply that to Y_b^k

$$Y_b^k = \bar{j}_k(\omega r_i)\bar{X}_b^k(r_i) + \bar{n}_k(\omega r_i)\bar{Z}_b^k(r_i) + \frac{h^2}{12}\,V_k(r_i)\,\rho(r_i)\left[\frac{\omega}{x^2} + j_k\,n_k\right]$$

now we take a derivative of ω

$$\frac{\partial}{\partial\omega}Y_b^k = \frac{\partial}{\partial\omega}\left[\bar{j}_k(\omega r_i)\bar{X}_b^k(r_i) + \bar{n}_k(\omega r_i)\bar{Z}_b^k(r_i) + \frac{h^2}{12}\,V_k(r_i)\,\rho(r_i)\,\left[\frac{\omega}{x^2} + j_k\,n_k\right]\right]$$
$$= \bar{X}_b^k(r_i)\frac{\partial}{\partial\omega}\bar{j}_k(\omega r_i) + \bar{j}_k(\omega r_i)\frac{\partial}{\partial\omega}\bar{X}_b^k(r_i) + \bar{Z}_b^k(r_i)\frac{\partial}{\partial\omega}\bar{n}_k(\omega r_i) + \bar{n}_k(\omega r_i)\frac{\partial}{\partial\omega}\bar{Z}_b^k(r_i)$$
$$+ \frac{h^2}{12}\,\rho(r_i)\,\left[\frac{\omega}{x^2} + j_k\,n_k\right]\frac{\partial}{\partial\omega}\,V_k(r_i) + \frac{h^2}{12}\,\rho(r_i)\,V_k(r_i)\frac{\partial}{\partial\omega}\,\left[\frac{\omega}{x^2} + j_k\,n_k\right]$$

we can use the following $\bar{n}_k = n_k\,\omega^{k+1}$ and $\bar{j}_k = j_k/\omega^k$

so

$$j_k\,n_k = \frac{1}{\omega}\,\bar{n}_k\,\bar{j}_k$$

then

$$\frac{\partial}{\partial\omega}\,\left[\frac{\omega}{x^2} + j_k\,n_k\right] = \frac{\partial}{\partial\omega}\,\left[\frac{\omega}{x^2} + \frac{1}{\omega}\,\bar{n}_k\,\bar{j}_k\right] = \frac{\partial}{\partial\omega}\,\left(\frac{1}{\omega}\,\left[\frac{1}{r^2} + \bar{n}_k\,\bar{j}_k\right]\right)$$
$$= -\frac{1}{\omega^2}\,\left[\frac{1}{r^2} + \bar{n}_k\,\bar{j}_k\right] + \frac{1}{\omega}\left[\frac{1}{r^2} + \bar{n}_k\,\frac{\partial}{\partial\omega}\bar{j}_k + \bar{j}_k\,\frac{\partial}{\partial\omega}\,\bar{n}_k\right]$$

and

$$\frac{\partial}{\partial\omega}\,V_k(r_i) = \frac{\partial}{\partial\omega}\,\left[\bar{j}_k(\omega r_<)\,\bar{n}_k(\omega r_>)\right] = \bar{n}_k(\omega r_>)\frac{\partial}{\partial\omega}\,\bar{j}_k(\omega r_<) + \bar{j}_k(\omega r_<)\frac{\partial}{\partial\omega}\,\bar{n}_k$$

let's go further

$$\frac{\partial}{\partial\omega}\bar{X}_b^k(r_i) = \frac{\partial}{\partial\omega}\,\left[X_b^k(r_{i+1}) + h f_2(r_{i+1})\right]$$
$$= \frac{\partial}{\partial\omega}X_b^k(r_{i+1}) + h\,\rho(r')\,\left[\,V_k(r')\,\frac{\partial}{\partial\omega}\,\bar{n}_k(\omega r') + \,\bar{n}_k(\omega r')\,\frac{\partial}{\partial\omega}\,\,V_k(r')\right]$$

let's apply $f_2(t) = \bar{n_k}(\omega r')\, V_k(r')\, \rho(r')$ then

$$\frac{\partial}{\partial \omega} f_2(t) = \frac{\partial}{\partial \omega}\, \bar{n_k}(\omega r')\, V_k(r')\, \rho(r') =$$
$$= \rho(r')\, V_k(r')\, \frac{\partial}{\partial \omega}\, \bar{n_k}(\omega r') + \rho(r')\, \bar{n_k}(\omega r')\, \frac{\partial}{\partial \omega}\, V_k(r')$$

and

$$\frac{\partial}{\partial \omega}\, X_b^k(r_{i+1}) = \frac{\partial}{\partial \omega}\, \bar{j_k}(\omega r') \int_r^\infty \bar{n_k}(\omega r')\, \rho(r') dr'$$
$$= \frac{\partial}{\partial \omega}\, (\bar{j_k}(\omega r')) \int_r^\infty \bar{n_k}(\omega r')\, \rho(r')\, dr' + \bar{j_k}(\omega r') \int_r^\infty \rho(r') \frac{\partial}{\partial \omega}\, \bar{n_k}(\omega r') dr'$$

17 Appendix II

Examples of the Program codes used in the precise calculations.

17.1 Program bessel

implicit real*8 (a-h,o-z)

17.1.1 Calculation of the $j_k(x)/omega^k$

```
omega=1.5d0
    h=0.2d0
    domega=0.001d0
    do l=-1,5
    write(*,*)
    do i=1,20
    r=0.0+(i-1)*h
    if (i.eq.1) r=0.001d0
    call bess(l,omega,r,sj)
    omega1=omega+domega
    omega2=omega-domega
    call bess bderiff(l,omega1,r,dddfsj1)
    call bess bderiff(l,omega2,r,dddfsj2)
    d=(dddfsj1-dddfsj2)/(2*domega)
    call bess bbderiff(l,omega,r,bfsj)
    omega1=omega+domega
    omega2=omega-domega
    call bess(l,omega1,r,sj1)
    call bess(l,omega2,r,sj2)
```

```
dsj1=(sj1-sj2)/(2*domega)
call bess diff(l,omega,r,dsj)
write(*,'(i5,f16.6,3d20.10)') l,r,sj,dsj,dsj1
enddo
enddo
stop
end
```

17.2 Subroutine bess(k,omega,r,sj)

```
implicit real*8 (a-h,o-z)
```

17.2.1 Calculation of the $j_k(x)/omega^k$

```
x=omega*r
    if (k.eq.-2) then
    if (dabs(x).lt.0.01d0) goto 300
    sinx=dsin(x)
    cosx=dcos(x)
    sj= -(sinx/x + cosx/x**2)
    sj=sj*omega**2
    return
    endif if (k.eq.-1) then
    if (dabs(x).lt.0.01d0) goto 300
    sinx=dsin(x)
    cosx=dcos(x)
    sj= cosx/x
    sj=sj*omega
    return
```

```
endif if (k.eq.0) then
if (dabs(x).lt.0.01d0) goto 300
sinx=dsin(x)
cosx=dcos(x)
sj= sinx/x
return
endif
if (k.eq.1) then
if (dabs(x).lt.0.01d0) goto 300
sinx=dsin(x)
cosx=dcos(x)
sj= sinx/(x*x)-cosx/x
sj=sj/omega
return
endif
```

17.2.2 Reference line of the calculations 300

```
if (dabs(x).le.0.5d0*(k+1)) then dfac=1.d0
do i=1,2*k-1,2
dfac=dfac*i
enddo
sj=r**k/(dfac*(2*k+1))
z=0.5d0*x*x
d=1.d0
fi=1.d0
i=0
```

17.2.3 Reference line of the calculations 200

```
i=i+1
    fi=-fi*z/(i*(2*k+2*i+1))
    d=d+fi
    if (dabs(fi).gt.1.d-16) goto 200
    sj=sj*d
    else
    sinx=dsin(x)
    cosx=dcos(x)
    sj0= sinx/x
    sj1= sinx/(x*x)-cosx/x
    do i=2,k
    sj=(2*i-1)*sj1/x-sj0
    sj0=sj1
    sj1=sj
    enddo
    sj=sj/omega**k
    endif return
    end
```

17.3 Subroutine naum(k,omega,r,sn)

```
implicit real*8 (a-h,o-z)
```

17.3.1 Calculation of the $n_k(x) * omega^{k+1}$

```
x=omega*r
    if (k.eq.-2) then
```

```
      if (dabs(x).lt.0.01d0) goto 300
      sinx=dsin(x)
      cosx=dcos(x)
      sn=cosx/x-sinx/x**2
      sn=sn/omega
      return
      endif
      if (k.eq.-1) then
      if (dabs(x).lt.0.01d0) goto 300
      sinx=dsin(x)
      cosx=dcos(x)
      sn=sinx/x
      return
      endif
      if (k.eq.0) then
      if (dabs(x).lt.0.01d0) goto 300
      sinx=dsin(x)
      cosx=dcos(x)
      sn=-cosx/x
      sn=sn*omega
      return
      endif
      if (k.eq.1) then
```

17.3.2 Reference line of the calculations 300

```
if (dabs(x).lt.0.01d0) goto 300
      sinx=dsin(x)
```

```
cosx=dcos(x)
sn=-cosx/(x*x)-sinx/x
sn=sn*omega**2
return
endif
```

17.3.3 Reference line of the calculations 210

```
if (dabs(x).le.0.5d0*(k+1)) then
dfac=1.d0
do i=1,2*k-1,2
dfac=dfac*i
enddo
z=0.5d0*x*x
sn=-dfac/r**(k+1)
d=1.d0
fi=1.d0
i=0
i=i+1
fi=-fi*z/(i*(2*i-1-2*k))
d=d+fi
if (dabs(fi).gt.1.d-16) goto 210
sn=sn*d
else
sinx=dsin(x)
cosx=dcos(x)
sn0=-cosx/x
sn1=-cosx/(x*x)-sinx/x
```

```
do i=2,k
sn=(2*i-1)*sn1/x-sn0
sn0=sn1
sn1=sn
enddo
sn=sn*omega**(k+1)
endif
return
end
```

17.4 Subroutine bess diff(k,omega,r,dfsj)

```
implicit real*8 (a-h,o-z)
```

17.4.1 Calculation of the $d[j_k(x)/omega^k]/domega$

```
x=omega*r
```

17.4.2 k =-1

```
if (k.eq.-1) then
if (dabs(x).lt.0.01d0) goto 400
sinx=dsin(x)
cosx=dcos(x)
dfsj=-sinx
return
endif
```

17.4.3 k = 0

```
if (k.eq.0) then
    if (dabs(x).lt.0.01d0) goto 400
    sinx=dsin(x)
    cosx=dcos(x)
    dfsj= (cosx-sinx/x)/omega
    return
    endif
```

17.4.4 Derivative bessel k =1

```
if (k.eq.1) then
    if (dabs(x).lt.0.01d0) goto 400
    sinx=dsin(x)
    cosx=dcos(x)
    dfsj= (3*cosx/x-3*sinx/x**2+sinx)/omega**2
    return
    endif
```

17.4.5 Reference line of the calculations 400

```
c - - - - - - - - - - - - - - - - - - - - - - - - - - - - if (dabs(x).le.0.5d0*(k+1)) then dfac=1.d0
    do i=1,2*k-1,2
    dfac=dfac*i
    enddo
    dfsj=r**k/(dfac*(2*k+1))
    z=0.5d0*x*x
    fi=-z/(2*k+3)
    d=fi
```

```
      i=1
```

17.4.6 Reference line of the calculations 200

```
i=i+1
      fi=-fi*z/((i-1)*(2*k+2*i+1))
      d=d+fi
      if (dabs(fi).gt.1.d-16) goto 200
      dfsj=dfsj*d*2/omega
      else
      sinx=dsin(x)
      cosx=dcos(x)
      sj0= sinx/x
      sj1= sinx/(x*x)-cosx/x
      do i=2,k
      sj=(2*i-1)*sj1/x-sj0
      sj0=sj1
      sj1=sj
      enddo
      dfsj=(x*sj0-(2*k+1)*sj)/omega**(k+1)
      endif
      return
      end
```

17.5 Subroutine bess deriff(k,omega,r,ddfsj)

```
implicit real*8 (a-h,o-z)
```

17.5.1 Calculation of the $d[j_k(x)/omega^k]/domega$

```
x=omega*r
      a=x**2/omega**k
      call bess(k-2,omega,r,sj)
      a=a*sj/omega**(k+1)
      b=x*(2*k-1)+r*(2*k+1)
      b=b/omega**k
      c=r-b
      c=c/omega**(k+1)-(k+1)*x/omega**(k+2)
      call bess(k-1,omega,r,sj)
      c=c*sj
      d=(2*k+1)**2/omega**(k+1)
      d=d/omega**(k+1)
      e=(2*k+1)*(k+1)/omega**(k+2)
      e=e+d
      call bess(k,omega,r,sj)
      e=e*sj
      ddfsj=a+c+e
      ddfsj=ddfsj/omega**(k+1)
      return
      end
```

17.6 Subroutine bess bderiff(k,omega,r,dddfsj)

```
implicit real*8 (a-h,o-z)
```

17.6.1 B part checkings without $omega^{k+1}$term

```
x=omega*r
    call bess(k,omega,r,sj)
    a=sj*(2*k+1)
    call bess(k-1,omega,r,sj)
    b=sj*x
    dddfsj=b-a
    return
    end
```

17.7 subroutine bess bbderiff(k,omega,r,bfsj)

```
implicit real*8 (a-h,o-z)
```

17.7.1 Calculation of the $d[j_k(x)/omega^k]/domega$

```
x=omega*r
```

17.7.2 B part calculation

```
a=(2*k+1)
    call bess diff(k,omega,r,dfsj)
    a=a*dfsj
    call bess diff(k-1,omega,r,dfsj)
    b=x*dfsj
    call bess(k-1,omega,r,dfsj)
    c=r*dfsj
    bfsj1=b+c-a
    bfsj1=bfsj1/omega**(k+1)
```

17.7.3 A part calculation

```
d=-(k+1)/omega**(k+2)*x
      call bess(k-1,omega,r,sj)
      d=d*sj
      e=(k+1)*(2*k+1)/omega**(k+2)
      call bess(k,omega,r,sj)
      e=e*sj
      bfsj2=d+e
```

17.7.4 A + B parts calculated together

```
bfsj=bfsj1+bfsj2
      return
      end
```

17.8 Program bessel

```
implicit real*8 (a-h,o-z)
      omega=1.5d0
      h=0.2d0
      domega=0.001d0
      do l=0,5
      write(*,*)
      do i=1,20
      r=0.0+(i-1)*h
      if (i.eq.1) r=0.001d0
      call naum(l,omega,r,sn)
      omega3=omega
```

```
      omega4=omega+2*domega
      omega5=omega+domega
      call naum(l,omega3,r,sn3)
      call naum(l,omega4,r,sn4)
      call naum(l,omega5,r,sn5)
      ddsn1=(sn4-2*sn5+sn3)/(domega)**2
      ddsn1=ddsn1
      cc write(*,*) dsn1 cc ddsn2=(sn5-sn3)/domega
      call naum deriff(l,omega,r,ddsn)
      write(*,'(i5,f16.6,3d20.10)') l,r,sn,ddsn,ddsn1
      enddo
      enddo
      stop
      end
```

17.9 program nauman

```
implicit real*8 (a-h,o-z)
      omega=1.5d0
      h=0.2d0
      domega=0.001d0
      do l=0,5
      write(*,*)
      do i=1,20
      r=0.0+(i-1)*h
      if (i.eq.1) r=0.001d0
      call naum(l,omega,r,sn)
      omega3=omega
```

```
      omega4=omega+2*domega
      omega5=omega+domega
      call naum(l,omega3,r,sn3)
      call naum(l,omega4,r,sn4)
      call naum(l,omega5,r,sn5)
      ddsn1=(sn4-2*sn5+sn3)/(domega)**2
      ddsn1=ddsn1
      call naum deriff (l,omega,r,ddsn)
      write(*,'(i5,f16.6,3d20.10)') l,r,sn,ddsn,ddsn1
      enddo
      enddo
      stop
      end
```

17.10 subroutine naum diff(k,omega,r,sn)

```
implicit real*8 (a-h,o-z)
      x=omega*r
      dsn=x
      call naum(k-1,omega,r,sn)
      dsn=dsn*sn
      return
      end
```

17.11 subroutine naum deriff(k,omega,r,ddsn)

```
implicit real*8 (a-h,o-z)
```

17.11.1 Calculation of the $d[n_k(x) * omega^{k+1}]/domega$

```
x=omega*r
    call naum(k-1,omega,r,sn)
    a=sn*r
    call naum(k-2,omega,r,sn)
    b=r**2*sn*omega**2
    ddsn=a+b
    return
    end
```